THE FORMATION OF COPPER TYPE SHEAR BANDS IN AL-1MG AND THEIR INFLUENCE ON RECRYSTALLISATION BEHAVIOUR

by

Alan Duckham

A thesis presented for the Degree of DOCTOR OF PHILOSOPHY in the Faculty of Engineering, University of Cape Town.

Department of Materials Engineering

August 1998

Abstract

Copper type shear band formation in Al-1Mg and its influence on recrystallisation phenomena has been investigated. This study includes the development of a suitable plane strain compression (PSC) apparatus, and an analysis of the deformation and recrystallisation structures which evolve from a matrix of experiments incorporating temperature, strain and strain rate variables.

A PSC test rig was purposely designed and built to facilitate the controlled high temperature deformation of aluminium specimens. The design of the apparatus ensured that strain distribution within a specimen is uniform while simultaneously limiting lateral spread. A small amount of lateral platen movement of the apparatus has been observed to cause asymmetric flow due to rotation of the plastic-rigid exit boundaries within the deforming specimens. Asymmetric flow compared to symmetric flow was found to have a negligible influence on the measured textures of the specimens studied.

The formation of shear bands during deformation, as characterised by optical and transmission electron microscopy, is seen to depend very critically on deformation temperature and strain rate and also to a large extent on strain. In particular a sudden transition from strong shear band formation to weak or non-existent shear band formation is observed at a value of Zener-Holloman parameter (Z) approximately equal to 1.0×10^{14} s^{-1}.

The influence of shear bands on recrystallisation behaviour in Al-1Mg has been studied by examining specimens annealed subsequently to PSC testing. The orientations of grains nucleating at shear bands were investigated from local orientation measurements performed on partially recrystallised specimens using the electron back scattered diffraction (EBSD) technique in a scanning electron microscope (SEM). Bulk texture measurements of fully recrystallised specimens were performed by X-ray diffraction (XRD). Nucleation at shear bands was observed to cause a random texture with weak peaks centred on the Goss and Q ideal orientations. This nucleation is responsible for the moderation of the potentially dominant Cube recrystallisation texture. In the absence of strong shear banding, the Cube recrystallisation texture was observed to increase dramatically in strength.

Acknowledgements

I would like to thank the following:

- Associate Professor RD Knutsen for his supervision, encouragement, assistance and guidance.
- Dr O Engler for valuable discussion and advice and for generating the ODFs corresponding to the local orientation measurements made.
- Mr G Newins for his invaluable assistance and advice in the designing and building of the PSC experimental apparatus, for the machining of countless specimens and for general workshop assistance.
- Mr R Hendricks and Mr N Dreze for their workshop assistance.
- Mr B Greeves, Mr J Petersen and Mr A Loedolff for their photographic assistance.
- Mr D Dean for his assistance in assembling the transformer for the PSC apparatus and other general electronic and computer assistance.
- Mrs M Topic for her laboratory assistance.
- Other staff and students, past and present, of the Department of Materials Engineering, UCT.
- The staff at the Electron Microscope Unit, UCT and in particular Mr D Gerneke for their assistance.
- MINTEK, South Africa for performing the hot rolling of the material investigated and performing the XRD measurements and data analysis necessary for the bulk texture results.
- Hulett Aluminium, South Africa for their financial support and for providing material.
- Alcan International, Banbury for providing material.
- The Foundation for Research Development, South Africa for their financial support.

- My wife, Elizabeth for her enormous support, patience, understanding and assistance, and for having to live the life of a "PhD widow" for several months. Thanks Babe.

List of Symbols and Abbreviations

β	angle of shear band to rolling plane
ψ	half scatter width
ε	logarithmic strain
$\dot{\varepsilon}$	strain rate
Δ	platen offset
σ	stress
λ	wavelength (of light)
Ω.cm	ohms centimetres
φ_1, φ_2, Φ	Euler angles describing crystal orientation
θ_b	misorientation across high angle boundary
γ_b	specific grain boundary energy
°C	degrees Celsius
(hkl) / {hkl}	index of plane / family of planes parallel to rolling plane
μm	microns (10^{-6} metre)
θ_s	misorientation across low angle boundary
γ_s	specific low angle boundary energy
[uvw] / <uvw>	index of direction / family of directions parallel to rolling direction
Al	aluminium
At %	atomic percent
AuPd	gold-palladium
C^{++}	computer programming language
Cu	copper
d	particle diameter
d_f	critical particle diameter for formation criterion of PSN
d_g	critical particle diameter for growth criterion of PSN
e^-	electron
Fe	iron
G	measured misorientation matrix
H_2O	water

HNO_3	nitric acid
k	shear stress
keV	kilo (10^3) electronvolts
kN	kilo (10^3) - newton
L	ideal misorientation matrix
M	misorientation matrix
Mg	magnesium
$mJ.m^{-2}$	millijoules per square metre
Mn	manganese
$MoK\alpha_1$	molybdenum $K\alpha_1$ X-ray
MPa	mega (10^6) –pascal
NaOH	sodium hydroxide
P_d	driving force for growth during nucleation of recrystallised grains
Q_b	activation energy for boundary diffusion
Q_v	activation energy for volume diffusion
r	particle radius
S	orientation density
s	subgrain size
Si	silicon
T	deformation temperature
Wt %	weight percent

ADC	**A**nalogue to **D**igital **C**onverter
b	Platen **b**readth / width
Brass	**Brass** ideal orientation
C	**C**ube ideal orientation
CD	**C**o-**d**irectional
CP	**C**o-**p**lanar
Cu	**C**opper ideal orientation
$Cube_{ND}$	**N**ormal **D**irection rotated **Cube** ideal orientation
$Cube_{RD}$	**R**olling **D**irection rotated **Cube** ideal orientation
DAC	**D**igital to **A**nalogue **C**onverter

DB / DBs	**D**islocation **b**oundary / **d**islocation **b**oundaries
EBSD	**E**lectron **B**ack **S**cattered **D**iffraction
ECC	**E**lectron **C**hannelling **C**ontrast
ESH	**E**lectro-**S**ervo **H**ydraulic
fcc	**F**ace **C**entred **C**ubic
FE	**F**inite **E**lement
G	**G**oss ideal orientation
h	Specimen **h**eight / thickness
MB / MBs	**M**icro**b**and / **m**icro**b**ands
MINTEK	Council for **Min**eral **Tek**hnology, Randburg, RSA
ND	**N**ormal **D**irection
ODF	**O**rientation **D**istribution **F**unction
OG	**O**rientated **G**rowth
ON	**O**rientated **N**ucleation
P	**P** ideal orientation
PSC	**P**lane **S**train **C**ompression
PSN	**P**article **S**timulated **N**ucleation
PTFE	**P**oly**t**e**t**ra**f**luoro**e**thylene (Teflon)
Q	**Q** ideal orientation
R	**R**etained rolling ideal orientation
RD	**R**olling **D**irection
RT	**R**oom **T**emperature
S	**S** ideal orientation
SAD	**S**elected **A**rea **D**iffraction
SB / SBs	**S**hear **b**and / **s**hear **b**ands
SEM	**S**canning **E**lectron **M**icroscopy
SFE	**S**tacking **F**ault **E**nergy
TD	**T**ransverse **D**irection
TEM	**T**ransmission **E**lectron **M**icroscopy
w	Specimen **w**idth
X	**R**andom orientation
Z	**Z**ener-Holloman parameter

Table of Contents

1. Introduction

The microstructural properties, and therefore also the mechanical properties, of thermo-mechanically processed metals and alloys depend very closely on the precise history of the thermo-mechanical process concerned. Such industrial processes include rolling, extrusion and hot press forming. The microstructural properties mentioned include grain size and shape, stored energy, precipitation and texture, which will influence mechanical properties such as strength, ductility and drawability. A well known example is the texture (or preferred orientation of grains) of rolled sheets of aluminium alloys that affects the drawing characteristics during cup forming in the manufacture of beverage cans. A strong or dominant Cube texture present in the rolled sheet in known to cause directionally dependent uneven or anisotropic drawing of the cups; a problem that is known as 'earing'. A more balanced or random texture in the rolled sheet will result in a more isotropically drawn cup and this can be achieved by altering the thermo-mechanical history during the rolling process necessary to produce the sheet from a cast ingot. In order to do so however, a detailed understanding of the microstructural processes involved is required.

Copper type shear bands are a well-known feature of the deformation microstructures of certain aluminium alloys, especially dilute aluminium alloys containing magnesium. Their formation is especially pronounced after high amounts of compression strain such as that caused by rolling. However, their formation is also thought to depend quite critically on certain other deformation variables such as temperature and strain rate. Furthermore, once present in the deformation microstructure, they are thought to affect subsequent recrystallisation behaviour that occurs during annealing. They thus have a very important effect on properties such as recrystallised grain size and texture.

In order to study the formation of copper type shear bands and hence also their subsequent effect on recrystallisation behaviour, it is necessary to reproduce the deformation conditions that are typical of an industrial process like rolling on a laboratory scale. Commercial trials on a larger scale are less flexible and far more expensive. One such laboratory scale simulation method is that of plane strain compression (PSC), which reproduces rolling deformation conditions fairly well and also allows for very good control of the deformation

variables of temperature, strain and strain rate. A further argument for the use of PSC testing instead of rolling trials is the possibility for rapid quenching of specimens after high temperature deformation.

1.1 Objectives

The objectives of this thesis were initially set as:

- To design and build a plane strain compression apparatus suitable for the intended experimental work. In particular, to provide a method of simulating the deformation mode of industrial rolling as well as reliably and accurately controlling the deformation variables of temperature, strain and strain rate.
- To investigate copper type shear band formation in the aluminium alloy, Al-1Mg as a function of the deformation parameters of temperature, strain and strain rate.
- To investigate the influence of copper type shear bands on the recrystallisation behaviour of Al-1Mg. In particular, to investigate grain nucleation at shear bands during recrystallisation and the subsequent effect on recrystallisation texture.

1.2 Experimental Approach

The experimental approach followed in pursuit of the research objectives was as follows:

- Plane strain compression tests were performed on laboratory scale samples of Al-1Mg over a matrix of deformation variables (temperature, strain and strain rate) in order to describe and map-out shear band formation as a function of these variables.
- Optical and transmission electron microscopy was employed to describe the extent of shear band formation.
- Specimens that exhibited strong and extensive shear band formation were subjected to a short 'flash anneal' in order to study nucleation at shear bands by the use of optical and scanning electron microscopy. In particular, the orientations of grains nucleating at shear bands were investigated by the analysis of diffraction patterns; the scanning electron microscope based technique of electron back scattered diffraction.

- Bulk texture measurements produced from X-ray diffraction analysis were used to investigate the effect of shear bands on both deformation and complete recrystallisation textures.

2. Literature Review

2.1 Material

The material under investigation is an Al-1Mg-0.3Fe-0.1Si alloy, that is an aluminium alloy containing 1 wt % (weight percent) magnesium, 0.3 wt % iron and 0.1 wt % silicon. In order to asses the effect of each of these alloying elements it is useful to review the relevant literature pertaining to pure aluminium, commercially pure aluminium (Fe and Si additions) and Al-Mg alloys.

2.1.1 High Purity Aluminium

2.1.1.1 General

Aluminium is an extremely useful engineering material due to a number of its properties. The most notable of these include its good corrosion resistance and low density, making it particularly suitable for applications in the fields of transport, packaging, building and domestic utensils. High purity aluminium (at least 99.9 % pure) is not very strong, possessing a yield strength of between 7 and 11 MPa in the annealed condition[1]. The addition of alloying elements significantly increases this figure.

An outstanding characteristic of simple aluminium alloys is the high amount of deformation obtainable during mechanical processing and in particular during high temperature mechanical processing. This is primarily due to the high level of dynamic recovery possible during deformation, which in turn is related to the high value of stacking fault energy (SFE). For pure aluminium this value is in the range[2], 170 to 200 $mJ.m^{-2}$. A stacking fault is the region between the two dissociated partial dislocations. The SFE of a material is an indication of the force per unit length pulling the dissociated partial dislocations together. The width of the stacking fault is inversely related to the SFE. This means that for a material like aluminium that has a high SFE, the width of the stacking fault is small and the two partial dislocations can easily recombine. Recovery processes like cross-slip and dislocation climb are thus enhanced.

2.1.1.2 Deformation

During the deformation of polycrystalline aluminium and other metals, the orientations of individual crystals or grains relative to the deformation geometry change as deformation progresses. This is due to the tendency of active slip systems to align either parallel (in the case of tension) or perpendicular (in the case of compression) to the major deformation axis. Taylor[3] was the first to propose a model for the preferred orientation of grains, or texture, that results when grains of different initial orientations become reorientated in specific ways. In rolling the orientations are measured relative to the rolling plane and the rolling direction. An ideal rolling orientation is described by a specific (hkl) plane, or family of {hkl} planes, parallel to the rolling plane and a specific [uvw] direction, or family of <uvw> directions, parallel to the rolling direction (see Figure 2.1). Such an ideal orientation in simply denoted, {hkl}<uvw>. Ideal orientations are also described by three unique Euler angles φ_1, Φ, and φ_2, which describe the orientations of three orthogonal crystal axes relative to the rolling geometry as is shown in Figure 2.2.

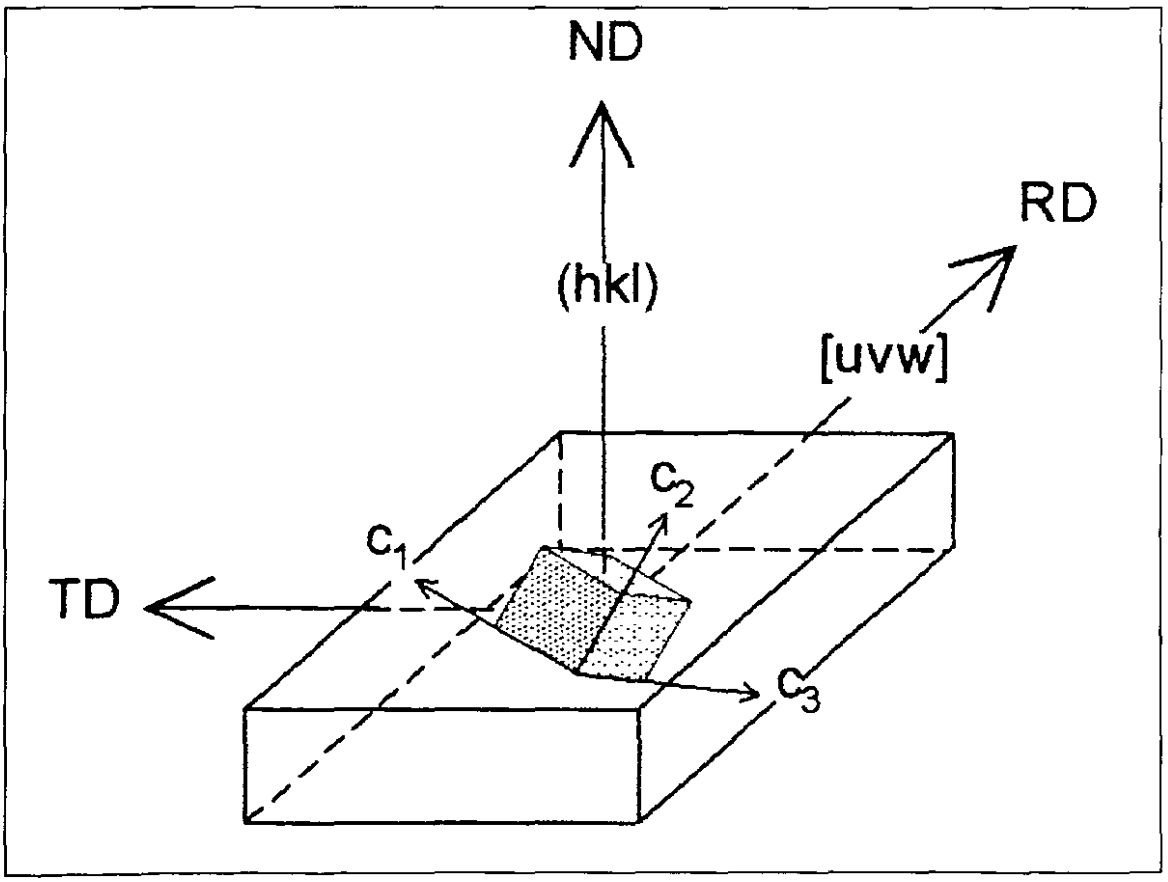

Figure 2.1 Definition of a crystallographic orientation in a rolled sheet by means of a parallel plane and direction to the rolling plane and direction (after Engler[4]).

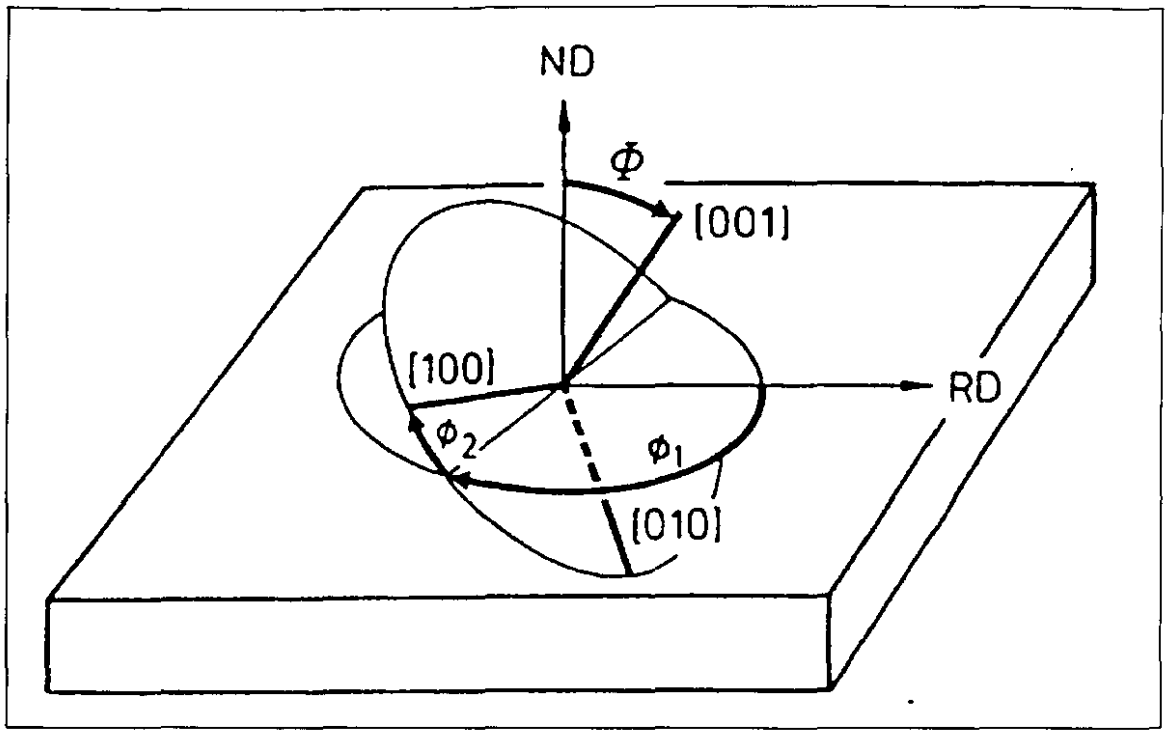

Figure 2.2 Definition of a crystallographic orientation in a rolled sheet by means of three Euler angles; φ_1, Φ and φ_2 (after Cahn[5]).

During the rolling of a pure face centred cubic (fcc) metal like aluminium that has a high SFE, a so-called pure metal or copper type rolling texture develops. This texture contains a wide spread of orientations and in its most elementary form consists of assemblies of orientations along two incomplete tubes or fibres in three-dimensional Euler angle orientation space. These fibres are known as the α- and the β-fibres (see Figure 2.3). The α-fibre, which exists mainly at very low degrees of rolling, runs from the Goss {011}<100> orientation to the {011}<211> Brass orientation. The β-fibre, the characteristic texture feature at medium to high degrees of deformation, follows a path from the {112}<111> Copper orientation (note the distinction between the copper texture and the Copper orientation) through the {123}<634> S orientation to the {011}<211> Brass orientation. The orientations along the β-fibre are of approximate equal intensity in the metal copper but the {112}<111> component is more highly developed in aluminium. On the other end of the spectrum, fcc metals with a low SFE (< 25 mJm^{-2}) develop a so-called alloy or brass (typical of 70:30 brass) type rolling texture. The alloy texture is characterised by a strong Brass {011}<211> orientation. Alloys with an intermediate SFE (25 – 80 mJm^{-2}) develop a rolling texture somewhere between the copper and brass textures.

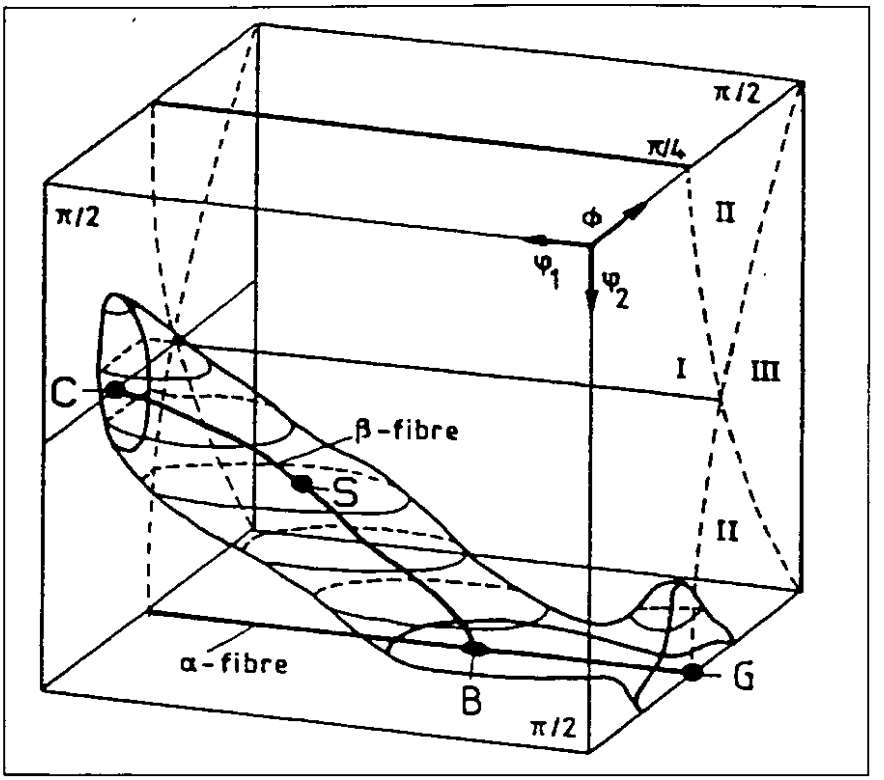

Figure 2.3 Schematic representation of the copper (pure metal) rolling texture in Euler angle space (after Lücke and Engler[6]).

2.1.1.3 Recrystallisation and the Cube Orientation

During annealing of aluminium after both hot and cold deformation recrystallisation can occur. This is known as static recrystallisation, as opposed to dynamic recrystallisation that occurs during deformation. The orientation of a recrystallised grain is often related to the orientation of the deformed region or grain in which it forms. Recrystallised grains will thus generally also exhibit a preferred orientation, or texture, relative to the original deformation geometry. The recrystallised texture of pure aluminium following rolling is dominated by the Cube, {001}<100>, orientation. In aluminium single crystal experiments, Tucker[7] was able to demonstrate the plastic anisotropy that results from an initial preferred orientation. During the deep drawing of cups from single crystals extra amounts of strain, known as ears, occurred. The position of the ears relative the rolling direction was found to correlate with the initial orientation of the crystal. In particular, earing occurring at 0° and 90° to the rolling direction was correlated to the Cube orientation. Panchanadeeswaran et al[8] have shown that a strong Cube texture in high purity polycrystalline aluminium causes similar anisotropic behaviour during cup drawing.

Due to its strong influence on mechanical properties the Cube orientation, and in particular its origin, has been the subject of intense investigation for some time now. A theory for the nucleation of grains with a Cube orientation in so-called transition bands was first proposed by Dillamore and Katoh[9] in 1974 and is referred to as the DK mechanism of Cube nucleation. These transition bands are thought to form during plane strain deformation when the cube orientation tends to split, rotating in opposite senses about the rolling direction (RD) axis towards two equivalent RD rotated cube orientations. In the centre of such transition bands there are thought to exist regions with cube or near cube orientations that act as nucleation sites during subsequent recrystallisation (see Figure 2.4). Direct evidence in support of this theory was first supplied by Ridha and Hutchinson[10] in work on rolled high purity copper. Dons and Nes[11] observed cube nucleation sites at transition bands in cold rolled and annealed aluminium, but these transition bands were centred around rotations about the transverse direction (TD) rather then the RD direction as predicted. Additional evidence of cube transition band formation[12] and cube orientated nuclei forming in transition bands[13,14] has been presented in more recent times.

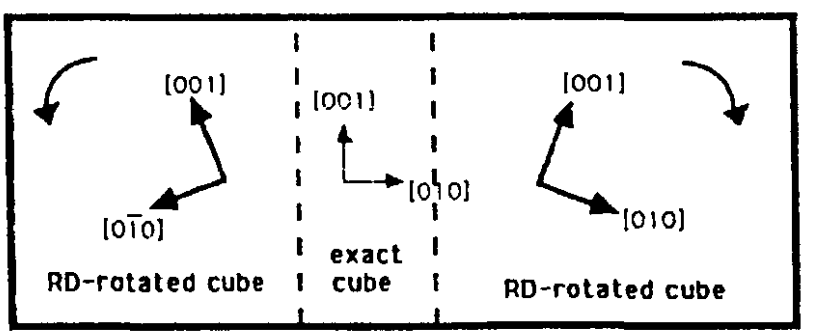

Figure 2.4 Schematic illustration of a transition band (cross-section in ND-TD plane) according to the DK mechanism of cube grain nucleation (after Doherty et al[15]).

From experiments and observations of aluminium deformed at high temperatures, an alternative theory has been proposed for cube orientated grain nucleation. Vatne et al[16] have demonstrated that cube orientated grains nucleate at bands that originate from original cube grains present before hot deformation. Their model[17] explaining this observation suggests that cube orientated grains are metastable during hot deformation and form elongated band like shapes from which cube orientated grains nucleate during subsequent annealing. The stability of the Cube orientated grains during deformation was seen to increase with deformation temperature and decrease with strain and strain rate. The stability of cube

orientated grains during hot or high temperature deformation has been demonstrated by a number of other researchers[12,18,19,20]. Maurice and Driver[12,21] have suggested that the increased stability of the cube texture during hot deformation compared to cold deformation is related to the onset of non-octahedral slip on {110} planes at higher temperatures. Hirsch[22] has expressed a similar view of multiple slip in proposing a high strain rate sensitivity model to account for observed deformation texture components (including cube) after the hot rolling of aluminium alloys.

The ideal Cube orientation is orientated at approximately 40° about the <111> axis to the major deformation texture component, the S orientation. Due mainly to this relative orientation and also because of its high rotational symmetry it therefore demonstrates strong growth characteristics following nucleation during annealing. It is a source of some debate whether it is due to this growth preference compared to other recrystallisation components – orientated growth (OG) - or due to its preferred nucleation – orientated nucleation (ON) - that the cube texture is so dominant in pure aluminium. Support for the OG mechanism contributing towards a strong cube texture is presented by Beck and Hu[23] for high purity aluminium and by Hirsch and Lücke[24] for a high purity Al-Fe alloy. Other researchers[25,26,27] contend that there is no direct support for OG and that the Cube texture is primarily due to ON because of the nucleation advantages available in both transition bands and cube bands retained during rolling. It is also thought that the dominance of the Cube texture is due to the combined effects of both ON and OG; that there is a preferred growth process out of a narrow spectrum of available nuclei. This point of view has been demonstrated by varying the starting texture before deformation, and thereby influencing nucleation sites, by Hirsch et al[28] for polycrystalline aluminium and by Akef et al[29] for single crystal aluminium. Other factors besides orientated nucleation and orientated growth have been suggested to account for the strong Cube texture. Nes and Solberg[30] have concluded that a favourable spatial distribution of nucleation sites will also contribute to the formation of a strong Cube texture.

2.1.2 Commercial Purity Aluminium

Commercial Purity aluminium as produced by the Hall process contains Fe and Si as major impurities. The solid solubility of Fe and Si in aluminium is limited; to about 0.025 wt %

at 600°C for Fe and this number decreases with temperature[31]. The excess Fe forms Al-Fe and Al-Fe-Si constituents or second phase particles during solidification and any subsequent annealing. Ito et al[32] used electron microscopical analysis to deduce the composition of these particles as Al_3Fe, Al_6Fe or α-AlFeSi for dilute Al-Fe-Si alloys. Cigdem and Bennet[33] found that the volume fraction of secondary phases increased with Fe content: from 5% for an Al-0.1Fe alloy to 16% for an Al-0.5Fe alloy. If Mn is present it tends to substitute for the Fe atoms to form phases of the type, $Al_6(Mn,Fe)$ and Al(Mn,Fe)Si as was shown by microprobe analysis on a Al-1.8Mn-0.2Fe-0.1Si alloy by Morris and Duggan[34]. The sizes of these second phase particles range from possessing a diameter of a fraction of a micron to that of tens of microns. The particles in the smaller size range (diameter less than 1 μm) are known commonly as dispersoids or precipitates while those in the larger size range are referred to as particles.

2.1.2.1 The R Recrystallisation Texture Component

For aluminium alloys containing even small amounts of Fe and Si, a second strong texture component besides the Cube component appears. This texture component is known as the R or Retained Rolling component and has the ideal orientation, {124}<211>. The R orientation is very close to the main rolling S orientation, {123}<634>. Beck and Hu[23] have suggested that, due to the closeness of the R and S orientations, the R orientated nuclei can easily form in the deformed microstructure by one or both of two mechanisms: (i) by continuous or *in situ* recrystallisation through extended recovery reactions when no large angle grain boundary movement is possible and (ii) by ordinary discontinuous recrystallisation at the grain boundaries of differently orientated deformed grains. Furthermore, a growth preference exists based on a 40°<111> orientation relationship between the R orientation and each of the symmetrically equivalent components of the S orientation. Recrystallisation experiments performed on high purity Al-Fe alloys by Ito et al[35] have confirmed that both the above mechanisms of R orientated recrystallisation are possible depending on the precipitation state of the second phase particles. At very high annealing temperatures, when all the Fe was in solid solution, the R orientation was found to form and increase in extent at the expense of the Cube orientation as the Fe content in solution increased. It was supposed that solute drag retards high angle boundary movement more so for the Cube orientated grains compared to the R orientated grains. A similar

experimental observation was made by Hutchinson and Ekström[31]. Their explanation of the increase in the R texture compared to the Cube texture was due to the higher number of R orientated nuclei compared to Cube nuclei, assuming that solute drag affected the grain boundary movement of grains of both orientations to an equal extent. For decreasing annealing temperatures, at which precipitates formed, Ito et al[35] found that again the R texture increased in strength at the expense of the Cube texture. This was explained by the effective pinning of high angle boundaries by precipitates - the Zener drag effect (see Eqn 2.1) - which weakened the Cube texture but not the R texture, as R orientated grains were still able to form by continuous recrystallisation. Evidence of continuous recrystallisation of the R texture has also been provided by Dermarkar et al[36].

Eqn 2.1

$$P_z = \frac{3F_v\gamma}{2r}$$

Where P_z is the Zener pinning pressure, F_v = volume fraction of randomly distributed spherical particles, γ = specific energy of boundary and r = radius of particles.

Humphreys[37,38] has recently proposed a unified theory (or model) of recovery, recrystallisation and grain growth applicable to cellular microstructures. The theory takes into account the orientation dependence of boundary energies and mobilities, and an extension of the theory includes the effects of a dispersion of second-phase particles. An analysis of subgrain growth based in this extended model predicts the conditions under which this may occur discontinuously and lead to complete softening of a deformed metal by subgrain growth alone in the absence of recrystallisation.

2.1.2.2 Particle Stimulated Nucleation (PSN)

The effect of larger second phase particles on the recrystallisation behaviour of aluminium alloys has been well documented. It is believed that particles with a diameter bigger than 1μm are responsible for the nucleation of new grains during annealing following deformation. This process is known as Particle Stimulated Nucleation or PSN. Humphreys[39] conducted *in situ* annealing experiments in an electron microscope on particle containing Al-Cu-Si single crystals. It was conclusively shown that PSN occurs in deformation zones adjacent to particles that form during deformation. A model was also proposed which both explains the formation of the deformation zones and the nucleation process that occurs within the deformation zones. The deformation zone is formed by

"turbulent flow" during deformation, resulting from the incompatibility between the particle and the adjoining matrix. It is therefore a region with a high dislocation density compared to the surrounding matrix, and is also highly misorientated with respect to the matrix. It is thus a good potential nucleation site. Nucleation originates at subgrains within the deformation zone followed by a rapid polygonisation process involving sub-boundary migration until the entire deformation zone is consumed. For nucleation to continue, growth into the neighbouring matrix has to occur. This often represents a barrier for further growth because of the lower dislocation density outside the zone. To overcome this barrier the nucleus is required to be larger than a critical radius, r:

Eqn 2.2
$$r > \frac{2\gamma}{P_d}$$

where γ represents the grain boundary energy and P_d the driving force due to the stored dislocation energy in the surrounding matrix. The size of the deformation zone is approximately equal to the particle size and therefore Eqn 2.2 represents the critical particle radius for successful PSN. Oscarsson et al[40] concluded that PSN was less favoured after rolling at elevated temperatures compared to cold rolling. This is presumably due to dynamic recovery that counteracts the formation of the deformation zone. Nes[41] proposed a more general model for PSN that accounted for Zener drag and suggested that the critical radius of a particle causing PSN should be:

Eqn 2.3
$$r > \frac{2\gamma}{P_d - P_z}$$

where P_z is the Zener pressure due to the drag from small dispersoid particles (as given in Eqn 2.1). Humphreys[37,38] recently proposed unified theory of recovery, recrystallisation and grain growth also explains the effect of a dispersion of second-phase particles on PSN. Vatne et al[42], from examinations of recrystallisation textures of commercial purity aluminium alloys, and Engler et al[43], from examinations of recrystallisation textures of an Al-Mg-Si alloy, observed that precipitates seem to have a higher retarding effect on PSN compared to the nucleation of Cube orientated grains. It is thought that this is due to the size advantage of Cube orientated nuclei.

The occurrence of PSN is thought to have a randomising effect on the recrystallisation texture of a deformed and annealed aluminium alloy. Studies have shown that increasing the number of potential PSN nucleation sites, that is by increasing the number of coarse particles present in the microstructure (by increasing alloy content or varying homogenising procedures following casting), leads to a weakening of the normally strong Cube dominated recrystallisation texture[42,44,45,46]. By measuring the individual orientations of grains formed by PSN, Oscarsson[47] concluded that no preferred orientation could be found for grains formed by PSN in a polycrystalline aluminium alloy. Ferry and Humphreys[48] have found that in single crystals of aluminium containing Si particles a growth preference exists for certain orientated grains formed by PSN. Engler et al[49] suggest that although PSN leads to a random texture in general, there is evidence of some preferred orientation, albeit weak. They concluded that PSN might sometimes lead to a preference for the P, {011}<122>, orientation and also cause scatter of the Cube orientation about the ND. This was attributed to a micro-growth selection process whereby nuclei with a 40°<111> orientation relationship with the surrounding matrix are favoured to grow further. Rabet et al[50] have also attributed an observed P texture to PSN while Rickert et al[51] have attributed a weak texture centred on a {001}<210> (ND rotated Cube) orientation to PSN.

2.1.3 Aluminium-Magnesium Alloys

Magnesium (Mg) is a highly effective solid solution substitutional strengthener of aluminium alloys. It is not the most effective element when measured in terms of atomic percent (at %) but is certainly very effective when measured in wt %. It also possesses the advantage over other alloying elements of being highly soluble in aluminium. The addition of 6 wt % Mg to aluminium causes an increase in measure yield strength from about 10 MPa to about 175 MPa in the annealed condition[1]. The addition of Mg also contributes towards good formability, corrosion resistance and finishing characteristics of aluminium alloys.

It is thought that the SFE of aluminium is greatly decreased by the addition of Mg. It has been suggested[2,52] that the addition of just 1 % Mg causes the SFE of an aluminium alloy to drop from about 170-200 $mJ.m^{-2}$ for pure aluminium to as low as 50 – 60 $mJ.m^{-2}$. Further addition of Mg is thought to further lower the SFE but at a reduced rate of decrease. This

lowering of the SFE is expected to have a profound influence on the dynamic recovery behaviour of aluminium alloys during deformation. This influence is especially noticed during the hot deformation of Al-Mg alloys when dynamic recovery behaviour would normally lead to flow softening in pure aluminium alloys. Several researchers[53, 54, 55] have demonstrated that the addition of Mg to aluminium causes an increase in flow stress during hot deformation and / or that it causes an increase in the amount of residual strain energy following hot deformation. It has also been shown that dynamic recovery improves for a particular Al-Mg alloy as the deformation temperature increases[55, 56, 57]. In particular, Poschmann and McQueen[57] showed that a transition in the microstructure of hot deformed Al-5Mg coincided with flow softening during deformation. This transition was characterised by a change from an initial dislocation wall structure into a subgrain structure characteristic of a recovered structure as deformation progressed.

The occurrence of dynamic recrystallisation during hot deformation of Al-Mg alloys has been well documented [52,55,58]. It is thought[52] that dynamic recrystallisation is caused by the reduction in the SFE in Al-Mg alloys which impedes dynamic recovery and consequently results in a high enough driving force for recrystallisation during hot deformation to occur. It appears that dynamic recrystallisation is restricted to Al-Mg alloys containing high amounts of Mg; about 5 wt % and above. The interaction of Mg atoms with dislocations is also thought to impede dynamic recovery. This interaction with dislocations is apparent in the dynamic strain ageing behaviour of Al-Mg alloys which results in "jerky flow", known as the Portevin-Le Chatelier effect, during tensile deformation[59].

2.2 Plane Strain Compression

2.2.1 Origin

The Plane Strain Compression (PSC) test used was first suggested by Orowan[60] in 1943 as a modified compression test which might simulate the yield conditions in rolling, and thereby obviate the correction factor by which the homogeneous yield stress must be corrected. The inhibited lateral spread that occurs in plain strain conditions (including rolling) results in a

measured yield stress equal to $1.155\sigma_0$, where σ_0 is the stress measured in homogeneous compression, according to the Von Mises criterion. The PSC test technique was first successfully implemented by Ford[61] in 1948 when it was used to determine cold rolling loads for copper and carbon steel. It is hence sometimes referred to as the Ford Plane Strain Compression Test. In 1952 Watts and Ford[62] took a more critical look at the geometry of the PSC test by investigating the effects of the ratio of platen width (b) to strip thickness (h) on platen pressure and yield stress.

2.2.2 Strain Distribution

The strain distribution in the region between the platens results from the material flow history during compression. The material flow is in turn governed by the prevailing slip-line field. A theoretical solution to the slip line field was first demonstrated by Hill et al[63] in 1951 who considered the problem of the compression of a rectangular block of material between two perfectly rough parallel platens, as in Figure 2.5 (a). The corners of each platen; A, B, C and D constitute singularities in the stress distribution and are therefore the most likely starting points in the construction of the slip-line field. Straight lines are drawn from the corners to meet the centre line at 45°. These lines form a boundary between rigid and plastic regions that form during compression. All other slip-lines are required to intersect orthogonally and to meet the platens either normally or tangentially. A slip-line field pattern similar to Figure 2.5 (b) is thus built up.

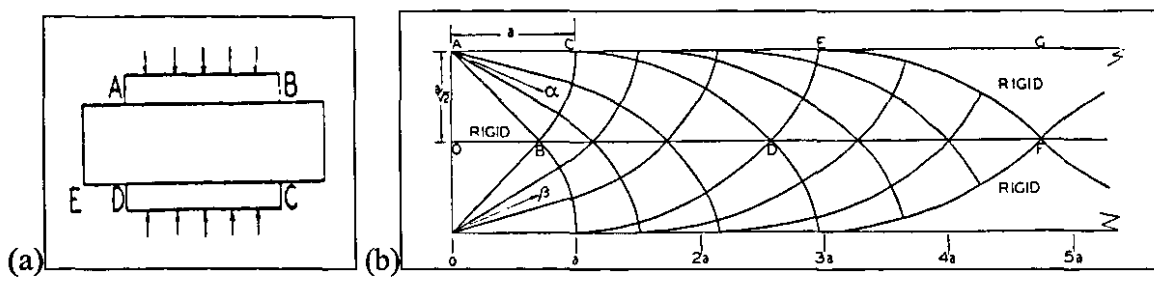

Figure 2.5 (a) Compression of a block between rough, rigid parallel platens as considered by Hill *et al* [63] and (b) Solution of slip-line field (half symmetry).

Green[64] developed solutions for the compression between parallel smooth platens at about the same time as Hill's[63] solution for rough platens. An example of one of these solutions is shown in Figure 2.6. It can be seen that the slip-lines meet the platens at an angle of 45° and that the starting slip line (originating at the corner of the platens) is not necessarily a

straight line. Green[64] also determined strain distributions experimentally by examining the distortion of ink grids stamped on plasticine blocks and the distortion of longitudinally strung out second phase particles in Al-7Mg blocks. Good agreement between these measured strain distributions and Green's model was obtained. A more rigorous development of Green's[64] solution has been presented by Collins[65]. For integral values of b/h, the slip-line field solution consists of straight lines as shown in Figure 2.7. The number of "crosses", where slip-lines intersect, corresponds to the particular b/h ratio. Thomason[66] reported that when a viscous lubricant is used it may become entrapped in the centre region of the platen / specimen interface. This implies that it is possible to obtain mixed friction conditions along the interface; that of almost zero friction at the centre and that of high friction at the edges. The slip-line field in such a case would then most likely be a mixture of the rough and the smooth solutions described.

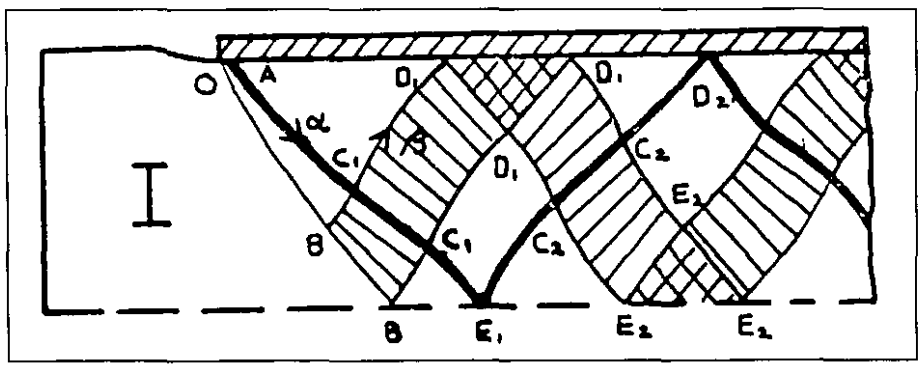

Figure 2.6 Solution of slip-line field for the case of parallel smooth platens (after Green[64]).

In 1985 Beynon and Sellars[67] developed a method (similar to that of Green[64]) of physically measuring the strain distribution of an aluminium alloy during hot PSC testing. The method involved splitting the specimens on the longitudinal axis of symmetry, scribing a grid on the longitudinal surface of one of the split pieces, clamping the split pieces together, performing a PSC test and finally analysing the strain distribution by examining the deformed grid. They found that strain distribution became more uniform as the starting ratio of b/h increased. Using the same method of determining strain distribution, Colas and Sellars[68] found that an increase in strain rate changed the range of strains in the strain distribution. This was attributed to localised heating effects related to higher strain rates. Timothy et al[69] were successfully able to reproduce the strain measured in the rolling of aluminium alloys by PSC tests. This was achieved by: (i) testing at the equivalent strains

measured at various depths in the rolled slab, (ii) maximising b/h according to the findings of Beynon and Sellars[67] and (iii) only conducting metallographic investigations close to the centre of PSC specimens where it was found that local strain was approximately equal to the nominal strain.

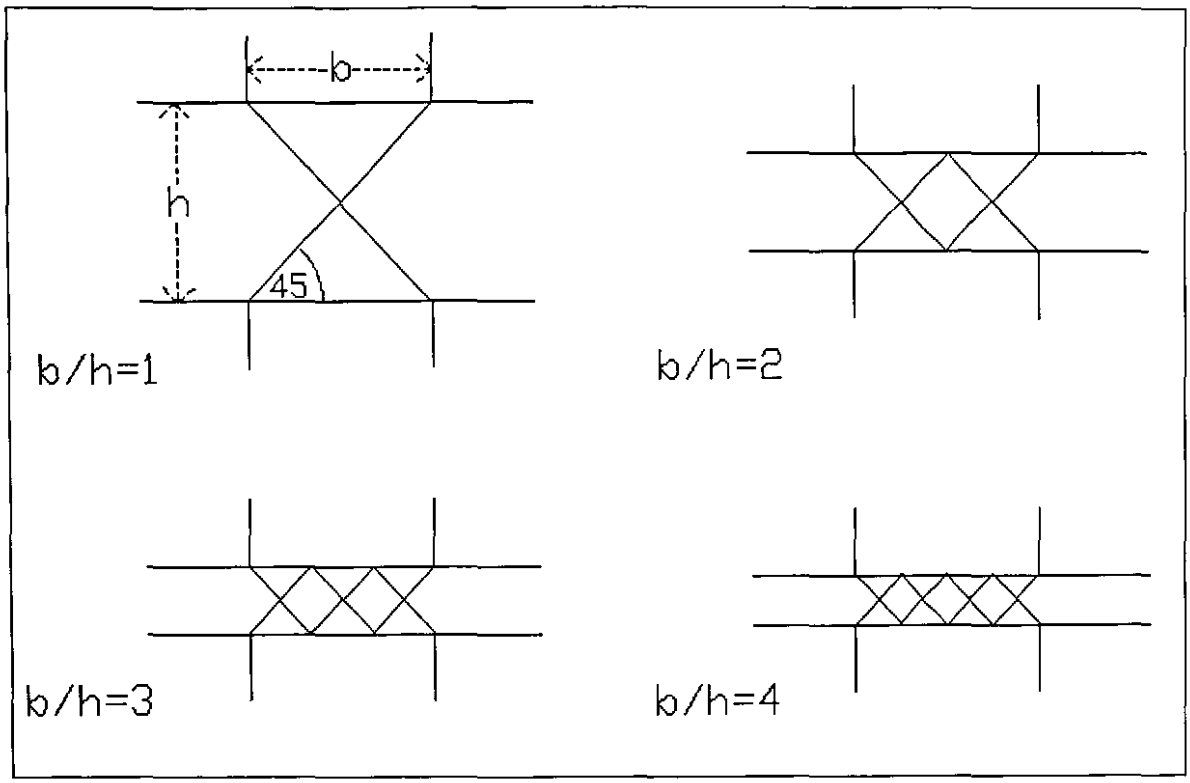

Figure 2.7 Slip-line field patterns for plane strain compression between frictionless parallel platens for integral values of b/h.

The determination of strain distribution during a PSC test can more conveniently be predicted by finite element (FE) modelling. As early as 1970, Lee and Kobayashi[70] used FE modelling to predict that strain distribution becomes less localised as the friction coefficient decreases. More recently, FE modelling has been conducted by Gelin et al[71] and Machio[72]. The FE predictions produced by Machio[72] indicate that strain distribution becomes less localised as the starting ratio b/h increases and as the value of the friction coefficient decreases (in agreement with the findings of Beynon and Sellars[67] and Lee and Kobayashi[70]). Furthermore, the predicted strain distributions as a function of b/h were in rough agreement with the slip line field solutions for integral values of b/h for smooth platens (Figure 2.7).

2.2.3 Reproducibility

It has been demonstrated recently by Shi et al[73] that careful consideration of details in PSC testing is important for reproducing results. These details include machine compliance, extrusion of lubricant, specimen / platen geometry, choice of lubricant and the condition of the platen surfaces. For instance it was found that PTFE (Teflon) tape was the best choice of lubricant as it leads to a very low coefficient of friction but it also causes the highest amount of lateral spread. Gelin et al[71] also found that PTFE caused the least friction followed by graphite and mineral oils, in that order. Furthermore, they successfully modelled the PSC test by the use of finite element (FE) analysis and were able to use their model to more accurately correct for the effects of friction and lateral spread.

2.2.4 Use

Since it was first used as a simple way of obtaining rolling loads by Ford[61] in 1948, PSC testing has been utilised increasingly in fundamental metallographic investigations. It represents a convenient method of simulating plane strain deformation that occurs in industrial processes like extrusion and rolling. The advantages of using PSC testing compared to running commercial trials are those of scale and control. PSC tests are conducted on laboratory scale specimens and precise control of deformation variables is possible. Furthermore, the fact that PSC testing closely resembles the deformation processes that occur in rolling means that a rolling geometry can be related to a PSC specimen. This means that texture studies conducted on PSC specimens can be related to rolling textures. PSC testing thus possesses a distinct advantage over other laboratory deformation processes.

The important deformation parameters in PSC testing include: strain, strain rate and deformation temperature. By varying these parameters in a controlled way researchers have been able to quantify deformation and annealing behaviour as a function of these parameters. The parameters of strain rate and temperature are generally described by a single parameter, Z, the Zener-Holloman[74] parameter. Z is also known as the temperature compensated strain rate and is expressed as:

Eqn 2.4
$$Z = \dot{\varepsilon} \exp\left(\frac{Q}{RT}\right)$$

where $\dot{\varepsilon}$ is the strain rate, Q is the activation energy, R is the gas constant and T is the deformation temperature. Castro-Fernandez et al[75] were able to obtain a relationship for the flow stress (σ) of an aluminium alloy (Al-1Mg-1Mn) in terms of the instantaneous values of strain and Z (Eqn 2.5). Furthermore they demonstrated relationships between subgrain size and flow stress (Eqn 2.6), and dislocation density and flow stress (for a constant value of Z). Wells et al[76] were similarly able to determine constitutive equations describing stress-strain behaviour for two Mg containing aluminium alloys in terms of deformation parameters. In addition they derived quantitative relationships between subgrain size, static recrystallisation kinetics, and final recrystallised grain size in terms of deformation parameters.

Eqn 2.5 $$Z = A\exp(\beta\sigma),$$ *A and β are constants*

Eqn 2.6 $$\sigma = a + bd^{-1},$$ *a and b are constants*

Much research has been conducted that concerns the effect of deformation variables on both deformation and recrystallisation textures. Bolingbroke et al[77] used a matrix of high temperature PSC tests on a commercially pure aluminium alloy to study deformation and recrystallisation textures in their investigation of the Cube texture. Vatne et al[16] conducted a similar study on an Al-1Mg-1Mn alloy in trying to determine the origin of cube nucleation. A large number of texture and grain orientation studies have also been conducted on aluminium alloys as a function of deformation parameters using the channel-die technique.[12, 21, 78]. This technique is similar to the PSC technique in terms of preventing lateral material flow during compression and it is therefore also loosely referred to as plane strain compression. It relies on the physical barriers of the channel to prevent lateral flow (see Figure 2.8) which means that the frictional forces resisting deformation are a lot higher compared to that in the normal PSC test.

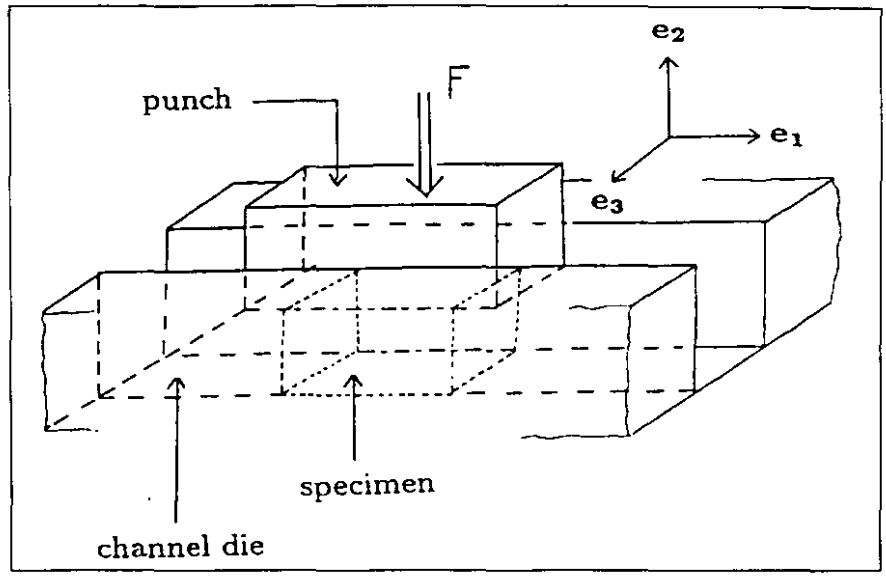

Figure 2.8 Schematic representation of Channel Die apparatus (after Harren et al[79])

The effectiveness of the PSC test in realistically simulating microstructural behaviour was demonstrated in a recent study by Furu et al[80]. The substructure evolution during different hot deformation processes including PSC, torsion, rolling and extrusion of different aluminium alloys was studied. It was found that the subgrain size after PSC testing was generally smaller compared to that measured after the other deformation techniques. This was attributed to the short delay time before quenching that is achievable after PSC testing. This would imply that the observed microstructure after PSC testing is a more accurate representation of the actual deformation microstructure that evolves during hot compression in comparison to that observed after deformation by the other techniques.

2.3 Shear Banding

2.3.1 Shear Banding in General

The term, 'shear banding', refers to a variety of localised regions or bands of shear deformation. Broadly speaking, there appear to be two categories into which the instances of shear banding may be divided: (i) shear banding during general states of stress and strain in the absence of softening caused by damage and (ii) shear banding that results from softening due to processes like micro-fracture and thermal softening caused by adiabatic heating[81]. The first of these two categories may be further subdivided, mainly according to

the scale of the shear bands involved. Bands of shear that run along the entire thickness of rolled sheets have been observed[82] and this type of shear banding is consequently referred to as sample scale shear banding. Shear Banding that is restricted to one or a few neighbouring grains has also been observed and this type is referred to as grain scale shear banding. Hatherly and Malin[83] categorised sample scale and grain scale shear banding for face centred cubic (fcc) metals in terms of the SFE of the material involved. Fcc metals with a low SFE ($\leq$ 20 mJ.m^{-2}), such as brass, demonstrate sample scale shear banding and consequently this type of shear banding is also referred to as brass type shear banding. In contrast, fcc metals with medium to high SFE ($\geq$ 40 mJ.m^{-2}), such as copper, demonstrate grain scale or copper type shear banding. As was mentioned previously, the SFE of Al-1Mg is in the region of 50-60 mJ.m^{-2} and it can thus be classified as having a medium to high SFE. This review will thus concentrate on the discussion of copper type shear banding.

2.3.2 The Formation of Copper Type Shear Bands

2.3.2.1 Observations

The formation of copper type shear bands during plane strain type compression has been well documented[6,10,79,84,85,86,87,88,89,90,91,92,93,94,95,96] in a variety of materials - such as Cu, Al-Mg alloys and Al-Cu alloys - that have a medium to high SFE. Shear bands are generally categorised as forming at medium to high strains but have been observed for strains as low as ε = 0.3 (25 % reduction)[79]. Their strength and frequency of formation, however, is strongly linked to an increase in strain. Furthermore, at low strains they are often observed to be restricted to single grains whereas at higher strains they appear to cross grain boundaries and are observed over several adjacent grains. They have been observed to occur at a variety of angles to the rolling plane, between 20° and 40°, with an average value of 35°. The tendency for shear banding to occur has not only been linked to composition but also to initial grain size, temperature of deformation and grain orientation. Ridha and Hutchinson[10] observed that the tendency for shear banding to occur increased as initial grain size increased during the cold rolling of Cu. Similar observations were made by Korbel et al[87] for Al-4.8Mg and by Engler[90] for Al-1.8Cu. Ridha and Hutchinson[10] also observed that the tendency for shear band formation decreased as the deformation temperature increased

from -100° to room temperature, while Nakayama and Morii[85] reported a similar observation for single crystal experiments on Al-3Mg as the rolling temperature was raised from room temperature to 200°C. The dependency of shear banding occurrence on grain orientation was clearly demonstrated by Morii et al[84] during single crystal experiments on Cu, Al and Al-3Mg. Shear banding was observed for single crystals of Al-3Mg with a (211)[$\bar{1}$11], Copper orientation, but not for single crystals of Al-3Mg with a (011)[$\bar{1}$00], Goss orientation. Morii et al[84] also demonstrated the influence of composition on shear band formation since no shear banding was observed for the Al single crystals.

2.3.2.2 Theories of formation

There does not appear to be a single accepted theory that fully explains the formation of copper type shear bands. There are theories based on continuum mechanics that attempt to predict the formation of shear bands and in particular the angle to the rolling plane at which they form. For these theories, plasticity is described solely by continuum shear flows that occur along the various slip systems of a crystal. Thus a mathematical description of plastic flow accounts for shear banding and discrete dislocation motion is not explicitly modelled. There are other theories and observations that attempt to describe shear banding at a more fundamental or microstructural level. Such theories are based on the observation that shear banding appears to be linked or preceded by the formation of microbands in the dislocation structure of the material concerned. These two groups of theories are examined further.

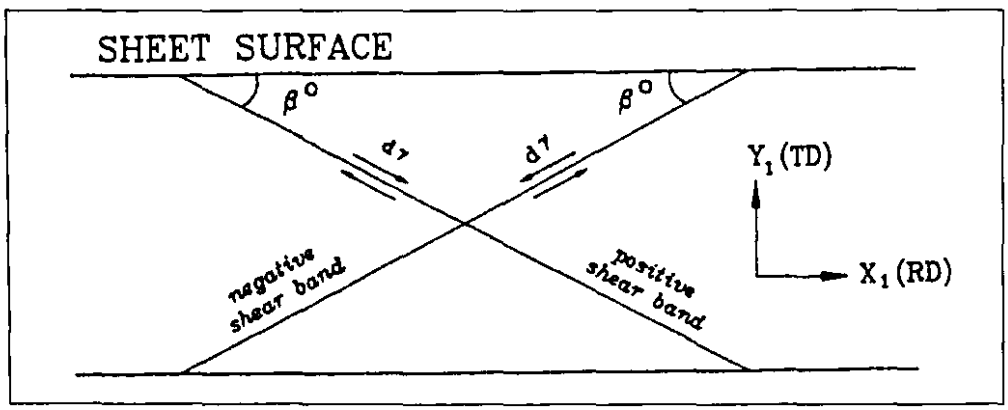

Figure 2.9 Geometry of shear bands indicating the angle to the rolling plane, β (after Lee and Chan[88])

There exist a number of continuum theories[88,97,98,99,100] that predict the angle to the rolling plane, β, at which shear bands form (see Figure 2.9). Dillamore et al[97] suggested that shear

occurs at an angle, β, such that the plastic work in deforming the material will be a minimum and not greater than that for homogeneous plane strain deformation. This criteria is defined as a minimum in the value of M′, the effective Taylor factor for the crystal concerned:

Eqn 2.7
$$M' = \frac{M}{\cos 2\alpha}$$

where α is the angular difference between β and 45° (45° is the angle of maximum resolved shear stress) and M is the Taylor factor which gives an indication of the shear strength of a crystal. Very often the variation of M′ with β does not exhibit a single minimum but rather is associated with a minimum plateau. There is thus a range of values of β that satisfy the principle of minimum work. Dillamore et al[97] thus suggested a further criterion in predicting β; that of plastic instability:

Eqn 2.8
$$\frac{1}{\sigma}\frac{d\sigma}{d\varepsilon} < 0$$

which can be written as:

Eqn 2.9
$$\frac{n}{\varepsilon} + \frac{m}{\dot{\varepsilon}} + \frac{1+n+m}{M}\frac{dM}{d\varepsilon} - \frac{m}{\rho}\frac{d\rho}{d\varepsilon} < 0$$

where n and m are the strain hardening and strain rate exponents, and ρ is the mobile dislocation density. A negative value of the term, dM/dε in Eqn 2.9, is quite possible since it corresponds to geometric softening by lattice rotation into a geometrically softer condition. The term (1/M)(dM/dε) is known as the texture softening factor and passes through minima as a function of β. These minima have been shown to correspond to measured experimental values of β. Lee and Chan[88] proposed an additional third criterion to the two proposed by Dillamore et al[97] to eliminate ambiguous predictions that are caused by the multiple minima of the texture softening factor. This criterion involves selecting from the possible solutions those values of β that give the minimum number of active slip systems.

It has been observed[84,85,86,87] that Copper type shear bands occur simultaneously with or are preceded by particular dislocation structures known as microbands (MBs). Microbands are long, thin (typically 0.1-0.3 μm) plate-like features that are confined to single grains and

appear after a certain finite amount of strain. Their walls consist of dislocation assemblies that lie parallel or very close to the {111} planes of the active slip systems of the grain involved. They are termed crystallographic due to this relationship with the active slip systems. Groupings or clusters of MBs have been observed to form a lamellae like dislocation wall structure. Similar lamellae structures have been observed in lower SFE materials like brass with the difference that the lamellae structure for the brass case consists of aligned twins[83]. In both cases (MBs or twins) it has been speculated that it is the lamellae structure that is associated with or leads to shear banding. Nakayama and Morii[85] speculate that shear bands nucleate within the lamellae MB structure. They contend that the dislocation MB wall structure causes long range internal stresses that increase with increasing strain. These long range internal stresses eventually cause co-operative movements of dislocations resulting in shear processes that cause fragmentation of the MBs into small blocks with large misorientations, i.e. shear bands. Korbel and Martin[86] speculate that groups of MBs generate large stress concentrations at their tips. On further deformation, when the MBs meet with a grain boundary, an elasto-plastic impulse is emitted and the MBs are thus able to penetrate into the neighbouring grain. When this happens the bands no longer possess a crystallographic relationship to the active slip systems and are hence known as shear bands. Wagner et al[89] have more recently suggested that MBs act as obstacles to dislocation glide on slip systems that intersect the MBs. Gliding is thus restricted to slip systems parallel to the MBs causing strong shear in the vicinity of the MBs. The angle at which shear bands form is then explained using a continuum approach based on that by Dillamore et al[97]. Support for this theory by Wagner et al[89] can be gathered from the work performed earlier by Juul Jensen and Hansen[101] who demonstrated that the plastic anisotropy they measured in tensile tests of commercial purity aluminium was caused by MBs. MBs were introduced into the microstructure of their material by prior cold rolling and differences in tensile flow stresses were attributed to the relative orientations of the MBs to the active slip systems.

Further theories of shear band formation include those of Shen[102] and Harren et al[79] that are based on geometrical softening caused by non-uniform lattice reorientation during deformation. The theory by Shen[102], for example, contends that during PSC the normal rolling orientations like those of Copper and Brass will form. Upon further deformation

these orientations rotate towards the Goss orientation, but this transformation is not homogeneous throughout the grain concerned. The active slip planes in the Goss orientation are inclined at an angle of 35° to the rolling plane and the concentration of strain in the Goss regions leads to shear bands being formed at the observed angle of 35° to the rolling plane.

2.3.2.3 Microband formation

If the occurrence of shear bands does indeed depend on the occurrence of MBs then it is logical to review the literature pertaining to the formation of MBs. Hughes[103] has recently described what is believed to be the precursor to MB formation by studying Al-5.5Mg cold rolled to low strains. A Taylor lattice with dislocations organised along {111} slip planes and long, straight dislocation boundaries (DBs) that lie parallel to the {111} slip planes has been described. MBs form by the paring of such DB's and thus create new misorientated regions that can accommodate further strain. Korbel et al[87] have suggested that MBs formed during the rolling of Al-4.8Mg are a form of dynamic recovery. A normal recovered cell structure is prevented from forming by the pinning of dislocations by the Mg atoms and hence MBs form due to the co-operative movement of pinned dislocations. Morii et al[84] have suggested that MB formation can be attributed to the asymmetry of slip for certain orientations. They contend that the amount of slip that occurs on the two co-planar (CP) slip systems of certain orientations is about twice as much as that occurring on the two co-directional (CD) slip systems in order to maintain orientation stability during deformation (see Figure 2.10). The localisation of slip on the CP planes thus causes MBs to form parallel to the CP slip systems. Winther et al[104] have produced a model for predicting MB formation based on the above suggestions by Korbel et al[87] and Morii et al[84] that achieves excellent agreement with experimental observations for single crystals and reasonable agreement for observations of polycrystalline materials.

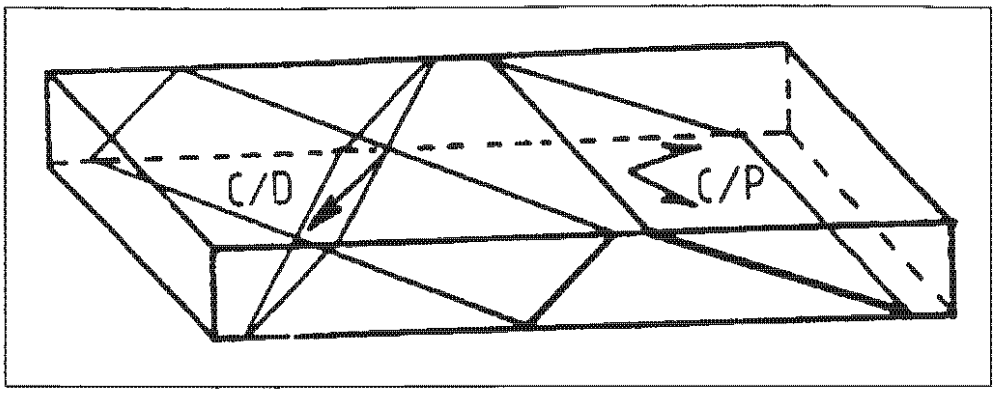

Figure 2.10 Schematic illustration of slip geometry in a {211}<111>, Copper orientated crystal. CP: co-planar slip systems, CD: co-directional slip systems (after Nakayama and Morii[85]).

It would seem that the formation of MBs, as is the case for SB formation, is dependent on deformation conditions and on grain orientation. At high temperatures of deformation MB formation appears to be inhibited. This has been shown by Nakayama and Morii[85] from observations of their single crystal experiments of Al-3Mg rolled at room temperature and 200°C. The dislocation structure of the non-shear banding case (rolling at 200°C) consisted of elongated subgrains bounded by two sets of operative slip planes in contrast to the shear banding case (rolling at room temperature) which consisted of clusters of MBs. Raghavan and Shapiro[105] found that the dislocation structure of Al-4Mg after torsion tests at 482°C consisted of equiaxed subgrains compared to a pronounced elongated cell structure after torsion tests at room temperature. Cizek et al[106] found that the microstructure of a commercial purity aluminium alloy contained no MBs or other pronounced special inhomogeneities after tensile deformation at 150°C. MB formation has also been shown to depend on the orientation of the deforming grain. Morii et al[84] found this for their single crystal rolling experiments on Al-3Mg. The dislocation structure of the orientation not exhibiting shear banding (the Goss orientation) consisted of elongated subgrains bounded by two sets of operative slip planes in contrast to that of the orientation exhibiting shear banding (the Copper orientation) which consisted of lamellae-like MB walls. Recently Godfrey et al[107,108] have demonstrated a similar orientation dependence of MB formation during the channel die compression of high purity Al single crystals. Layered dislocation walls lying close to CP slip planes (which might be classified as MBs) were observed after deformation of Copper orientated crystals while a very homogeneous cell block structure defined by dislocation walls lying on two active slip planes was observed after deformation

of Brass orientated crystals. It must be emphasised that shear bands were not observed in either case.

2.3.3 Influence of Copper Type Shear Bands on Deformation Texture

The formation of Copper type shear bands has been observed to coincide with certain features of deformation texture. Lücke and Engler[6], Engler et al[91], and Wagner et al[92] observed a stabilisation of the Goss orientation and a higher relative rate (compared to the other major deformation orientations) of increase of the Brass orientation for both Al-1.8Cu and Al-3Mg alloys as strain increased. These observations were linked to the simultaneous occurrence and increase in extent of copper type shear bands. A simple TD rotation in the Copper orientated grains, associated with shear band formation, was thought to lead to the Goss orientation which then rotates to the Brass orientation after further strain. In addition, Wagner et al[92] observed the appearance of the Q, {013}<231>, orientation after strains of 90 % and above for Al-3Mg. The Q orientation was thought to form due to a compensating shear in the regions neighbouring shear bands by the activation of the CD slip systems, which leads to 45° ND rotated Cube orientation, {001}<110>. The Q orientation is metastable and since it is only 10° away (in orientation space) from the {001}<110> orientation it is believed to form in the scattering of the {001}<110> orientation.

Wagner et al[89] were able to expand on the above observations by using the Electron Back Scattered Diffraction (EBSD) technique to measure local orientations in and around shear bands in Copper orientated single crystals of Al, Cu and Al-1.8Cu. They observed both positive and negative TD rotations of the Copper orientation inside shear bands and positive TD rotations adjacent to shear bands. They theorised that shear bands are in fact composed of microscopic shear bands, that experience a positive TD rotation towards the {001}<110> orientation, and intermediate regions between the microscopic shear bands that experience a reactive negative TD rotation towards the Goss orientation (see Figure 2.11a). The same reactive stresses that lead to the Goss orientation in the intermediate regions are also thought to lead to the {001}<110> orientation in the regions adjacent to the shear bands (Figure 2.11b). The orientation rotation is opposite in sense for this case because of the different relevant operational plane and direction (rolling plane and direction compared to shear plane and direction). Jasienski et al[94,95] have made observations supporting those of

Wagner et al[89] for Copper orientated single crystals[94] of Cu and for polycrystalline[95] Cu which exhibited copper type shear banding. They observed scattering of the Copper orientation towards the {001}<110> and {111}<112> orientations. The {001}<110> scatter was observed to occur within newly formed shear bands and the {111}<112> is thought to rotate towards the more stable Goss orientation.

It is interesting to note that a texture characterised by a major {001}<100> component and a minor {111}<112> is often referred to as the Shear texture that is found in rolling. Choi[109] et al demonstrated how the deformation texture of a rolled sheet of high purity Al, exhibiting high levels of friction between the rolls and the sheet, varied from a typical Copper texture measured at the centre of the sheet to this Shear texture measured near the surface of the sheet.

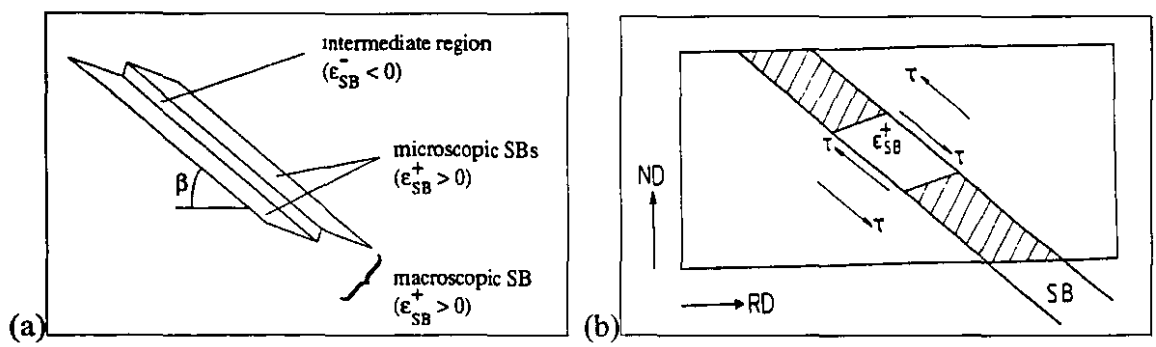

Figure 2.11 Schematic representations of positive and negative TD rotations in and around shear bands: (a) indicates a macroscopic SB composed of microscopic SBs (exhibiting positive rotations) and intermediate regions (exhibiting negative rotations) (b) indicates the reactions stresses in the vicinity of macroscopic SBs that lead to positive rotations (after Wagner et al[89]).

2.3.4 Influence of Copper Type Shear Bands on Recrystallisation

Shear bands are regions with high misorientations with respect to the matrix and are also regions with high dislocation densities and therefore it would seem that they should be favoured sites for heterogeneous nucleation. The orientation of grains nucleating in or near shear bands should be related to the local orientations at shear bands that form during deformation. Furthermore, if grains nucleated at shear bands possess a sufficient growth capacity it can be expected that they will have an effect on the total recrystallisation texture.

The first serious attempt to observe the influence of shear bands on recrystallisation texture was that by Ridha and Hutchinson[10] in 1982. SEM and optical microscopy revealed grain nucleation within shear bands in a Cu alloy after annealing for a short period of time. The corresponding complete recrystallisation texture formed after a longer annealing time was a weak, almost random texture. This was in contrast to a sharp cube recrystallisation texture corresponding to a non-shear banding condition of a similar alloy of Cu. Local orientations of grains nucleated at shear bands, determined from TEM analysis of Kikuchi patterns, revealed no preferred orientation. These grains were, however, twinned which complicated the analysis. It was reasoned that shear bands lead to a randomisation of the recrystallisation texture by the nucleation of random orientated nuclei and, in addition, by the destruction of the sites of Cube orientated nuclei by cutting through the Cube transition bands. Recently Jasienski et al[110] used the techniques of EBSD (SEM) and selected area diffraction, SAD, (TEM) to measure the local orientations of grains nucleating at shear bands in Copper orientated single crystals of Cu. Peaks in the texture measured in this way were found at the following orientations: {554}<441>, {031}<413>, Goss and {114}<221> with a TD spread towards a weak {001}<111>.

Koken and Embury[96] studied the kinetics of recrystallisation at shear bands for an Al-4.8Mg alloy. They observed that grain nucleation occurs more rapidly at shear bands compared to alternative nucleation sites like grain boundaries. They also found that the growth of grains nucleated at shear bands was slower in comparison to those nucleated at grain boundaries and at higher annealing temperatures the recrystallisation microstructure was dominated by those grains nucleated at grain boundaries.

The largest body of literature pertaining to the influence of copper type shear bands on recrystallisation appears to have been produced by Lücke, Engler, Wagner, Heckelmann, Hirsch and colleagues[6,90,92,93,111,112] concerning their work stretching over the last 8-10 years on Al-1.8Cu, Al-3Mg, and Al-4.5Mg-0.7Mn. Collectively they have shown that a recrystallisation texture characterised by strong peaks around the Goss, Q and perhaps also the P - {011}<122> - orientation, accompanied by a reduction in the strength of the Cube orientation is associated with the formation of shear bands during deformation. The Goss and Q orientations are thought to result from positive and negative TD rotations in Copper

and S orientated grains associated with the formation of shear bands as was discussed in the previous section (2.3.3). The Goss and Q orientations are metastable, in that they possess a low rate of further rotation, and are thus always present for possible nucleation during annealing. The P orientation is thought to originate from the divergent rotation of the Q orientation towards the P orientation after further strain. Nucleation of P orientated grains is thus thought to be from transition bands, similar to the Dillamore Katoh[9] mechanism for Cube nucleation. The P, and to a lesser extent, the Goss and Q orientations possess good growth relationships of about 40° around the <111> axis to the S and Copper rolling orientations.

Lücke and Engler[6], Engler[90], Wagner et al[92], and Engler et al[112] all demonstrated evidence of grain nucleation at shear bands in polycrystalline alloys. In addition, Lücke and Engler[6] measured the texture of grains nucleated at shear bands in single crystals of Al-1.8Cu by means of local orientation measurements. The texture they measured showed peaks around the Q orientation and an orientation in between the Goss and Brass orientations. Engler[90] made local orientation measurements of newly formed grains in a partially recrystallised state of polycrystalline Al-1.8Cu. A distinction was made between grains nucleating at shear bands and grains nucleating at band-like structures parallel to the RD, presumed to be Cube bands. Two different textures were calculated corresponding to measurements of these two groups of nucleated grains. The texture corresponding to the presumed Cube bands demonstrated a Cube texture with only minor scatter. The texture corresponding to the shear bands was less well defined with notably less occupation of the exact Cube orientation. No peaks at the Goss and Q orientations were observed although a minor peak near the P orientation was observed. It was emphasised that the number of orientations measured was too low for any quantitative assessment to be made. There exists an experimental difficulty in obtaining a suitable partially recrystallised state for the polycrystalline alloys concerned due to the very fast kinetics involved in recrystallisation.

The effect of annealing temperature on shear band influenced recrystallisation texture has also been investigated to some extent. Wagner et al[92] found that by increasing the annealing temperature from 310°C to 450°C for Al-3Mg, an increase in the random and Q components of the recrystallisation texture was observed at the expense of the Cube and R components.

Heckelmann et al[111] made a similar observation for the recrystallised texture of cold rolled Al-3Mg in that a distinct weakening of the Cube component was noticed as the annealing temperature was increased from 300°C to 450°C. These effects of annealing temperature are thought[92] to be due to the decreased growth preference of the Cube and R orientated grains at higher temperatures. This observation would seem not to coincide with that made by Koken and Embury[96].

3. Experimental Methods

3.1 Material

3.1.1 Chemical Composition

The alloy investigated was an aluminium alloy containing a nominal amount of 1 wt % Mg: Al-1Mg. The chemical composition of the alloy is indicated in Table 3.1. In addition to the Mg there are also significant amounts of Fe and Si present in the alloy, 0.34 wt % Fe and 0.13 wt % Si. These two elements are known to promote the formation of second phase particles.

Mg	Fe	Si	Zn	Ti	Mn	Cu	Cr	Al
0.90	0.34	0.13	0.011	0.011	0.003	0.002	0.001	balance

Table 3.1 Chemical composition (weight %) of Al-1Mg

3.1.2 History

The material was supplied by Alcan International, Banbury, England in the form of a slice from a cast slab. The microstructure of the received material is indicated in Figure 3.1 and is typical of a cast structure with a coarse grain structure (Figure 3.1a) and accumulations of second phase particles along dendrites and grain boundaries (Figure 3.1b). Blocks of size 250 mm x 160 mm x 45 mm were sectioned and machined from the centre of the slice of the cast slab for hot rolling. The hot rolling was performed by MINTEK, Randburg, South Africa according to a rolling schedule proposed by the author, which is indicated in Table 3.2. A total reduction of 70 % was achieved and the exit temperature of the last reduction pass was below 300 °C. This ensured that the coarse distribution of second phase particles was broken up and also ensured that a finer grain size was achievable after subsequent annealing.

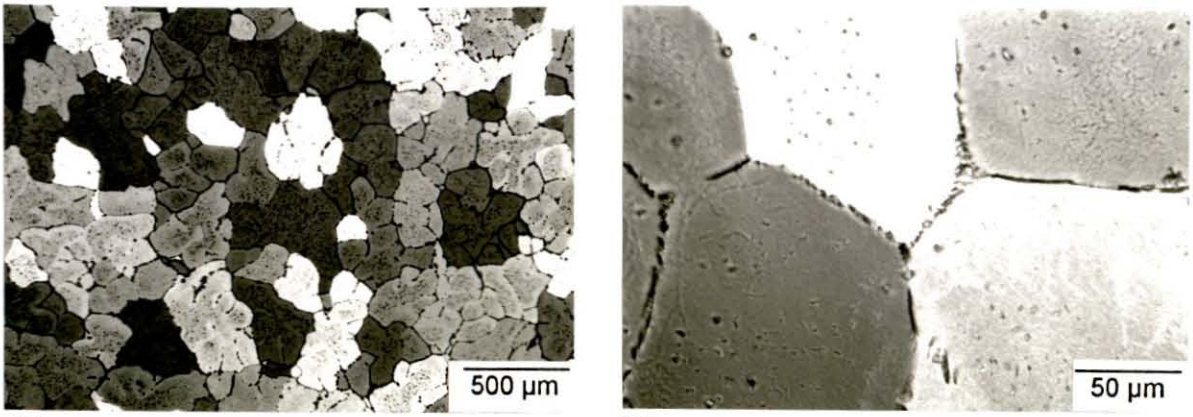

(a) (b)

Figure 3.1. Microstructure of cast material, showing (a) a coarse grain structure and (b) second phase particle accumulations.

Pass	Entry Temp (°C)	Exit Temp (°C)	Entry Gauge (mm)	Exit Gauge (mm)
1	500	275	45	30
2	465 - 480	420 - 450	30	20
3	430 - 450	225 - 300	20	14

Table 3.2. Hot rolling schedule performed on cast material.

Following the hot rolling the material was annealed for 2 hours in an air furnace at a temperature of 400°C with the intention of producing a finer equiaxed recrystallised starting grain structure. The microstructure of the material before and after annealing is shown in Figure 3.2a and Figure 3.2b respectively. Figure 3.2b reveals a partially recrystallised microstructure (less than 50 % recrystallised) as opposed to the more ideal fully recrystallised microstructure that was sought. This partially recrystallised microstructure still however represented a constant starting state for all the subsequent testing performed and at least substantially lowered the dislocation density of the material in comparison to its state following the hot rolling. The constant starting state of the material must be stressed here, and it is also worth mentioning that the highest deformation temperature employed during subsequent PSC testing was 400°C, which is equal to the annealing temperature employed. Furthermore, the time-scale of heating and holding during testing was substantially shorter (order of a few minutes) compared to that during annealing (order of hours). Due to the bimodal distribution of grain size resulting from the mixture of smaller

recrystallised grains and larger as deformed grains, it is not really meaningful to state an average starting grain size. The recrystallised grains are equiaxed and about 50 μm in diameter, while the as deformed grains are highly elongated with typical dimensions of about 500 μm in the RD and about 100 μm in the ND.

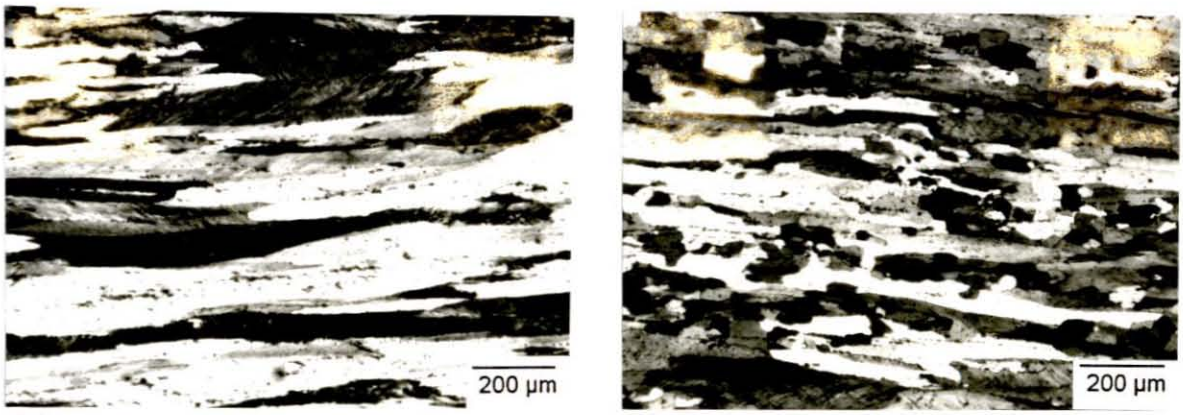

(a) (b)

Figure 3.2. Microstructure of material after (a) hot rolling and (b) subsequent annealing.

3.1.3 Particle Size Distribution

The particles size distribution of large (diameter > 1 μm) second phase particles in the starting material (after hot rolling and annealing) was measured. The diameters of over 500 large particles were measured and a histogram showing the distribution of these particle sizes is shown in Figure 3.3. From Figure 3.3 it can be seen that the size distribution of large particles in the starting material was log-normal. The mean and the standard deviation of the measured diameters were calculated to be 2.7 μm and 1.5 μm respectively.

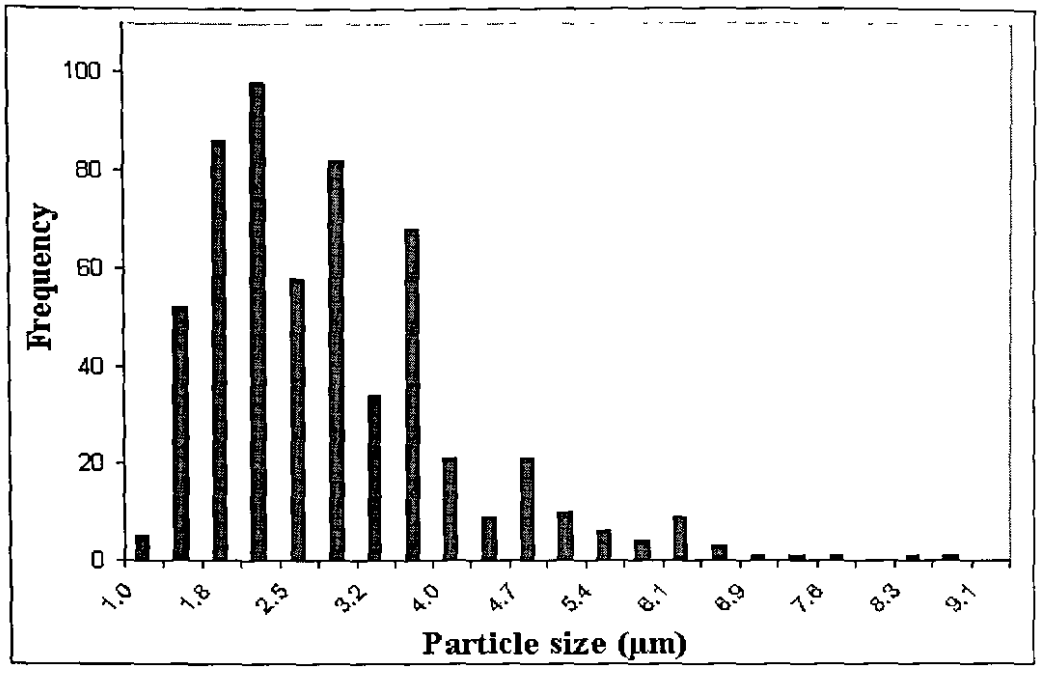

Figure 3.3 Particle size distribution of starting material following hot rolling and annealing.

3.1.4 Specimen Orientation

Rectangular specimens for PSC were machined from the centre thickness of the hot rolled plate (centre 10 mm of 14 mm gauge). Their orientation with respect to the plate geometry was such that the simulated rolling direction resulting from plane strain compression coincided with the original hot rolling direction of the plate as is shown in Figure 3.4.

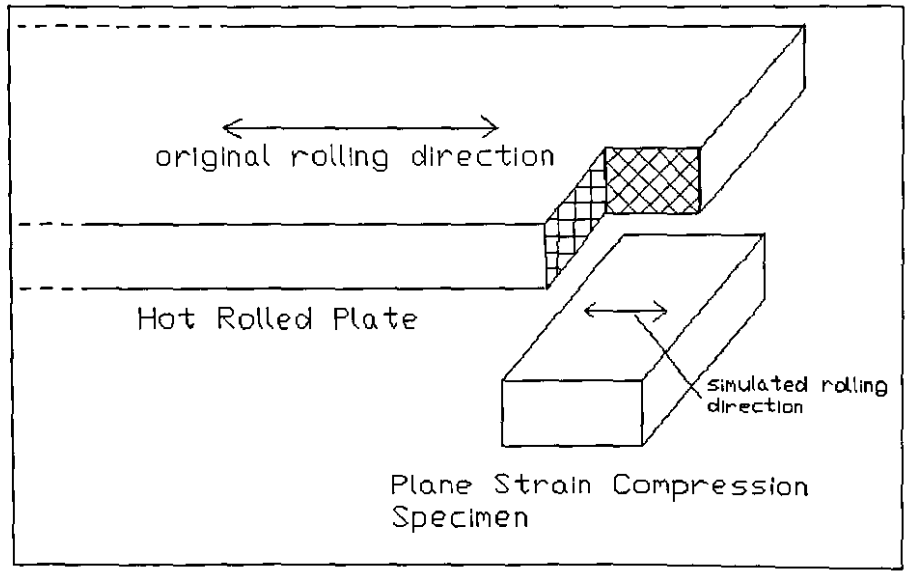

Figure 3.4 PSC specimen orientation with respect to the hot rolled plate geometry.

3.2 Plane Strain Compression

3.2.1 Configuration

A typical configuration for a PSC test in shown in Figure 3.5. A specimen of width, w, and thickness, h, is compressed between two platens of breadth, b. As the thickness of the specimen decreases, material flows in the length direction of the specimen but not in the width direction. Material flow is thus biaxial or plane strain. Material flow in the width direction is constrained by the unstressed material on either side of the platens. For this constraint to be completely effective (i.e. for negligible lateral spread), the ratio of specimen width to platen breadth (w/b) must be 5 to 1 or greater. The ratio of platen breadth to specimen thickness (b/h) has important consequences for the uniformity of strain distribution in the specimen in the region between the platens.

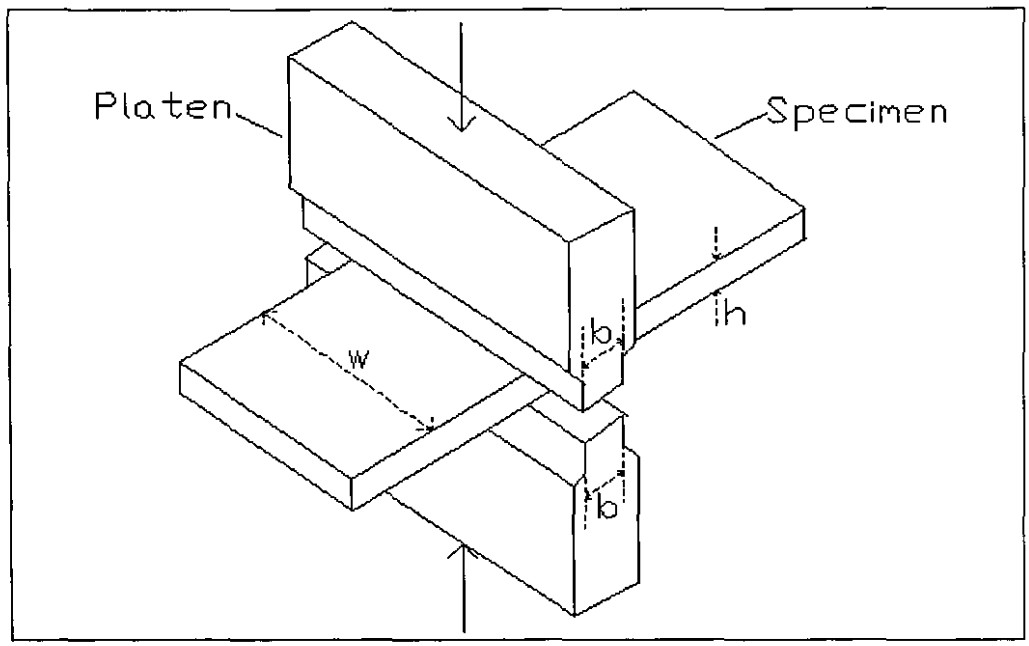

Figure 3.5 Typical configuration for a PSC test.

For a rigid-plastic material, deformation under plane strain conditions is pure shear strain and can only be produced by a pure shear stress (k). Applying Von Mises criterion results in:

Eqn 3.1

$$\sigma = 2k = \frac{2}{\sqrt{3}}\sigma_0 = 1.155\sigma_0$$

where σ is the stress measured in plane strain compression and σ_0 is the stress measured in homogeneous compression (no constraints).

3.2.2 Rig Design

3.2.2.1 Criteria

The purpose of design was to build apparatus capable of achieving plane strain compression of metals at deformation conditions comparable to those encountered in industrial processes like rolling. In particular the design of the apparatus was required to:

- ensure that large reductions (at least 90 %) of specimens was possible
- ensure that compression was indeed plane strain or as close as possible to plane strain
- ensure that strain distribution within a specimen was as homogeneous as possible
- enable controlled and uniform heating of the specimens
- allow for rapid quenching of specimens following hot deformation
- measure load, displacement and temperature variables
- make provision for the adequate control of the compression process to:
  - precisely set strain amounts
  - precisely set strain rates
  - precisely set temperatures

In addition to the above criteria, the design also allowed for multiple successive compression stages at the same or different temperatures.

3.2.2.2 Compression

In satisfying the criteria of plane strain compression and homogeneous deformation, the relative sizes of w, b and h (confer Figure 3.5) are of critical importance. The platen / specimen geometry was thus optimised and this is dealt with in detail in section **3.2.3**. More generally, compression of a rectangular metallic specimen was achieved between 2 steel platens attached to an electro-servo hydraulic (ESH) universal testing machine. Figure 3.6 represents a schematic diagram of the PSC rig while photographs of the rig are shown in Figure 3.7. The bottom platen was fixed to the base of the ESH testing machine by means of a secure base plate, while the top platen was attached to the movable piston of the ESH machine. The movement of the entire assembly of the top platen and the piston was

controlled by four guiding bars attached to the bottom base plate (as are visible in Figure 3.7a) in order to limit lateral movement. The prevention of lateral movement could not entirely be achieved and the minor amount of lateral movement that did occur was observed to influence material flow during testing. This subject is dealt with in considerable detail in Chapter 4. The ESH machine was chosen because of its availability, its load capabilities (maximum force of 250 kN) and the fact that it has a relatively high maximum cross-head speed of about 100 mm.s^{-1}. The high cross-head speed meant that a relatively high strain rate was achievable; a strain rate of 10 s^{-1} was possible for a specimen with an initial thickness of 10 mm.

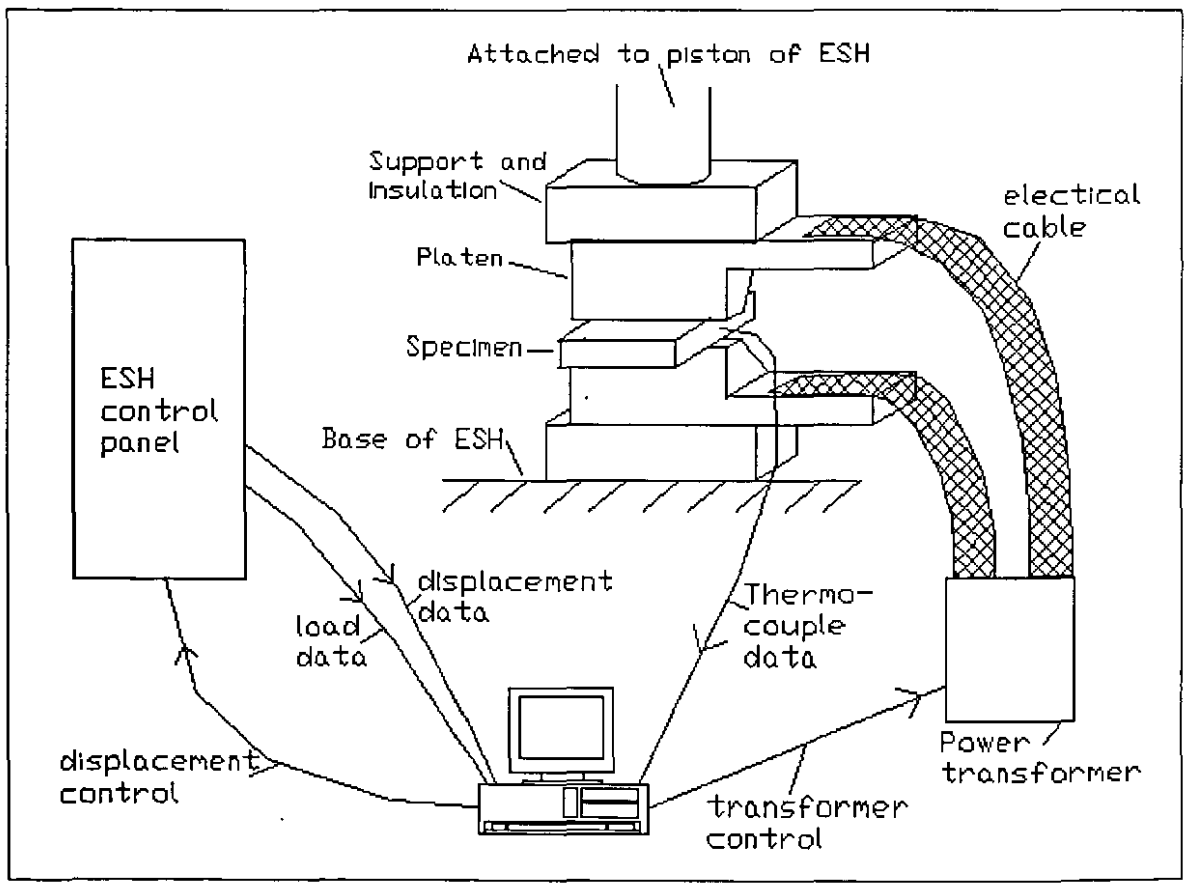

Figure 3.6. Schematic representation of PSC rig.

(a)

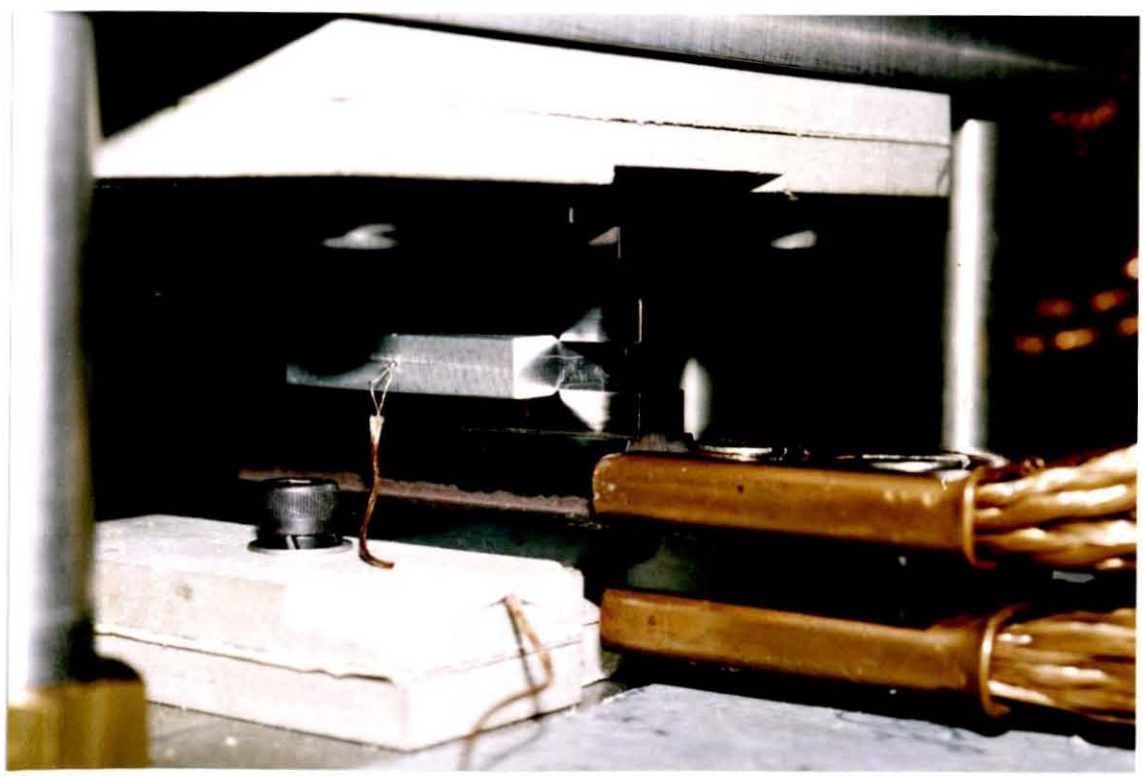

(b)

Figure 3.7 Photographs of PSC rig: (a) general view showing attachment to ESH testing machine, (b) close-up view of specimen being compressed between platens.

3.2.2.3 Heating

For high temperature compression specimens had to be heated. The heating method chosen was that of direct electrical resistance heating. This method has the advantage of heating a correctly positioned specimen to a required temperature accurately and fairly rapidly. It has the added advantage of good specimen accessibility following a test to allow for rapid quenching of the specimen. The same method is used by the commercial Gleeble system[113] used for high temperature compression. A high amperage current was passed through a specimen in contact with the two platens, which then heated up due to its resistance to the current. Figure 3.6 shows how current was fed from a custom built power transformer to the platens in contact with the specimen via thick ribbon cable so as to minimise electrical losses and facilitate the cooling of the cables. Since the resistivity of the steel platens was considerably higher than that of the aluminium specimen, the platens were designed to taper down towards the contact area with the specimen so that the resistance provided by the specimen was mainly due to a constriction of current flow. The temperature of the specimen was measured by a thermocouple inserted into a narrow hole drilled into the side (centre thickness and centre length) of the specimen.

The temperature uniformity of the heated specimens prior to compression was assessed both experimentally and by finite element (FE) modelling[114]. The temperature distribution within the specimens (Figure 3.8) produced from the FE modelling revealed that a temperature gradient existed along the width (the w dimension shown in Figure 3.5) of the specimen. This temperature gradient was confirmed experimentally. A higher temperature was observed at the end of the specimen opposite to the end at which both electrical cables were attached to the platens. This was thought to be due to the nature of the current flow through the specimen produced from such a configuration (the configuration shown in Figure 3.6). An alternative configuration (that shown in Figure 3.9 and also visible in Figure 3.7), resulting from the positioning of the platens such that the electrical cables were attached to each of the platens at opposite ends in relation to the specimen, was experimentally found to produce a more uniform and acceptable distribution of temperature within the specimen.

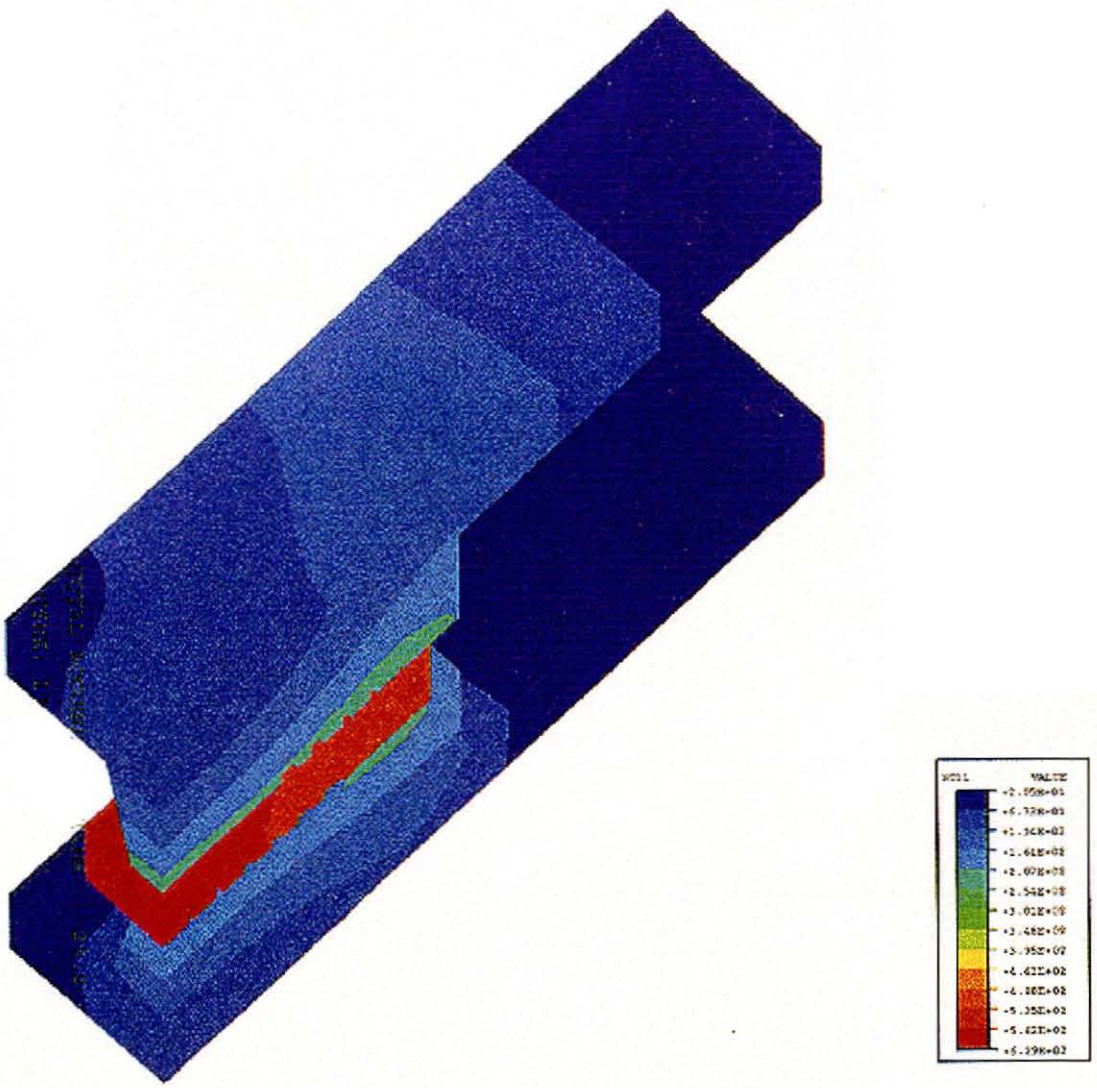

Figure 3.8 Contour plot produced from finite element modelling showing temperature distribution within a PSC specimen and platens. Half symmetry is shown.

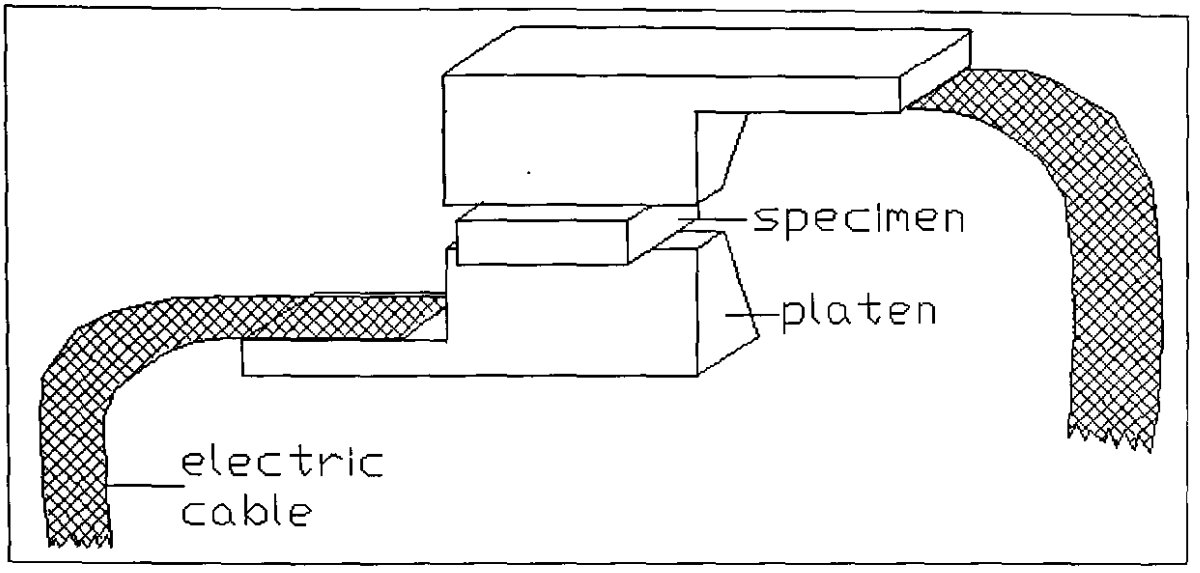

Figure 3.9 The exact configuration of platen positioning employed during PSC that resulted in very good temperature uniformity within the specimens prior to compression.

3.2.2.4 Control

Due to the design criteria set for the control of strain, strain rate and temperature, it was decided to subject the heating and compression processes to automation via computer control. Figure 3.6 illustrates the interface between the 386 PC used (via a PC30 analogue-to-digital-converter/digital-to-analogue-converter, ADC/DAC, card) and the ESH control panel, thermocouple and transformer. Load and displacement data were sampled from the ESH control panel while temperature data was sampled from the thermocouple. Control of the displacement of the moving platen (and hence also of the compression of the specimen) was achieved by a voltage output to the ESH control panel, while control of the temperature of the specimen was achieved by a voltage output to the power transformer. Displacement control was such that a constant strain rate was possible by exponentially lowering the speed of the cross-head during compression to compensate for the reduction in gauge length (or thickness) of the specimen. Custom software was written (in C++) for the control of the heating, deformation and data sampling processes. A source code listing is included in Appendix A. The sequence of events and the control of an entire PSC test are summarised in the form of a flow diagram in
Figure 3.10.

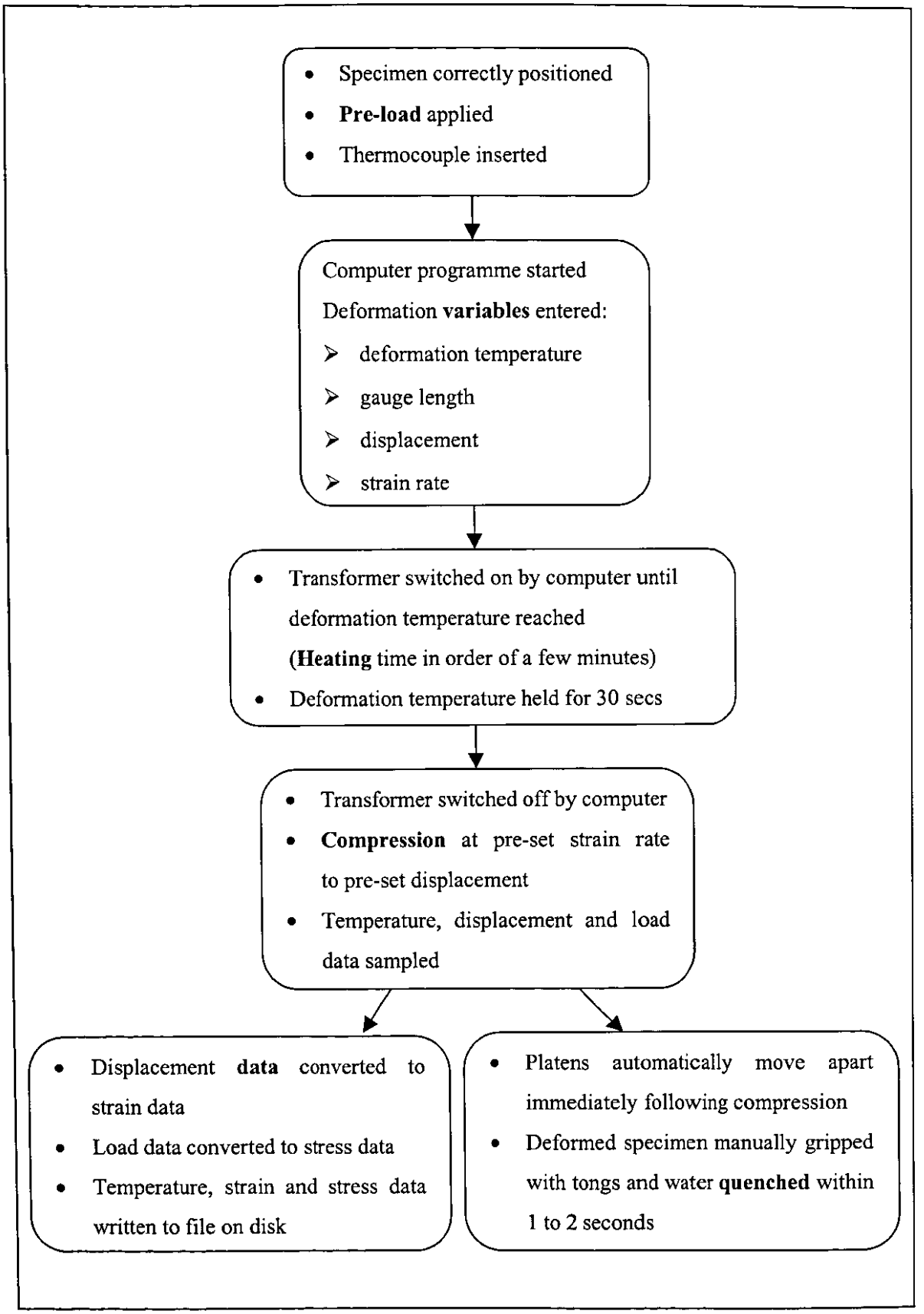

Figure 3.10 Flow diagram showing sequence of events and control during a PSC test.

3.2.2.5 Data

For each compression test, load, displacement and temperature data were collected, processed and stored (written to a computer file on disk). Temperature data was collected in voltage form before being converted to degrees Celsius. Load and displacement data were also collected in voltage form before being converted into kN and mm respectively. Load data was converted into true stress data according to Eqn 3.2, which was then written to file.

Eqn 3.2
$$\sigma = \frac{1}{1.155} \cdot \frac{load}{area}$$

Displacement data had to be first corrected for rig compliance, as the displacement measured was that of the cross-head and therefore included both the displacement of the specimen and the elastic displacement of the rig. The rig stiffness was thus measured (see Figure 3.11) as a function of load and used to calibrate the displacement of the specimen. The corrected displacement data was then converted into true strain data according to Eqn 3.3 and then written to file.

Eqn 3.3
$$\varepsilon = 1.155 \cdot \ln\left(\frac{h_0}{h}\right), \qquad h_0 = \textit{initial thickness},\ h = \textit{current thickness}$$

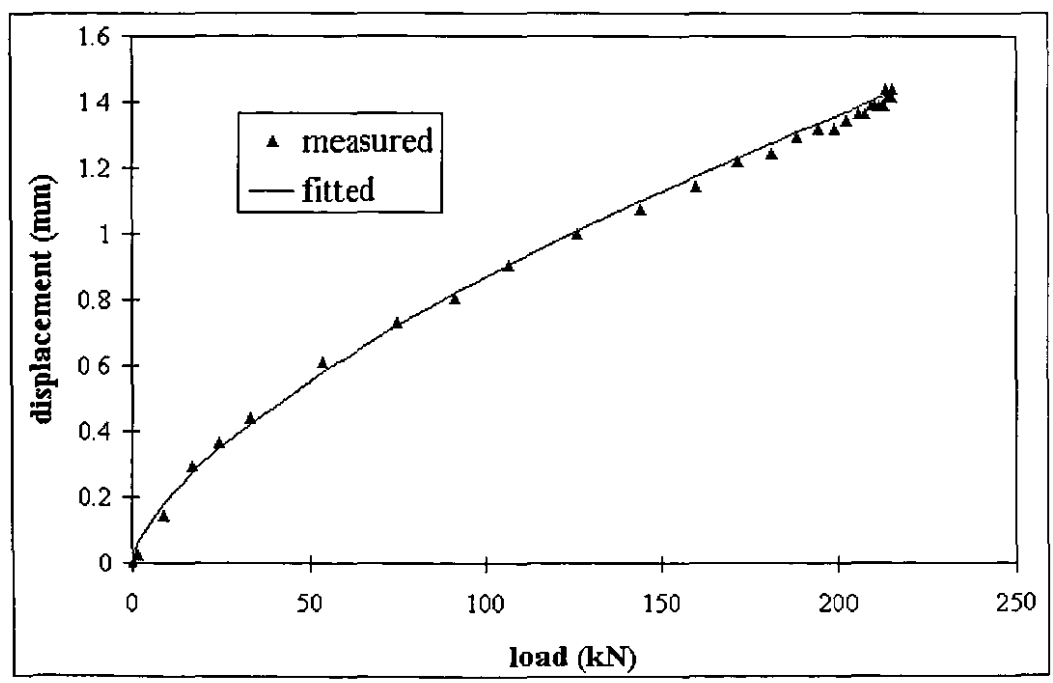

Figure 3.11 Calibration curve for PSC rig stiffness

3.2.3 Optimisation of Platen / Specimen Geometry

3.2.3.1 Dimension Limitation

The absolute values of specimen width, w, specimen thickness, h, and platen breadth, b, were ultimately limited by the maximum load (250 kN) available for compression. The limited load available meant a maximum contact area (the product of w and b) allowable for the stress required for compression. However, the uniformity of strain distribution in the region of interest between the two platens depends on the size of b (actually the ratio, b/h). As is shown in the next section (**3.2.3.2**), the larger the value of b, the more uniform is the distribution of strain. The ratio, w/b, is in turn critical in determining plane strain conditions. This means that there should be a limit on the value of b allowable. The approach followed involved first determining the lowest acceptable value for the ratio w/b (and hence the highest relative value of b) in producing plane strain or almost plane strain conditions, and then calculating the highest possible value for b without exceeding the allowable maximum contact area.

3.2.3.2 Strain Distribution with Thickness

Strain distribution in PSC specimens is shown in Figure 3.12 for different values of b/h. The strain distribution patterns appear to be fairly consistent with that predicted from the slip-line field solutions for integral values of b/h for a frictionless platen case (Figure 2.7). Figure 3.12a, which corresponds to a starting value of b/h = 0.9 and a final value of b/h = 1.5, shows a strain distribution that is highly concentrated in the centre. This agrees very well with the slip line field corresponding to b/h = 1 (Figure 2.7) which consists of 2 intersecting slip lines forming 1 'cross'. Figure 3.12b corresponds to a starting value of b/h = 1.3 and a final value of b/h = 2.2. It shows a strain distribution with a central bulge flanked by two constrictions. This strain distribution agrees very well with that predicted from the slip-line field for b/h = 2 (Figure 2.7) consisting of 2 'crosses'. So it is confirmed that the larger the starting value of b/h (or the larger b is for a fixed h), the more uniform the initial and hence the final strain distribution will be.

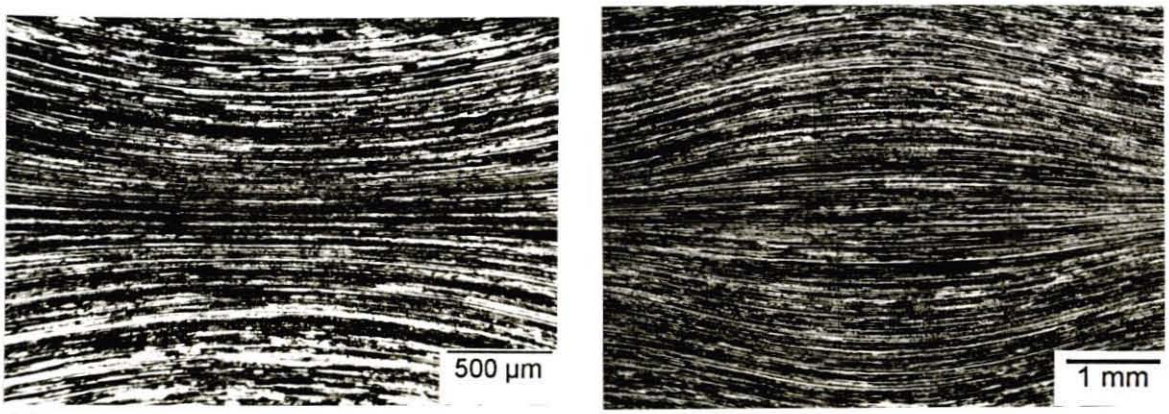

(a) (b)

Figure 3.12 Strain distribution in PSC specimens for different starting b/h ratios: (a) starting b/h = 0.9 and final b/h = 1.5, (b) starting b/h = 1.3 and final b/h = 2.2.

3.2.3.3 Lateral Spread

A set of compression tests for various values of the contact area ratio, w/b, were performed in order to determine the lowest acceptable value for w/b. Tests were performed for a specimen thickness, h, of 10 mm, a platen breadth, b, of 10 mm and specimen widths, w, of 25 mm, 30 mm, 35 mm, 40 mm and 45 mm. The specimens were all compressed to a strain of 90 % (ε = 2.66) and their lateral spreads after compression were measured as a percentage of their original widths. The results of these tests are shown in Figure 3.13, where percentage lateral spread is plotted as a function of w/b. Since lateral spread increases as strain increases, Figure 3.13 therefore also shows percentage lateral spread per unit value of strain as a function of w/b. It can be seen from Figure 3.13 that lateral spread decreases exponentially to a limiting value of about 5 % per unit strain as w/b increases. A value of 7 % per unit strain is reached for a w/b ratio of 4.0 and it was thus deduced that this value of w/b was the smallest allowable value that did not significantly compromise a plane strain mode of deformation.

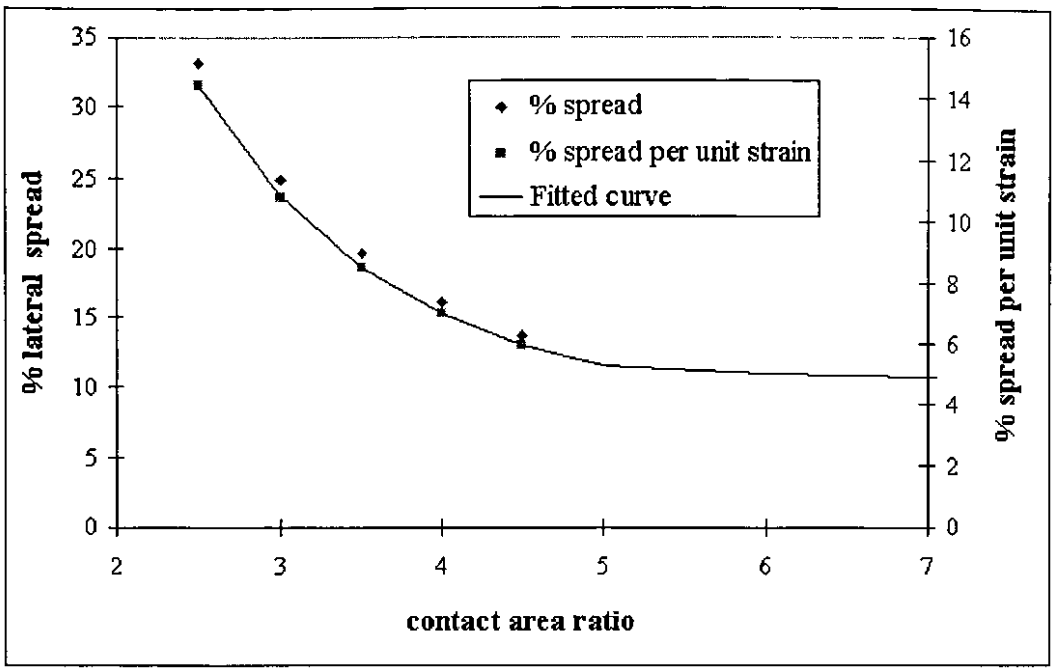

Figure 3.13 Lateral spread of PSC specimens as a function of contact area ratio, w/b.

A consequence of lateral spread is the fact that contact area increases and therefore a higher load is required to produce the same stress on a specimen. This was an additional reason for ensuring that the ratio of w/b used was not too low. Figure 3.14 shows how the measured final stress after compression (calculated assuming a constant contact area) increases along a similar trend compared to lateral spread as w/b decreases.

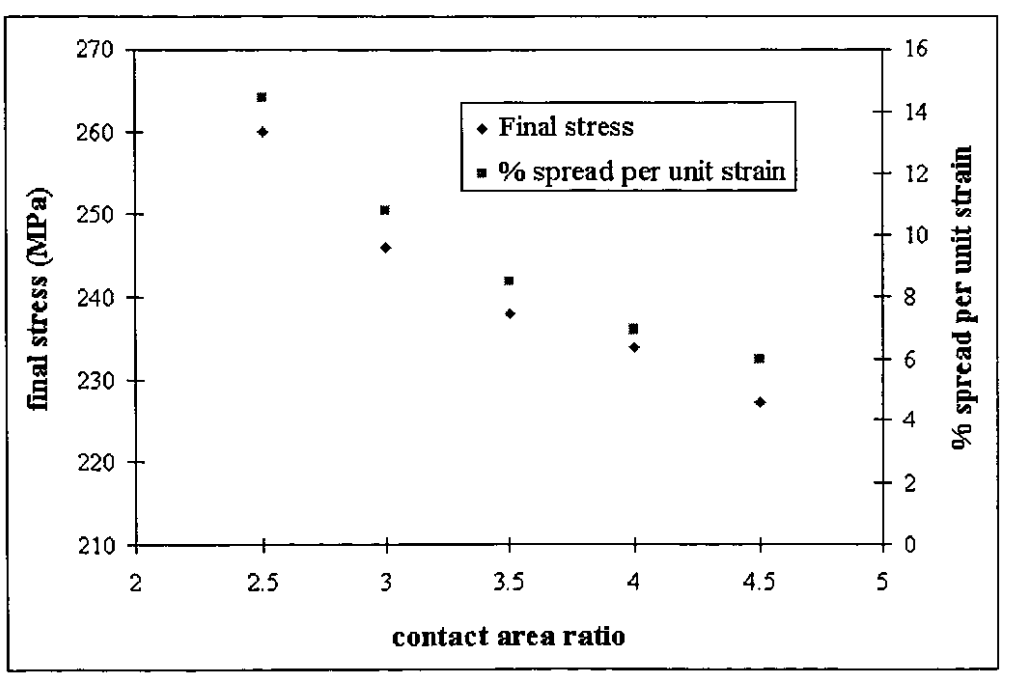

Figure 3.14 Effect on lateral spread on contact area and compression load.

3.2.3.4 Platen and Specimen Dimensions

The platen and specimen dimensions used allowed for a contact area ratio of specimen width, w, to platen breadth, b, of 4:1. The values of w and b were calculated to allow b to be as large as possible while ensuring that the maximum required stress was achievable. The maximum required stress was measured to be ≈ 270 MPa (true stress as given by Eqn 3.2) from the compression of specimens of Al-1Mg to a reduction of 95 % (at room temperature) using a smaller contact area than that intended (by using platens with a value of b = 10 mm). The value of b was thus set at 13 mm and the value of w set at 52 mm. Figure 3.15 shows the design for the platen used. The platens were made from a high tensile steel, V155, which has a relatively low electrical resistivity of 19×10^{-6} Ω.cm. The specimens used were simple rectangular blocks of dimension 52 mm x 33 mm x 10 mm.

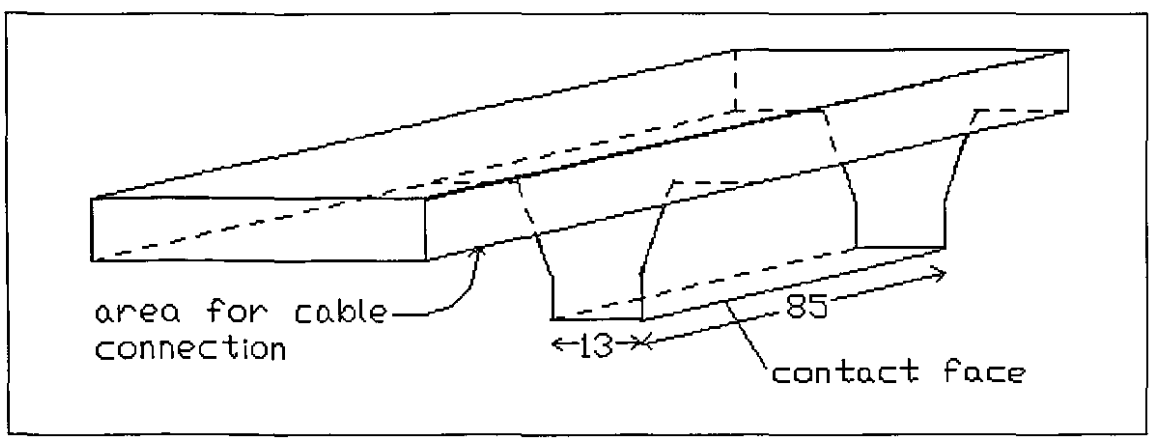

Figure 3.15 Design of platen used for PSC

3.2.4 Lubrication

Although it is known that PTFE (Teflon) tape is the best choice of lubricant, its use was not considered practical due to the resistive heating method employed. It was thus decided to use graphite as a lubricant due to its relatively good friction characteristics and the fact that it allowed for the conduction of an electrical current through the specimen. All specimens were ground to a standard finish of 800 grit on silicon carbide paper. Platen surfaces were inspected regularly for any signs of damage and were given a light grind with 1200 grit silicon carbide paper prior to each test. Graphite particles were applied to the contact surfaces by means of a soft graphite pencil after which an oil based graphite suspension was sprayed onto the surfaces. This form of lubrication was found to work well up to a

deformation temperature of 400°C. For deformation temperatures of 450°C and above some break down in lubrication was noticed. This break down was observed to cause a change in strain distribution within specimens. Strain appeared to be more concentrated in the centre of the specimens and the strain distribution resembled that for a lower starting value of b/h.

3.2.5 Quenching

For high temperature PSC tests, specimens were quenched immediately following deformation to prevent static annealing of the deformed microstructure. The method employed consisted of manually removing the deformed specimen immediately following deformation and dropping it into water. It was possible to consistently quench specimens within 1 to 2 seconds following deformation. Specimens were discarded if this condition could not be met.

3.3 Heat Treatments

In order to study recrystallisation behaviour deformed specimens were subjected to various annealing heat treatments in a salt bath at annealing temperatures of between 420°C and 550°C. A salt bath, as opposed to a conventional air furnace, was used to enable rapid heating of specimens. This meant that it was possible to conduct very short, controlled heat treatments in order to produce partially recrystallised microstructures. A partially recrystallised microstructure was necessary for the study of grain nucleation events that occur in the beginning stages of recrystallisation.

3.4 Optical Microscopy

3.4.1 Sectioning

PSC specimens were sectioned in the equivalent (compared to rolling) longitudinal plane for microscopical investigations. The longitudinal plane is the plane that contains the normal and rolling directions (ND and RD). This is shown schematically in Figure 3.16

where the hatched area represents the plane of view. Investigations concentrated on the centre region of the hatched area where strain was found to be the most uniform in distribution. Furthermore, the hatched area was mid-way or at least close to mid-way across the transverse direction, thus ensuring that the plane of view was always at or very close to the geometric centre of the specimen.

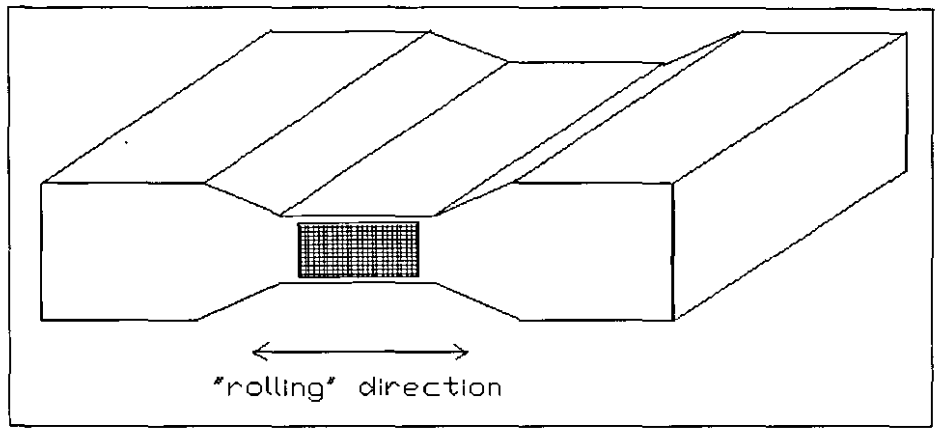

Figure 3.16 Plane of view (hatched area) chosen for microscopy of PSC specimens

3.4.2 Preparation

Following sectioning, specimens were hot mounted in resin for grinding and polishing. Hot mounting was performed at the relatively low temperature of approximately 70°C and therefore it did not have any significant effect on the microstructures of the specimens examined. Specimens were ground on silicon carbide paper to a finish of 1200 grit. They were then mechanically polished in two stages: a diamond polish using particles of 3μm in size followed by a final polish using a suspension of fine colloidal silica. Specimens were then anodised electro-chemically using Barkers reagent (2.5 % Fluoroboric Acid in H_2O). Anodising conditions used were: 2.5 minutes, 30 volts dc, at room temperature.

3.4.3 Microscopy

The anodic layer deposited on the specimens was anisotropic due to the different grain orientations at the surface of the specimen. This allowed grain contrast - in shades of grey - to be viewed when illuminating with polarised light. Colour contrast of grains was achieved by inserting a quartz λ compensation plate into the light path. The light microscope used was a Reichert MeF3 A with which all light micrographs were taken.

3.4.4 Grain Size Measurements

The average grain sizes of fully recrystallised samples were determined manually by the linear intercept method. Micrographs representing three fields of view of each condition were analysed, representing between 120 and 700 grains depending on the grain size concerned. An uncertainty error of less than 10 % was obtained for all the measurements performed.

3.5 Microtexture Investigations

3.5.1 Sample preparation

The aim of sample preparation was to achieve a perfectly smooth surface free of any mechanical deformation caused by grinding and polishing. Specimens were mounted in resin, ground, and mechanically polished in a similar way to that for optical microscopy (section **3.4.2**). They were then electro-chemically polished using a solution of 55 % HNO_3 in Dimethylformamide. Polishing conditions were: 3 seconds at 10 volts dc at a temperature of 20°C. Finally the resin was sputter coated with AuPd by placing a mask over the sample surface.

3.5.2 EBSD Technique

Individual grain orientation measurements were made using electron back-scatter diffraction (EBSD) in a scanning electron microscope (SEM). The EBSD system used is illustrated schematically in Figure 3.17. The SEM used was a LEICA Instrument S440 located at the Electron Microscope Unit, also at the University of Cape Town. Samples were inserted into a sample holder machined to an inclined angle of 70.5° to the horizontal. Samples were thus highly inclined to the electron beam in the SEM. The resulting back scattered electrons formed diffraction patterns (Kikuchi patterns) that were detected by a phosphor screen placed inside the SEM chamber. The diffraction pattern image on the phosphor screen was recorded by a low light video camera placed adjacent to a port in the SEM chamber. The video signal was then fed to a computer containing a frame grabber card. The image was enhanced by multiple sampling and averaged by the computer

software used. The enhanced pattern image was then displayed on a monitor. From the displayed captured image the zone axes were manually located using a computer mouse, and the pattern was then indexed by the computer algorithm. The system was calibrated by indexing a diffraction pattern produced from a Si single crystal that was placed adjacent to the sample in the sample holder.

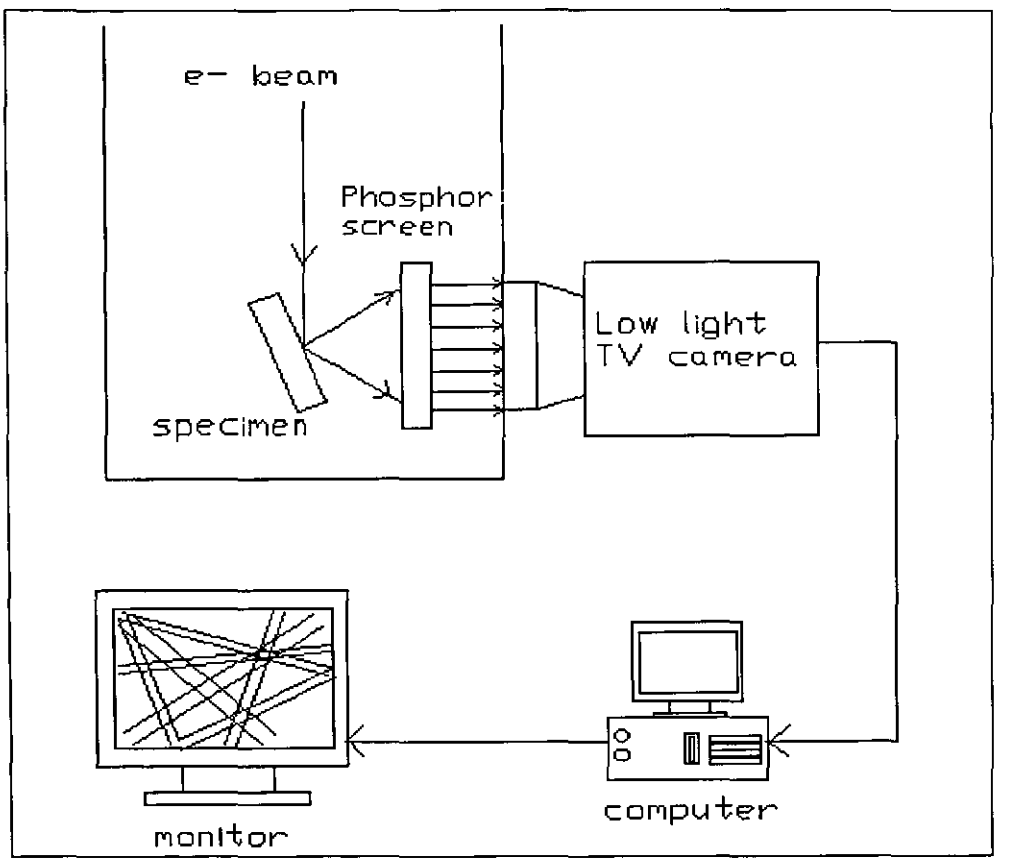

Figure 3.17 Schematic diagram of EBSD system in SEM

3.5.3 Orientation Imaging

Orientation imaging refers to the method whereby the orientations of single grains are related to their position in the microstructure. An image of the microstructure of the region under investigation was obtained by channelling contrast of back scattered electrons measured by a back scatter detector placed immediately below the phosphor screen in the SEM chamber. Once a grain's orientation was measured, the orientation was related to a specific grain in the image by means of a numbering system. In this way an orientation image was produced.

The measured orientations of individual grains were related to ideal orientations (see Table 3.3). If the misorientation between the measured orientation and a specific ideal orientation was found to be less than 15°, the measured orientation was then classed as having the ideal orientation. If a measured orientation could not be matched to an ideal orientation in this way, it was then classed as having a random orientation. Misorientations between measured and ideal orientations were calculated by assuming cubic and orthorhombic symmetry. The calculations were performed by custom written software (source code listed in Appendix B) which made use of matrix algebra to calculate the misorientations as follows:

Eqn 3.4 $$M = L^{-1}G$$

where M, L and G represent the misorientation, ideal and measured orientation matrices respectively.

Since unrecrystallised regions of the microstructure appeared somewhat mottled (due to the high dislocation densities which affected electron channelling in these regions) in the back scatter images, it was not always possible to relate nucleated grains to specific aspects of the deformation structure, especially shear bands. Samples were therefore prepared for optical microscopy immediately following EBSD imaging so that an optical image of the same regions investigated in the SEM could be obtained. In this way additional information could be added to the orientation image produced. In order to obtain an optical image, the relevant area of the sample had to be located. This was facilitated by micro-hardness indentation marks that acted as navigation marks that had been made prior to any EBSD measurements and SEM imaging.

3.5.4 Texture Representation

Orientation distribution functions (ODFs) were generated from local orientation measurements performed on certain partially recrystallised specimens. A detailed description of ODFs is given in section **3.6.3**. In this instance ODFs were generated by the superposition of the calculated Gauss–peaks corresponding to each measured grain orientation. Each grain orientation was assigned the same weight and no attempt was made

to correct for volume effects that might have resulted from grains of different orientations having different sizes. The Gauss type distribution corresponding to each grain orientation was calculated from the orientation density S that decreases exponentially as a function of the angular distance ψ from the exact orientation according to:

Eqn 3.5

$$S(\psi) = S_0 \exp\left[-\left(\frac{\psi}{\psi_0}\right)^2\right]$$

Where ψ_0 is the half scatter width and S_0 is equal to 1 for single grain orientation measurements.

3.6 Macrotexture Investigations

3.6.1 Sample Preparation

Macro or bulk texture measurements were performed on the mid thickness plane of PSC specimens. Specimens were thus ground and mechanically polished to the mid thickness plane before being chemically polished. Chemical polishing was performed in a solution of 15 % NaOH in H_2O (with a spoon of table sugar added) for a period of 15 to 20 minutes. Specimens were then cleaned in a 10 % HNO_3 solution for 10 seconds.

3.6.2 X-ray Diffraction Measurements

X-ray diffraction was performed on PSC samples in order to measure their bulk or average textures (preferred orientation of grains). All X-ray diffraction measurements were performed at MINTEK, Randburg, South Africa using a Siemans D500TT X-ray diffractomer fitted with a molybdenum anode tube and an Euler cradle. Textures were quantified via incomplete pole figures measured from an area of approximately 200 mm^2 using Mo$K\alpha_1$ radiation in back reflection mode.

3.6.3 Data Representation

The traditional form of representation of bulk texture measurements has, until fairly recently, been by means of pole figures. Pole figures, however, are two dimensional

projections of three dimensional orientation distribution space. A full description of orientation distribution is given by the orientation distribution function (ODF). A mathematical method has been used to calculate the bulk texture ODF's represented in this work from four incomplete pole figures; those of (111), (200), (220) and (311). This method is the so-called series expansion method (lmax = 22) that uses generalised spherical harmonics. The ODF plots have been reduced to $0° \leq \varphi_1, \phi, \varphi_2 \leq 90°$ in Euler angle space due to the cubic-orthorhombic symmetry of the samples measured. The plots consist of φ_2 constant sections (in 5° intervals) with density contours plotted at 15 % intervals of the maximum intensity value (times random value). Volume fractions of ideal orientations have been calculated by integration over 15° around the ideal orientation peaks. This fact explains why some volume fraction charts presented in Chapters 4 and 5 (Figure 4.7b, Figure 5.12 and Figure 5.14) indicate cumulative volume fractions greater than 100 %. The overlap that results from ideal orientations that are separated by less than 15° in orientation space accounts for this. The ideal orientations considered in this study are those listed in Table 3.3, which provides both the Miller indices and Euler angles for each orientation.

Orientation	Euler angles			Miller indices
	φ_1	ϕ	φ_2	{hkl}<uvw>
Cu (Copper)	90°	35°	45°	{112}<111>
S	59°	33°	65°	{123}<634>
Brass	35°	45°	0°/90°	{011}<211>
Goss	0°	45°	0°/90°	{011}<100>
Cube	0°	0°	0°/90°	{001}<100>
$Cube_{ND}$ (ND rotated Cube)	22°	0°	0°/90°	{001}<310>
$Cube_{RD}$ (RD rotated Cube)	0°	22°	0°/90°	{013}<100>
R (retained rolling)	63°	31°	60°	{124}<211>
Q	45°	15°	10°	{013}<231>
P	70°	45°	0°/90°	{011}<122>

Table 3.3 Euler angles and Miller indices of ideal orientations considered.

3.7 Transmission Electron Microscopy

3.7.1 Sample Preparation

A rod, 3 mm in diameter, was machined from the centre of PSC specimens in the way indicated in Figure 3.18. Part of the rod's outer diameter was machined flat to indicate its relative orientation to the PSC specimen; the flattened section corresponded to the rolling plane of the PSC specimen. Thin discs were sliced from this rod to prepare specimens for transmission electron microscopy (TEM) that would result in a longitudinal view relative to the compressive geometry. These discs were mechanically ground to a thickness of about 100 μm before being electro-chemically polished. Polishing was by means of controlled twin-jet polishing using a solution of 20 % HNO_3 in methanol at 20 volts and at a temperature of -20°C.

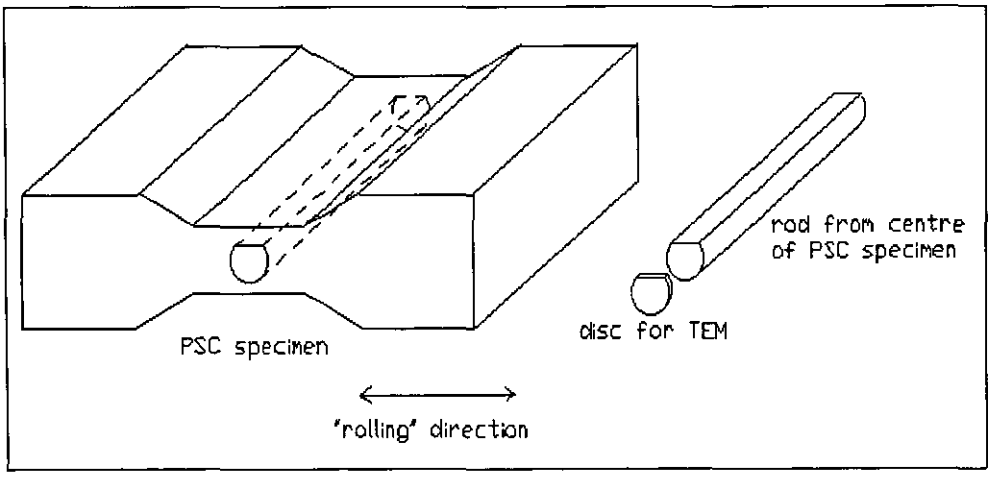

Figure 3.18 Orientation of TEM specimens in relation to PSC geometry.

3.7.2 Microscopy

Transmission electron microscopy was carried out on a Jeol 200CX microscope at an accelerating voltage of 200 keV. Bright field images were obtained and the orientations of the images were recorded relative to the specimen orientation in the sample holder. In so doing it was possible to record the relative orientation of the images to the deformation geometry by means of the flattened section of the specimen that corresponded to the rolling direction.

4. Asymmetric Flow During Plane Strain Compression

4.1 Description

Asymmetric flow was observed to sometimes occur during plane strain compression. The longitudinal view of specimens in situ after deformation is depicted in Figure 4.1. The specimen cross sections depicted are a true representation of their shape after compression to strains of $\varepsilon = 2.7$. Figure 4.1a shows the configuration that would be expected and is indeed observed for a symmetrical deformation; a typical "dog bone" shape that is symmetrical about both the normal direction (ND) and rolling direction (RD). Figure 4.1b, in contrast, shows the shape observed for an asymmetrical deformation, which is asymmetrical about the ND and RD axes. Both tests depicted in Figure 4.1 were performed under identical conditions (at room temperature, to strains of $\varepsilon = 2.7$ and at strain rates of 1 s^{-1}) on two hot rolled and annealed Al-1Mg specimens. These specimens were sectioned parallel to the longitudinal plane (i.e. the plane containing the ND and RD) at a point midway across the transverse direction (TD) to produce longitudinal views of the specimen segment in contact with the platens at the end of the test (Figure 4.2). Each view is a montage of optical micrographs that serve to illustrate the flow pattern involved by the elongated grain morphology that is revealed. The flow pattern shown in Figure 4.2a, which corresponds to the specimen with an external symmetrical shape (Figure 4.1a), is clearly symmetrical about the central ND and RD axes and is also uniform across most of the ND-RD plane. The pattern depicted in Figure 4.2b, which corresponds to the specimen with an external asymmetrical shape (Figure 4.1b), on the other hand lacks this symmetry and the region of uniform strain is very limited.

The development of an asymmetrical flow pattern, as shown in Figure 4.2b, was traced by sectioning PSC specimens after fixed strain increments. Figure 4.3 depicts the flow patterns of Al-1Mg-1Mn specimens after strains values of $\varepsilon = 0.55$, $\varepsilon = 0.97$, $\varepsilon = 1.6$ and $\varepsilon = 2.2$. The overall shapes of the specimens deformed to strains of 0.55 and 0.97 remained

symmetrical with resultant symmetrical flow patterns as shown in Figure 4.3a and Figure 4.3b respectively. The shape of the specimen deformed to a strain of 1.6 appeared to be slightly asymmetrical and its corresponding flow pattern (Figure 4.3c) appears to exhibit some loss of symmetry. The shape of the specimen strained to a value of 2.2, however, was definitely asymmetrical as was its corresponding flow pattern that is shown in Figure 4.3d. It must be emphasised that asymmetrical flow was not always detected even at strains up to $\varepsilon = 2.7$. There was also a greater tendency for asymmetric flow to occur in the Al-1Mg-1Mn alloy compared to the Al-1Mg alloy.

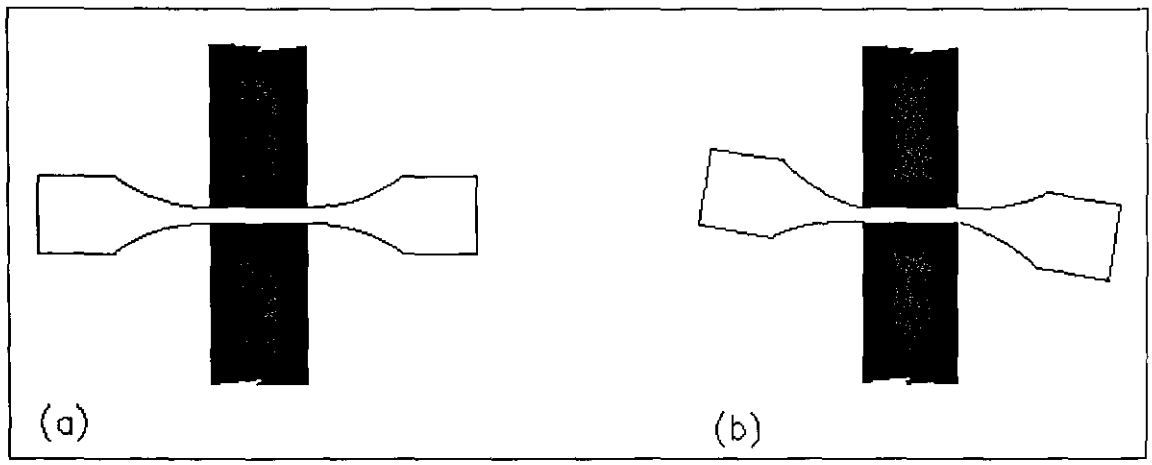

Figure 4.1 Schematic representation of deformed specimens in relation to platens for (a) symmetrical and (b) asymmetrical deformation

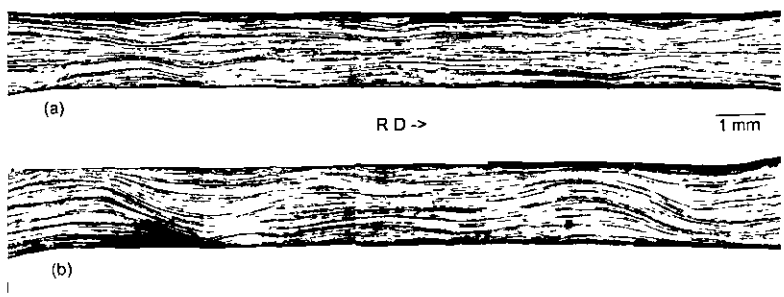

Figure 4.2 Optical micrographs showing longitudinal views of two Al-1Mg specimens: (a) deformed symmetrically and (b) deformed asymmetrically. Sections shown correspond to the specimen segments in contact with the platens as in Figure 4.1.

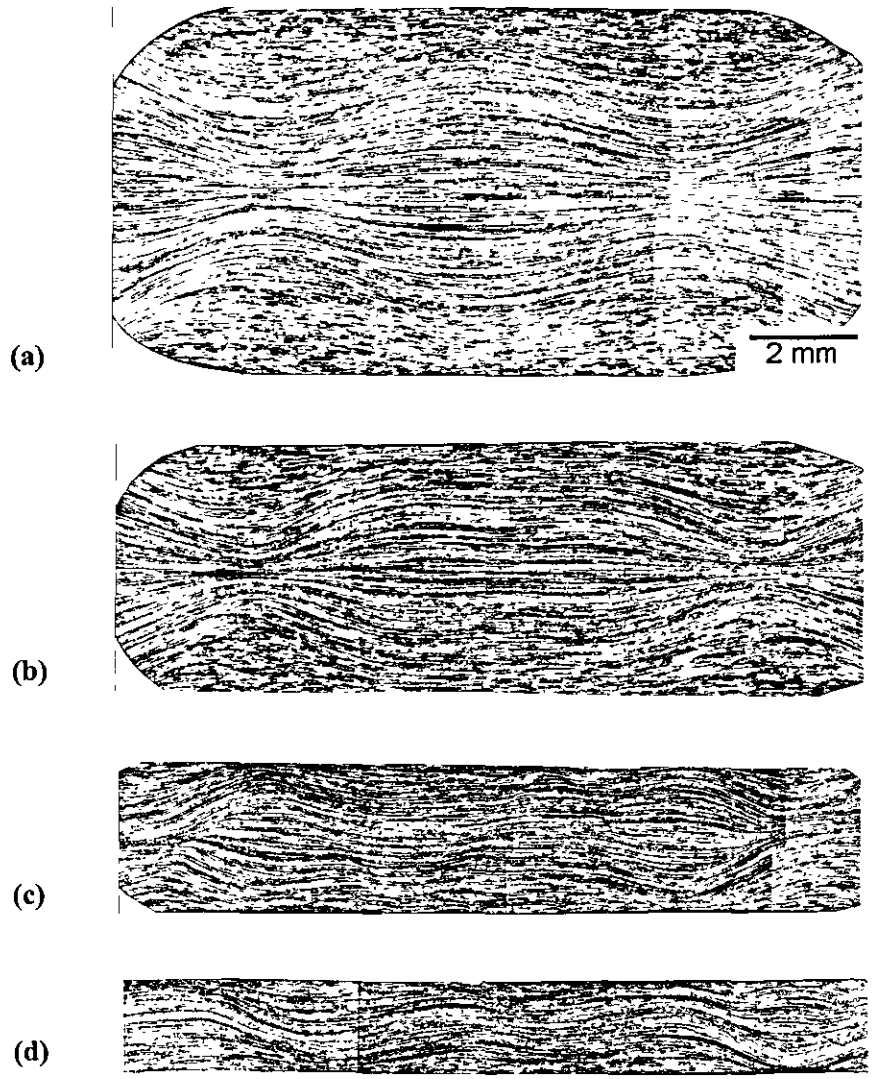

Figure 4.3 Asymmetric flow pattern development during incremental straining of Al-1Mg-1Mn specimens: (a) $\varepsilon = 0.55$, (b) $\varepsilon = 0.97$, (c) $\varepsilon = 1.6$ and (d) $\varepsilon = 2.2$.

4.2 Lateral Offset of Platens

Although the platens of the PSC rig were perfectly aligned both before and after deformation and although the apparatus was constructed to minimise lateral movement of the platens (section **3.2.2.2**), the geometric change in the specimens when asymmetric deformation took place suggested that a possible lateral offset of the platens occurred during loading. Several PSC tests were thus performed whilst the lateral displacement of the platens was monitored by observing several dial gauges set up at strategic positions. A

maximum lateral displacement of 0.20 mm was detected when a test resulted in asymmetric flow as shown in Figure 4.1b. This translates to an offset of only 1.5% of the width of the platens. In addition, the lateral offset was noted to occur at a critical load coinciding approximately with the strain at which asymmetrical flow was observed to occur (see Figure 4.3) which suggests a limit in the machine compliance. However, the fact that lateral offset sometimes did not occur (for identical loading conditions), suggests that there may be an exacerbating factor that promotes lateral offset. This factor is most likely that caused by the variation in local friction conditions between the platens and the specimen. An increase in friction locally will inhibit the lateral flow of material and therefore exert a lateral force on the platens. The fact that the critical load for the onset of lateral displacement was more easily exceeded for the Al-1Mg-1Mn alloy compared to the Al-1Mg alloy is due to the higher flow stress intrinsic for the former alloy. This also explains why the onset of asymmetric flow was observed at a lower critical strain for the Al-1Mg-1Mn alloy.

4.3 Analysis

The analysis of asymmetric flow during PSC is dependent on the slip-line field that is applicable. The determination of the complete slip-line field in non-trivial due to the friction conditions which are involved, which are somewhat intermediate between smooth and perfectly rough interface conditions. It is not the intention of this analysis to develop a complete slip-line field for the two situations of symmetric and asymmetric flow depicted in Figure 4.1. Rather, attention will be placed on the plastic-rigid boundaries between the deforming (plastic) material and the overhanging non-deforming (rigid) material. These boundaries, which are initiated at the sharp corners of the platens and spread inwards until they meet near the geometric centre of the specimen, form the basis for the construction of the rest of the slip-line field. Hill et al[63] have shown that for rough platens the plastic-rigid boundary is a straight line that meets the centre-line at 45° for any value of the b/h - platen breadth to specimen height – ratio (see Figure 2.5b). This is based on the assumption that the platens are of equal width and that indentation is symmetrical. Green[64] has shown that the plastic-rigid boundary is not necessarily a straight line, although it still meets the centre-line at 45°, for smooth platens (Figure 2.6). However, for integral values of b/h the plastic-

rigid boundary was shown to be a straight line for smooth platens. For high amounts of strain several integral values of b/h are derived for relatively small increments in strain. In this study for example, b/h has an integral value when h = 2.2 mm and again when h = 1.85 mm. Thus it is at least reasonable to assume a straight-line representation of the plastic-rigid boundary for intermediate friction conditions and for high strain amounts. A further factor influencing the present choice of plastic-rigid boundary is the exact nature of friction at the interface. Thomason[66] has reported that viscous lubricants, like that used in this study, may become entrapped in the centre region of the platen / specimen interface. This leads to much higher than average friction conditions at the edges of the platens, whereas the friction might approach zero at the centre of the platens. The slip-line field at the platen edges is thus more likely to resemble the field corresponding to rough platens than for smooth platens, and consequently a straight line boundary is more likely.

The case of compression between platens of unequal breadth has been investigated by Johnson and Kudo[115]. They found it necessary to modify the slip-line field solution presented by Hill et al[63] for rough interface conditions. The plastic-rigid boundary was assumed to be made up of two perpendicular straight lines of equal length, originating from the die edges and meeting at some point other than the centre thickness line. In this way the slip-line field can always be started by drawing a right-angled isosceles triangle between the edges of the two platens. An example of a slip-line field calculated by Johnson and Kudo[115] that corresponds to a difference in platen breadth of 2Δ is presented in Figure 4.4.

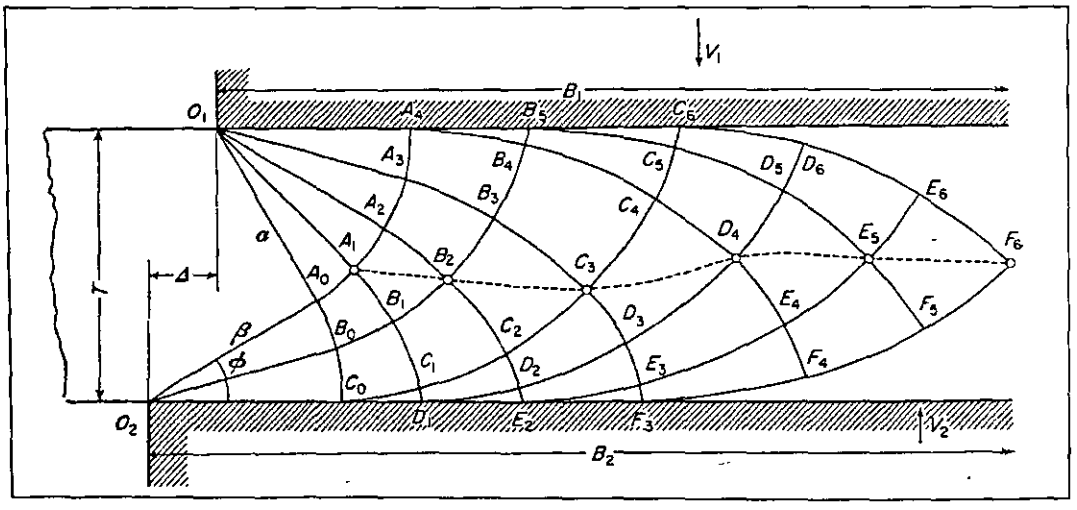

Figure 4.4 Slip-line field for compression between perfectly rough platens of unequal breadth, 2Δ, as calculated by Johnson and Kudo[115].

On the basis on the aforementioned arguments, the plastic-rigid boundaries for the symmetric and asymmetric flow situations shown in Figure 4.1 are presented in Figure 4.5. When the platens are perfectly aligned (Figure 4.5a), the plastic-rigid boundaries meet the specimen centre thickness line at an angle of 45° and thus define the start of a symmetrical flow pattern about both the specimen horizontal (RD) and vertical axis (ND). If the platens are offset by some value Δ (Figure 4.5b), then the plastic-rigid boundaries meet at some point above or below the specimen centre thickness line. It is obvious that an asymmetrical flow pattern will develop from the resultant slip line field. In this case both boundaries (left and right hand sides) have rotated in a clockwise sense, by an amount of rotation that is related to the offset Δ. Johnson and Kudo[115] have shown that for the similar case of platens of unequal breadth, the velocity of the narrower platen is higher than that of the broader platen by an amount that is proportional to half the difference in platen breadth, Δ. In fact it is reported that when Δ is equal to or greater than the specimen thickness (when $\varphi = 0°$ in Figure 4.5), then the velocity of the broader platen is zero and indentation from this platen ceases. The situation in Figure 4.5b can thus be described in the following way. If the velocity (V) of the platens at the edges is considered with respect to the specimen, then $V_A > V_B$ and $V_{A'} < V_{B'}$. In other words the rate of indentation is higher at A and B' than at their respective opposite edges B and A'. Since there is no rotation of the platens, the specimen has to rotate in order to satisfy the above velocity conditions. The rotation of the specimen causes the geometry in Figure 4.1b to arise, and the rotation of the plastic-rigid exit boundaries causes the flow pattern shown in Figure 4.2b and Figure 4.3d to develop.

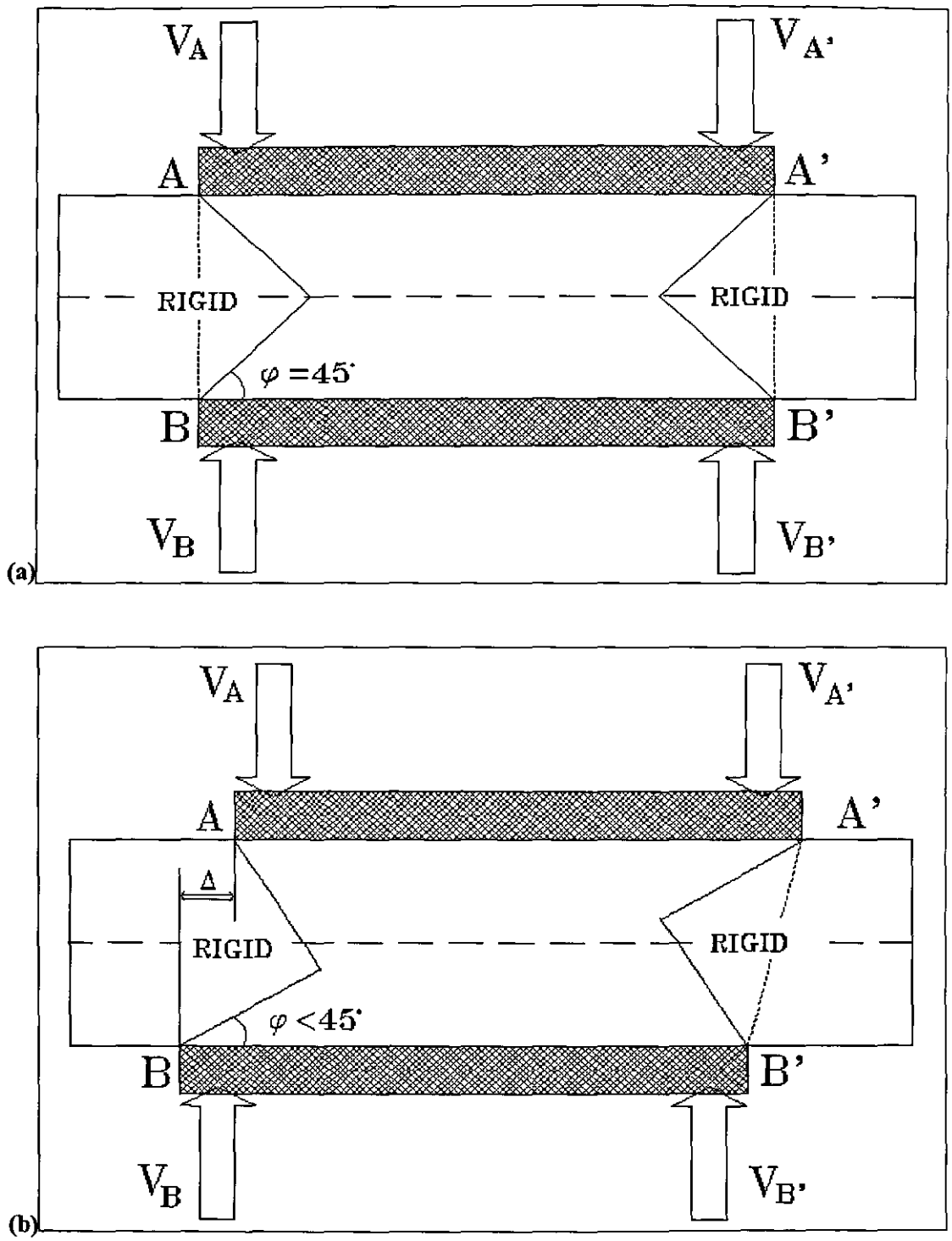

Figure 4.5 Schematic representation of the plastic-rigid exit boundaries for (a) perfectly aligned platens and (b) lateral platen offset equal to an amount of Δ.

4.4 Implications

4.4.1 Apparent Influence on Shear Band Formation

It has been described how asymmetrical deformation results in non-uniform material flow as is illustrated in Figure 4.2b and Figure 4.3d. This non-uniform flow is characterised by curved regions of elongated grains as opposed to uniform flow where grain elongation is more parallel to the rolling direction (see Figure 4.2a for example). Very strong shear band formation was observed in these curved elongated grain regions that characterise asymmetrical flow (Figure 4.6). Specimens that have experienced asymmetrical flow thus appear to exhibit a higher density of shear band formation compared to specimens that have experienced symmetrical flow for otherwise identical conditions of deformation. Furthermore, it could be concluded that specimens that are asymmetrically deformed experience a higher amount of shear strain. The effective strain of these specimens could thus be significantly higher than the value of the nominal strain applied.

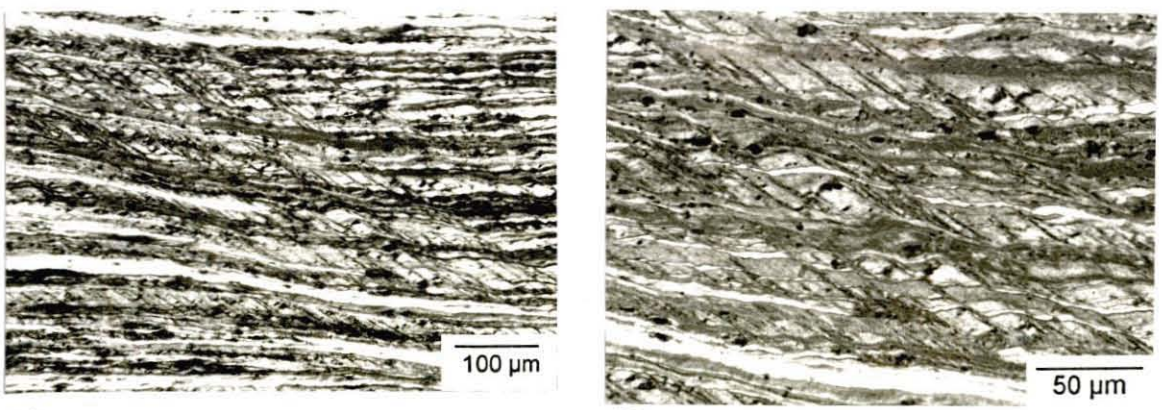

Figure 4.6 Optical micrographs (longitudinal view) illustrating the very strong shear band formation that occurs in regions of curved or non-uniform material flow that is characteristic of asymmetrical deformation.

4.4.2 Influence on Texture Formation

The influence of asymmetric flow on texture formation was studied by measuring both the as deformed and the recrystallised textures (bulk texture measurements) of specimens exhibiting symmetric and asymmetric flow. The specimens chosen were in fact the same specimens that are depicted in Figure 4.1 and Figure 4.2 and again it must be noted that, apart from the flow characteristics exhibited, the deformation conditions were identical for the two specimens. Figure 4.7a shows that asymmetrical flow had very little effect on the values of the deformation texture components compared to symmetrical flow. The deformation texture corresponding to asymmetrical flow is only slightly weaker than that corresponding to symmetrical flow, as can be seen by the lower value of the maximum intensity level of the ODFs concerned (8.1 compared to 11.3) and the slightly reduced volume fractions of the main deformation texture components (Brass, Cu and S). Asymmetrical flow also had very little effect on the recrystallisation texture produced as can be seen from Figure 4.7b. A weakening of recrystallisation texture caused by asymmetrical flow could perhaps be observed from a reduction in the maximum intensity levels of the ODFs concerned (6.6 compared to 8.3). A small, but hardly significant, increase in the Q volume fraction at the expense of the Cube and the Goss volume fractions appeared also to be caused by asymmetrical flow compared to symmetrical flow.

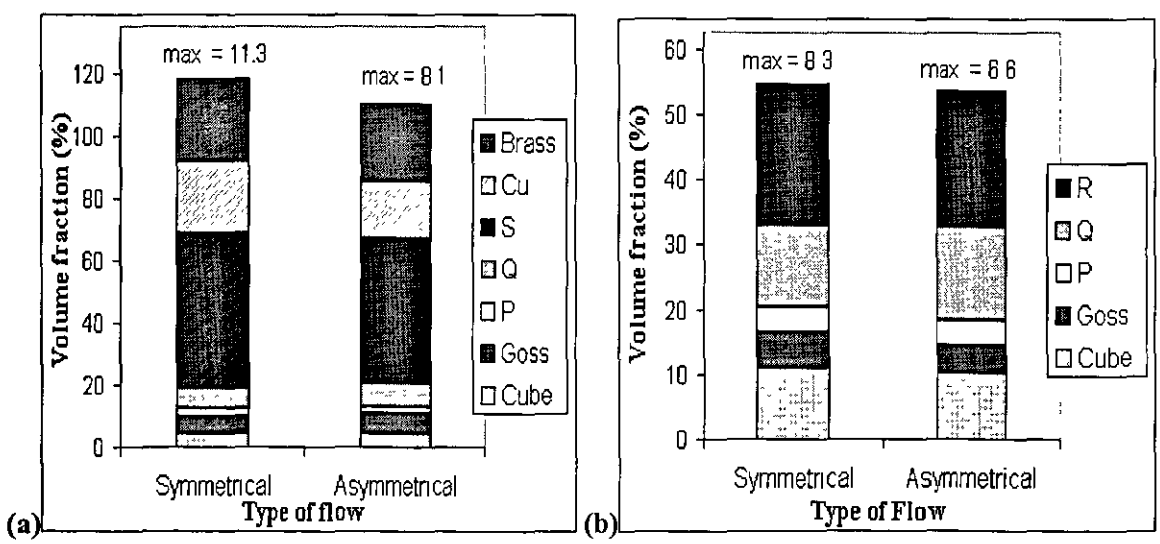

Figure 4.7 The effect of asymmetric flow on the (a) deformation texture components and (b) recrystallisation texture components. (Deformation conditions identical: room temperature, strain rate = 1 s^{-1}, strain of ε = 2.7). Max refers to maximum intensity level of corresponding ODF plot.

4.4.3 Further Implications

Although it has been demonstrated that asymmetric flow has little apparent influence on measured texture formation, it nevertheless remains a concern for microstructural and texture studies. The texture measurements were conducted on the mid-thickness plane (RD-TD plane at mid ND) which was also sectioned from the centre three-quarters of the RD. The possible effects of asymmetrical flow where in this way minimised. The approach for selective sampling adopted by Timothy et al[69] is therefore emphasised. Less careful selection of texture samples from the PSC specimens might well have resulted in significant differences being observed between specimens demonstrating asymmetrical and symmetrical flow. For example, if measurements were performed at say the quarter thickness plane it is possible that more variation in texture results might have been recorded. Of course the situation might become a lot more critical as the amount of lateral offset, Δ, increases.

An asymmetric flow pattern has been described for the compression of material between parallel rotating platens with particular reference to the changing plastic-rigid exit boundaries[116,117]. Collins[116] has suggested that the oscillatory strain-rate field corresponding to this situation might be the same as that which arises during the actual cold rolling of metals. It is thus worth noting that although symmetrical flow and homogeneous strain is being sought during PSC testing, asymmetrical flow caused by lateral platen offset may be of some use for studying certain situations which arise during actual cold rolling.

5. Results

5.1 Shear Band Formation

The deformation variables of strain, temperature and strain rate were observed to have a profound influence on the strength and extent of shear band formation during plane strain compression of Al-1Mg. The description of shear band formation was based mainly on optical microscopical observations of as deformed specimens. Plane strain compression tests were conducted for a matrix of deformation variables: for strains of $\varepsilon = 0.25$ to 3.1 and for temperatures from room temperature to 400°C (for a constant strain rate of 1 s^{-1}). Tests at strain rates of 0.1 s^{-1} and 7.5 s^{-1} were also conducted for certain values of strain and deformation temperature. Both symmetrically and asymmetrically deformed specimens were considered for investigation.

5.1.1 The Effect of Strain

Plane strain compression tests at room temperature and at a fixed strain rate of 1 s^{-1} were performed to strains of $\varepsilon = 0.25$, 0.6, 1.1, 1.6, 2.7 and 3.1 in order to asses the influence of strain on shear band formation. The strength of shear band formation was found to be proportional to the amount of strain experienced during compression. In general, the higher the strain, the more pronounced was the shear band formation that was observed.

For high amounts of strain, $\varepsilon = 2.7$ and $\varepsilon = 3.1$, shear banding was observed in nearly all grains and shear bands were observed to cross several adjacent grains (see Figure 5.1a). The strength of the shear banding could be inferred from the very clear contrast of the bands produced in the optical micrographs (resulting from polarisation differences at the anodic surface of the samples due to orientation differences in the shear bands) and also from the degree of distortion of the grain boundaries by the shear bands.

For medium amounts of strain, $\varepsilon = 1.6$, the strength of shear banding was still observed to be strong compared to higher strain amounts, although less distortion of grain boundaries

was observed and shear bands did not appear to cross as many adjacent grains (see Figure 5.1b).

For low strains amounts, $\varepsilon = 0.6$ and 1.1, the strength of shear banding was observed to be of moderate proportions compared to higher strains. Shear bands appeared to be less well formed in general, as was observed from a lower degree of orientation contrast and less grain boundary distortion (see Figure 5.1c).

For very low amounts of strain, $\varepsilon = 0.25$, shear banding was observed to be very weak. Typically, very fine banding (not obvious shear banding) was observed with a few isolated instances of actual shear banding (see Figure 5.1d).

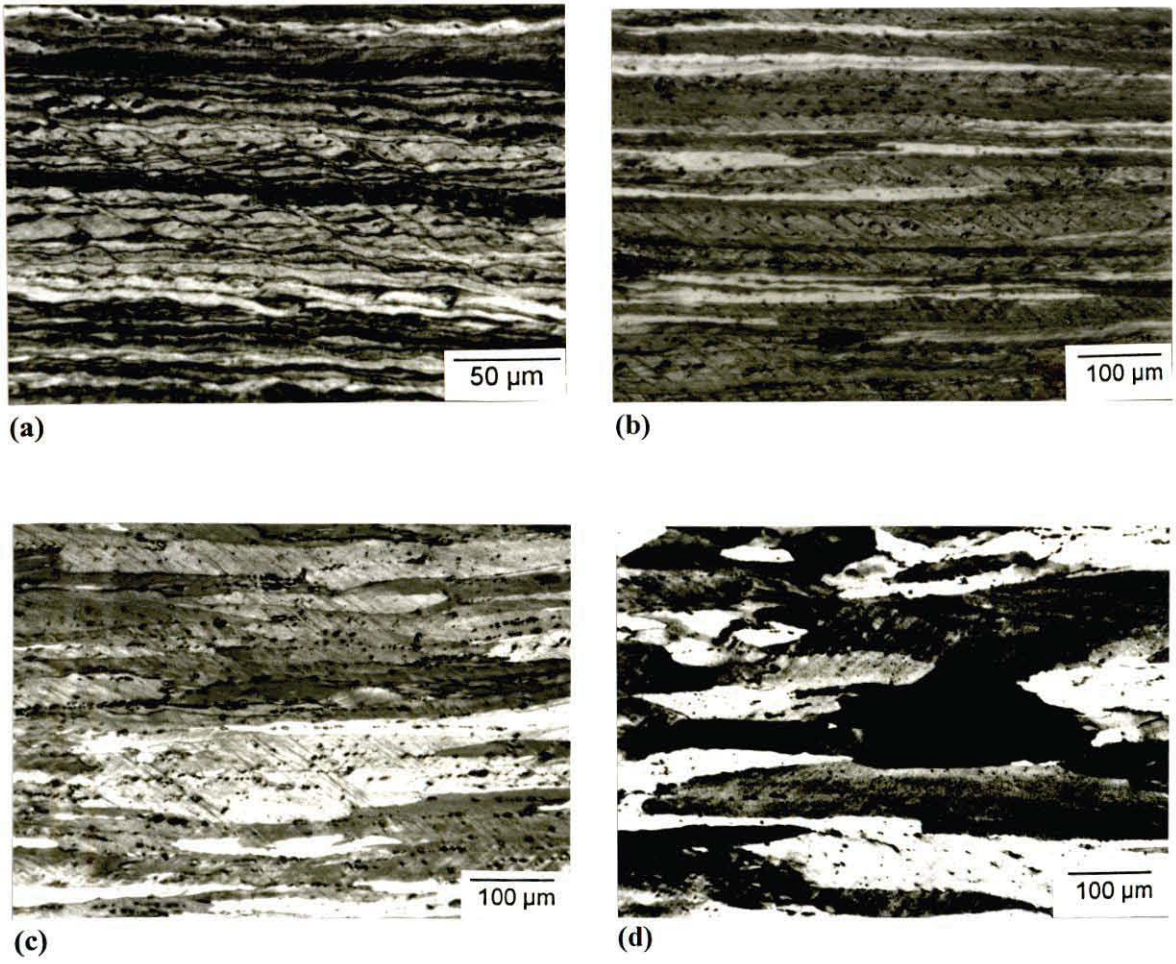

Figure 5.1 Optical micrographs showing the extent of shear banding for different strains (deformation temperature = room temperature, $\dot{\varepsilon} = 1s^{-1}$): (a) $\varepsilon = 3.1$, (b) $\varepsilon = 1.6$, (c) $\varepsilon = 1.1$ and (d) $\varepsilon = 0.25$.

The effect of strain on shear band formation was also investigated for deformation temperatures higher than room temperature. The combined effects of strain and deformation temperature on shear band formation are summarised in Figure 5.2. A similar variation in shear band formation with strain was observed for deformation temperatures up to and including 250°C as compared to room temperature. The effect of deformation temperature on shear band formation will be dealt with in further detail in the next section **(5.1.2)**.

5.1.2 The Effect of Deformation Temperature

5.1.2.1 Optical Observations

The effect of deformation temperature on shear band formation was evaluated by performing plane strain compression tests at a fixed strain rate of 1 s^{-1}, at strain amounts varying from $\varepsilon = 0.25$ to 3.1, and temperatures equal to room temperature, 100°C, 200°C, 250°C, 300°C, 350°C and 400°C. The results of these tests are summarised in Figure 5.2. From Figure 5.2 it can be seen that deformation temperature has very little effect on shear band formation for temperatures up to 250°C for all strains. At 300°C some weakening was observed for all strains, while for temperatures of 350°C and above a significant weakening was observed for all strains. This trend is further reflected in Figure 5.3 which reveals the extent of shear band formation for a strain of $\varepsilon = 2.7$ and deformation temperatures equal to room temperature, 200°C, 300°C and 350°C. The micrographs corresponding to deformation temperatures of room temperature (Figure 5.3a) and 200°C (Figure 5.3b) reveal little difference in the apparent strength of the shear bands observed. The micrograph corresponding to a deformation temperature of 300°C (Figure 5.3c) shows a small relative weakening in comparison, while that corresponding to a deformation temperature of 350°C (Figure 5.3d) shows a significant weakening to the extent that shear bands appear not to have formed.

There thus seems to be a critical value of deformation temperature, or range of deformation temperature, above which the formation of shear bands is significantly impeded for all values of strain. For a strain rate of 1 s^{-1} this critical temperature would appear to lie between 300°C and 350°C.

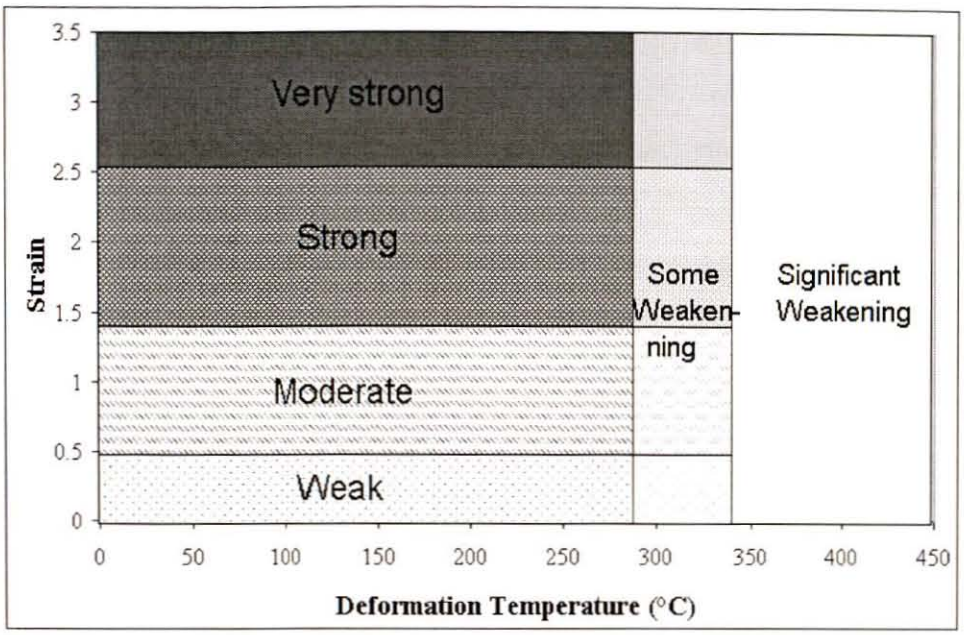

Figure 5.2 Shear band formation mapped out as a function of both deformation temperature and strain (for a constant strain rate of $1s^{-1}$).

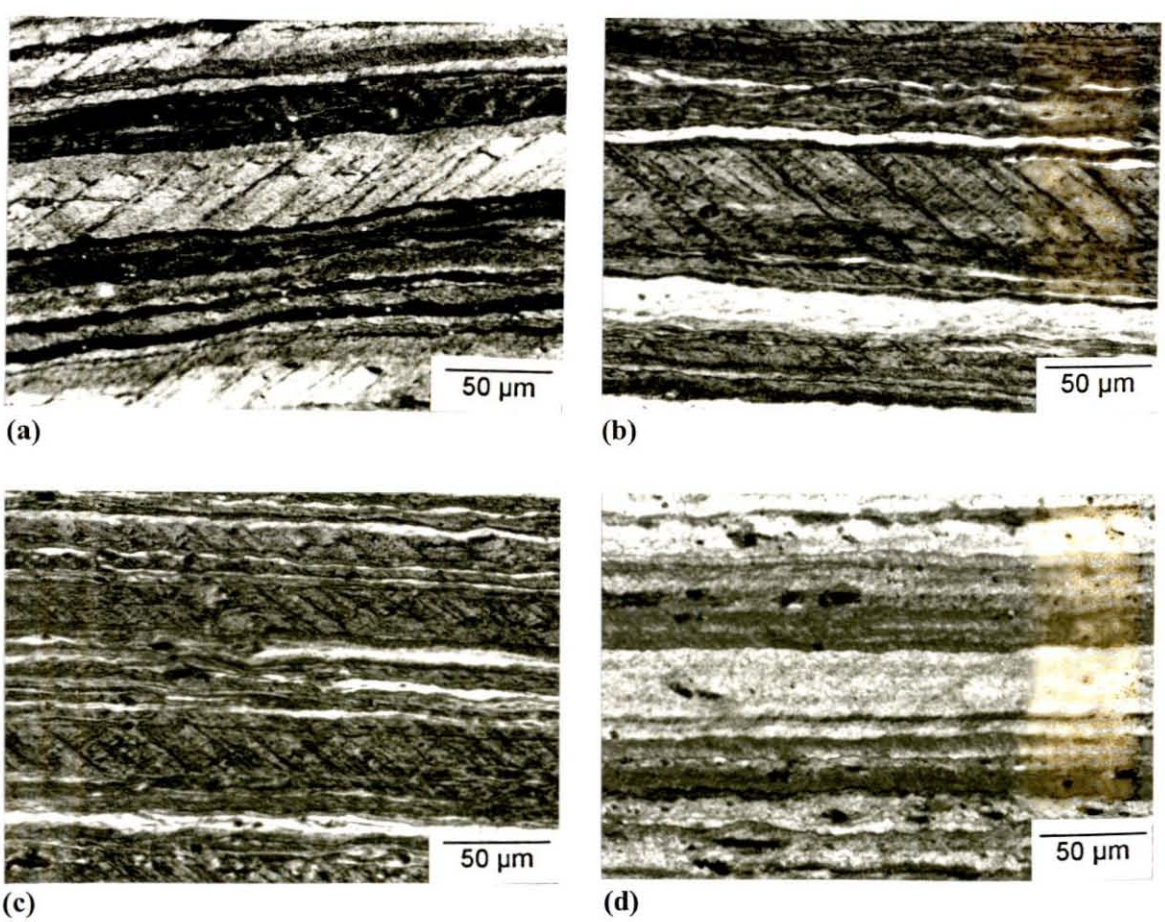

Figure 5.3 Optical micrographs showing the extent of shear banding for different deformation temperatures (strain of $\varepsilon = 2.7$, strain rate of $1s^{-1}$): (a) Room Temperature, (b) 200°C, (c) 300°C and (d) 350°C.

5.1.2.2 TEM Observations

The effect of deformation temperature on dislocation structures was investigated by means of transmission electron microscopy. The dislocation structures corresponding to deformation at room temperature (strain rate of 1 s^{-1} and strain of $\varepsilon = 1.1$) are shown in Figure 5.4a. This represents a longitudinal view of the compression sample containing the rolling and normal directions with the rolling direction approximately parallel to the horizontal edge of the micrograph. A distinct microband structure can be observed with the bands aligned at approximately 35° to the horizontal, and therefore also the rolling direction. A macroband or shear band can also be observed. The dislocation structures corresponding to deformation at 350°C (strain rate of 1 s^{-1} and strain of $\varepsilon = 1.1$) are shown in Figure 5.4b. Again a longitudinal view is represented. In contrast to Figure 5.4a, Figure 5.4b reveals a more recovered equiaxed substructure.

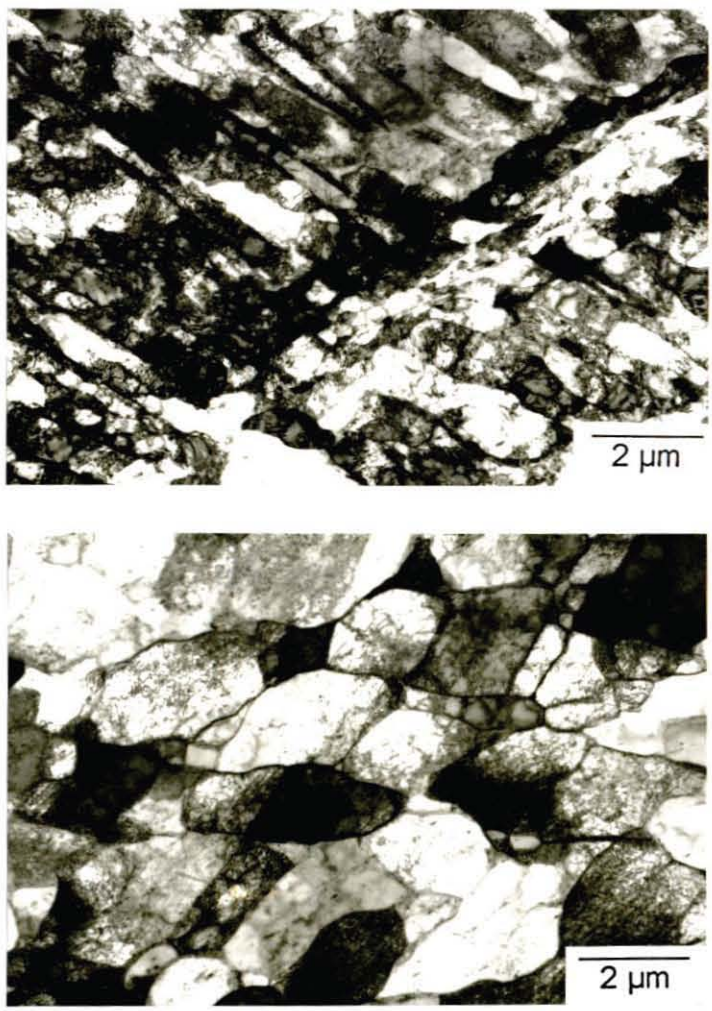

Figure 5.4 TEM micrographs revealing dislocation structure after deformation at (a) room temperature and (b) 350°C. (Strain amount of $\varepsilon = 1.1$ and strain rate = $1s^{-1}$).

Furthermore, a sudden rapid drop in hardness can be observed as the deformation temperature increases between 300°C and 350°C. This corresponds to the temperature range over which a significant weakening in shear band formation was observed (see Figure 5.2 and Figure 5.3).

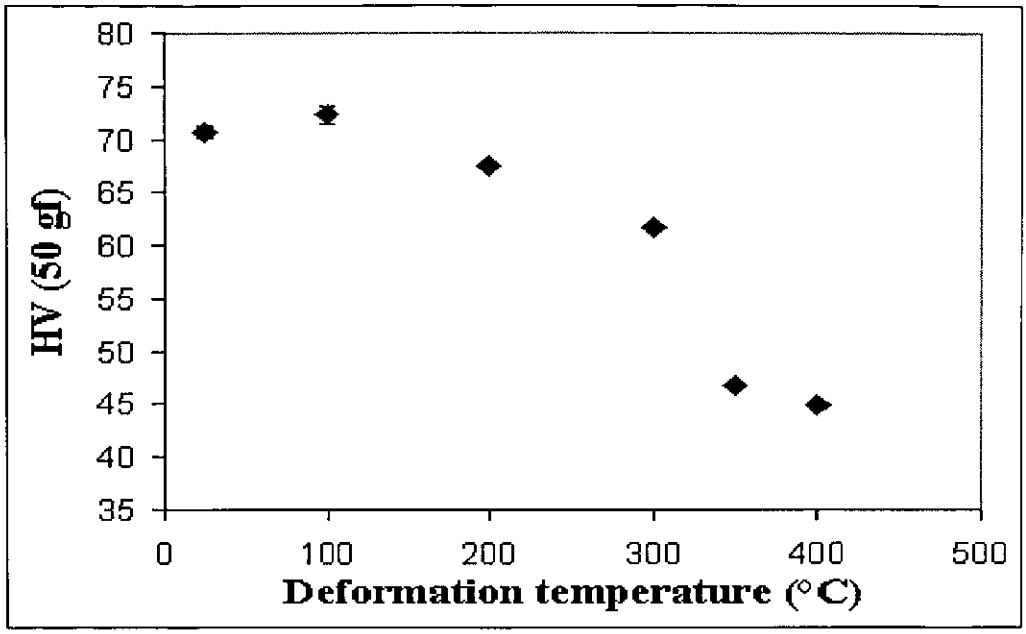

Figure 5.6 Measured hardness of as deformed specimens as a function of deformation temperature (for a constant strain rate of $1s^{-1}$ and for a constant strain of $\varepsilon = 2.7$).

5.1.3 The Combined Effect of Strain Rate and Deformation Temperature

A decrease in strain rate during deformation is thought to have a similar effect, in terms of dynamic recovery rates, to that of an increase in deformation temperature and vice versa. The combined effects of strain rate and deformation temperature are often represented by the single parameter, Z (the Zener-Holloman parameter), as given in Eqn 2.4. PSC tests were thus conducted at critical values, in terms of shear band formation, of deformation temperature (300°C and 350°C) and at strain rates of 0.1 s^{-1}, 1 s^{-1} and 7.5 s^{-1} in order to vary Z. The value of Q (activation energy) used to calculate the respective values of Z was 156 $kJ.mol^{-1}$).

5.1.3.1 Optical Observations

It was the intention to conduct a PSC test at 300°C and at a strain rate of 0.1 s^{-1} (nominal Z value of $1.7x10^{13}$ s^{-1}) to produce a similar value of Z compared to that of a PSC test

conducted at 350°C and at a strain rate of 1 s^{-1} (Z value of $1.2x10^{13}$ s^{-1}). The latter combination of deformation temperature and strain rate was observed to lead to a significant weakening in shear band formation (see Figure 5.2 and Figure 5.3d). If it were true that an increase in the rate of dynamic recovery causes a weakening of shear band formation, then it would be expected that the former combination of deformation temperature and strain rate would similarly lead to a significant weakening in shear band formation (because of the similar values of Z). However, for the relatively low value of strain rate of 0.1 s^{-1}, there was an associated problem of a drop in deformation temperature during compression. An effective temperature of 267°C (as opposed to 300°C) calculated from the measured temperature during compression, results in an effective value of Z = $1.3x10^{14}$ s^{-1} (as opposed to $1.7x10^{13}$ s^{-1} for 300°C). This value of Z is in fact closer to that for a PSC test conducted at 300°C at a strain rate of 1 s^{-1} (Z = $1.7x10^{14}$ s^{-1}), which represents deformation conditions leading to strong shear banding with some weakening observed (see Figure 5.2 and Figure 5.3c). The extent of shear banding after a PSC test at a nominal deformation temperature of 300°C (effective temperature of 267°C) and at a strain rate of 0.1 s^{-1} (strain of $\varepsilon = 2.7$) can be inferred from Figure 5.7a. There is clear evidence of shear banding although it would appear that there is a further weakening of the shear bands that can be noticed from their reduced contrast with the matrix (compare with Figure 5.3c).

Figure 5.7b shows the extent of shear band formation for a PSC test conducted at a deformation temperature of 350°C and at a strain rate of 7.5 s^{-1} resulting in a Z value of $9.2x10^{13}$ s^{-1}. This value of Z lies between that for a deformation temperature = 350°C and a strain rate = 1 s^{-1} (Z = $1.2x10^{13}$ s^{-1}), a virtually non shear banding case (see Figure 5.3d), and that for a deformation temperature = 267°C and a strain rate = 0.1 s^{-1}, a weakening shear banding case (Figure 5.7a). Figure 5.7b more closely resembles Figure 5.3d than Figure 5.7a in that shear banding appears to be significantly weakened to the point of not occurring.

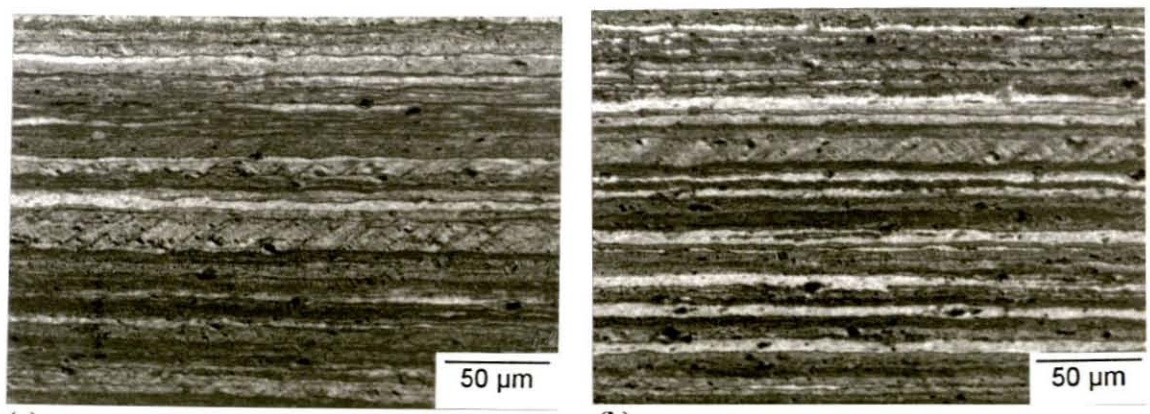

Figure 5.7 Optical micrographs showing the extent of shear banding following deformation at (a) an effective deformation temperature = 267°C and a strain rate of 0.1 s^{-1} (Z = $1.3x10^{14}$ s^{-1}) and (b) a deformation temperature = 350°C and an effective strain rate of 7.5 s^{-1} (Z = $9.2x10^{13}$). Strain of ε = 2.7 for both (a) and (b).

5.1.3.2 Flow Stress Measurements

The effect of strain rate on the amount of dynamic recovery can be further inferred from the variation of measured flow stress during PSC tests due to a change in strain rate. From Figure 5.8 it can seen how flow stress decreases as strain rate decreases, for a constant deformation temperature of 300°C, implying that a lower strain rate during PSC allows for more dynamic recovery. This trend is observable even though the effective deformation temperature decreases as strain rate decreases (i.e. the effective deformation temperature is 267°C as opposed to 300°C at 0.1 s^{-1}).

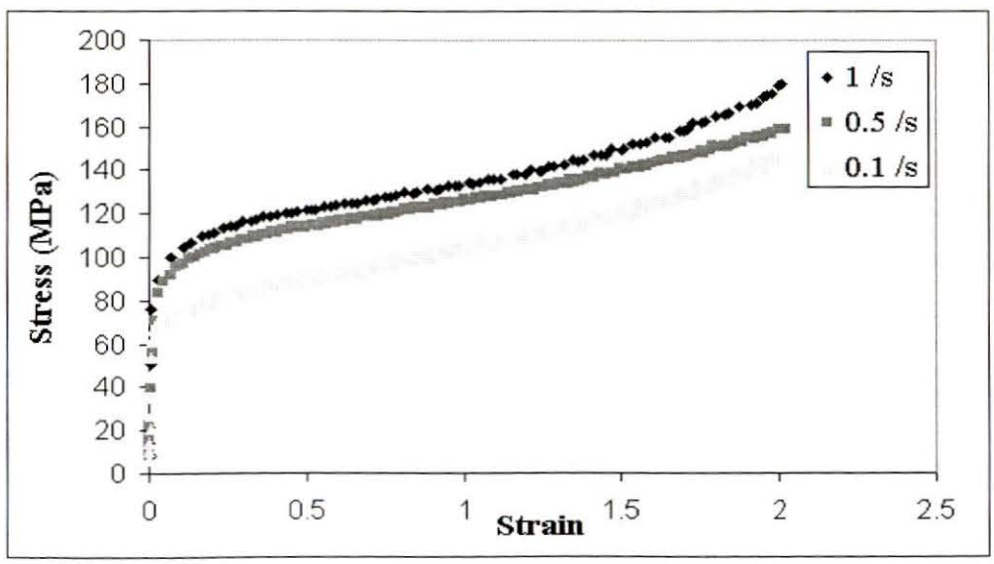

Figure 5.8 The influence of strain rate on flow stress during PSC (for a constant deformation temperature of 300°C).

5.1.3.3 Hardness Measurements

Hardness measurements as a function of both strain rate and deformation temperature (i.e. Z) are presented in Figure 5.9. The four deformation conditions represented correspond to deformation conditions of: temperature = 300° and strain rate = 1 s^{-1} ($Z = 1.7x10^{14}$), temperature = 267°C and strain rate = 0.1 s^{-1} ($Z = 1.3x10^{14}$), temperature = 350°C and strain rate = 7.5 s^{-1} ($Z = 9.2x10^{13}$), and temperature = 350°C and strain rate = 1 s^{-1} ($Z = 1.2x10^{13}$). These measurements were performed on as deformed PSC specimens after a strain of ε = 2.7. A similar trend compared to flow stress behaviour is observed as Z decreases. That is, a decrease in hardness is observed to occur as Z decreases. This further confirms the observation that dynamic recovery increases as Z decreases.

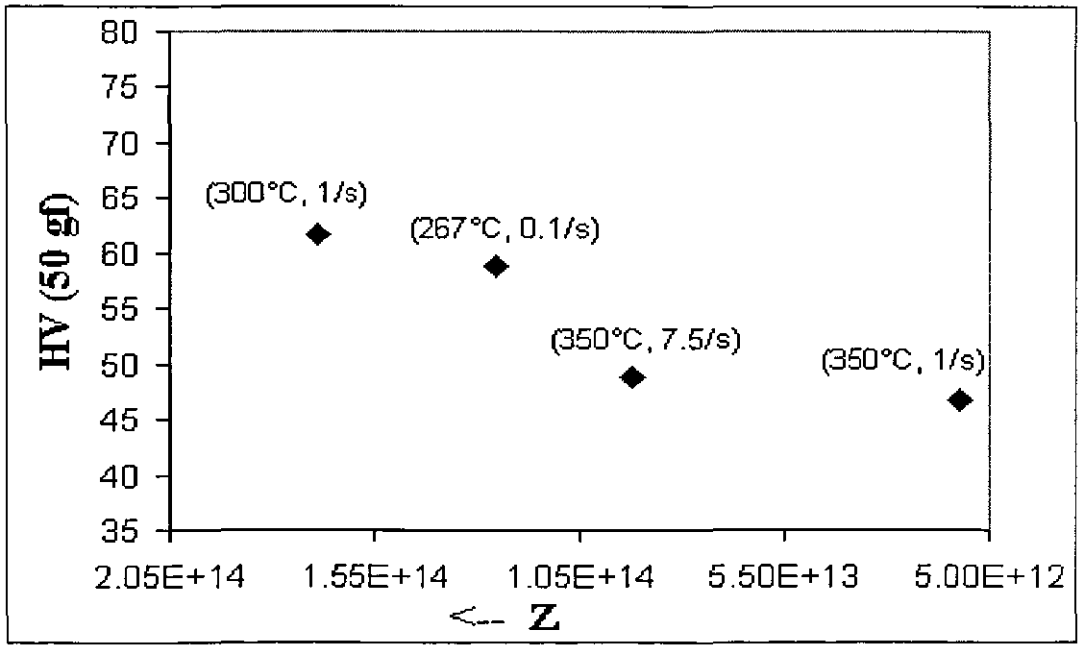

Figure 5.9 Measured hardness of as deformed specimens as a function of strain rate and deformation temperature, represented by Z (for a constant strain of ε = 2.7).

5.2 Deformation Textures

Deformation textures were measured from bulk X-ray diffraction measurements on as deformed (i.e. immediately quenched after deformation) PSC samples.

5.2.1 Starting Texture

As was discussed in detail previously (see section 3.1.2), the starting condition of the PSC specimens was characterised by a partially recrystallised microstructure following hot rolling and annealing. The texture of the starting material condition was measured by X-ray diffraction at the mid-thickness plane of the PSC specimens. An ODF representation of the measured texture is given in Figure 5.10, which reveals a fairly weak texture resulting from a mixture of deformation components (Brass, Copper and S) and recrystallisation components (a Cube texture with strong ND scattering and an enhanced Goss orientation).

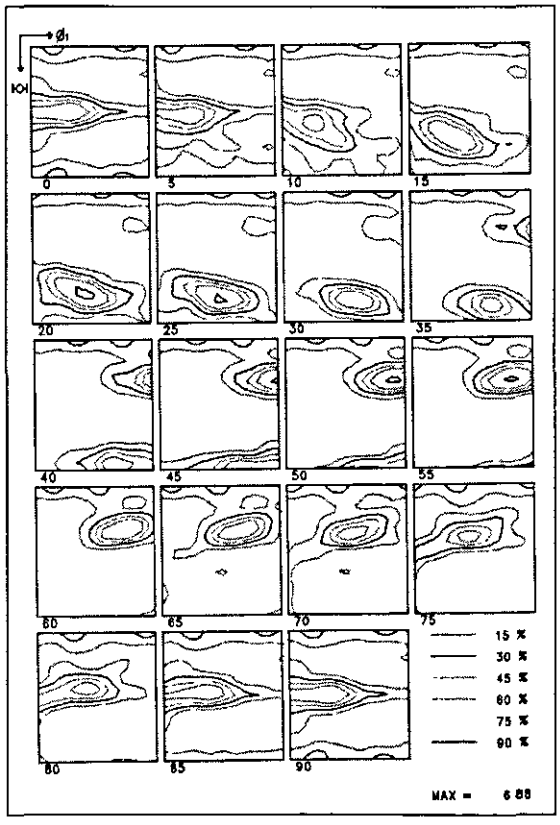

Figure 5.10 ODF bulk texture representation of starting material condition.

5.2.2 The Effect of Strain

The effect of the amount of strain on deformation texture was investigated by measuring the as deformed textures of PSC specimens deformed to strains of ε = 1.6, 2.7 and 3.1 (for a constant deformation temperature of room temperature and a constant strain rate of 1 s^{-1}). ODF plots representing deformation textures after strains of ε = 1.6 and ε = 3.1 are presented in Figure 5.11. The two ODF plots are very similar in appearance and there is not much difference in intensity levels. They both represent typical Copper deformation textures and also demonstrate a very long α-fibre (Goss to P). Furthermore, there is not much difference between the relative volumes of the different components of the deformation texture as a function of strain as is shown in Figure 5.12.

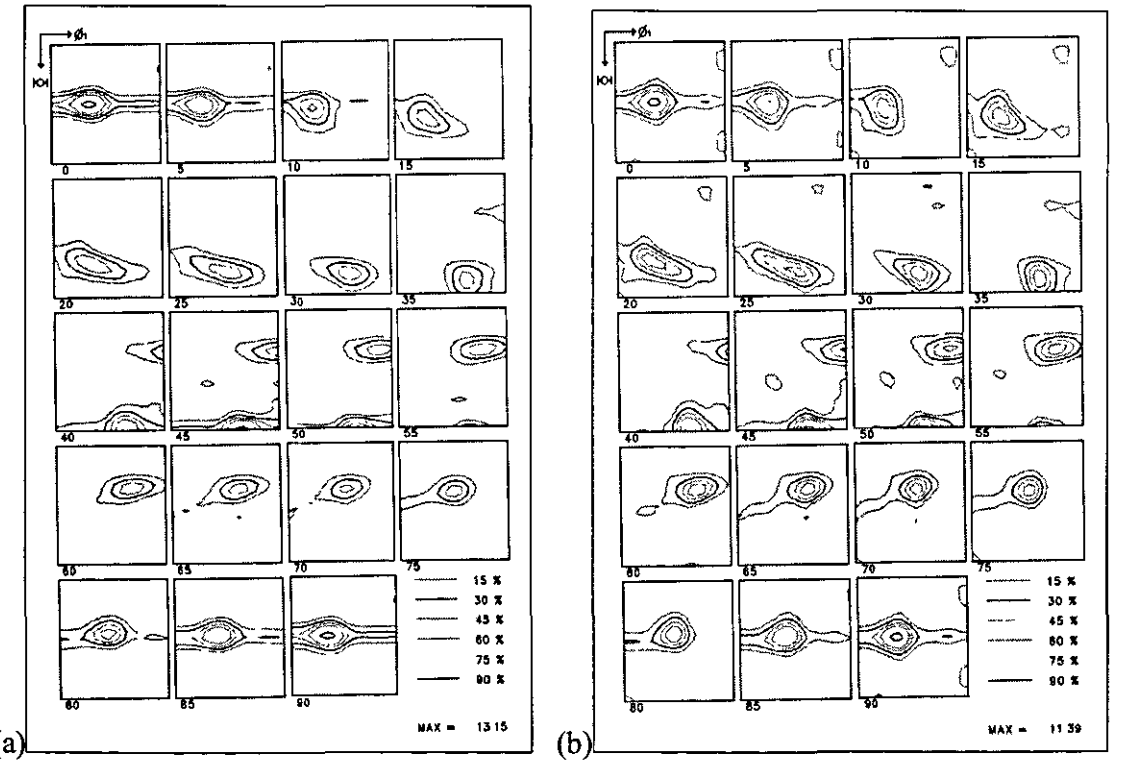

Figure 5.11 ODF plots representing as deformed textures after PSC tests to strains of (a) ε = 1.6 and (b) ε = 3.1, (for a constant deformation temperature = 25°C and a constant strain rate = 1 s^{-1}).

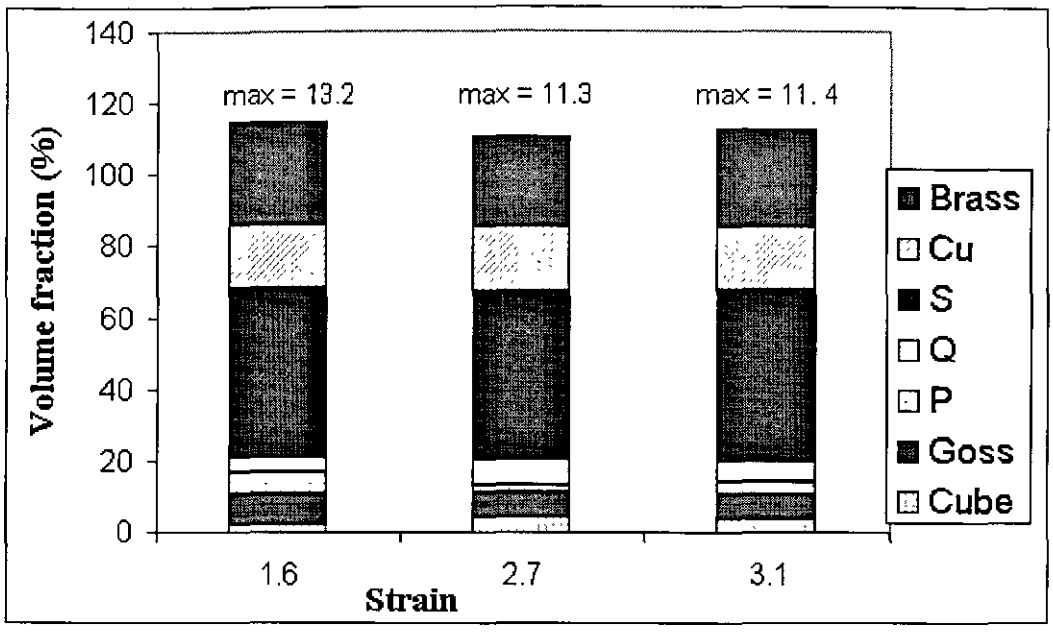

Figure 5.12 The effect of strain on the relative volumes of the different deformation texture components (constant deformation temperature = 25°C and constant strain rate = 1 s^{-1}). Max values refer to maximum intensity levels of corresponding ODF plots.

5.2.3 The Effect of Deformation Temperature

The effect of deformation temperature on deformation texture was investigated by measuring the as deformed textures of PSC specimens deformed at temperatures of room temperature, 300°C, 350°C and 400°C (for a constant strain amount of $\varepsilon = 2.7$ and at a constant strain rate of 1 s^{-1}). ODF plots representing the deformation textures of the two extreme values (room temperature and 400°C) of deformation temperature are shown in Figure 5.13. There is little difference in terms of the general appearance of the two plots. Both represent a typical copper deformation texture with strong peaks apparent around the Brass orientation and weaker peaks around the P and Goss ideal orientations. There are certainly no signs of recrystallisation texture components in Figure 5.13b (corresponding to deformation at 400°C). The main difference between the two plots is that of measured intensity. The plot corresponding to deformation at room temperature (Figure 5.13a) has a maximum intensity level of 11.3 times random, while the plot corresponding to deformation at 400°C (Figure 5.13b) has a maximum intensity level of 21.1 times random. These observations are reinforced by a plot of the relative values of the various deformation texture components as a function of deformation temperature (Figure 5.14). From this plot it can be observed that the main deformation texture components (especially the S and

Brass components) increase as deformation temperature increases. There is no measurable variation of the Q, P, Goss and Cube components as a function of deformation temperature.

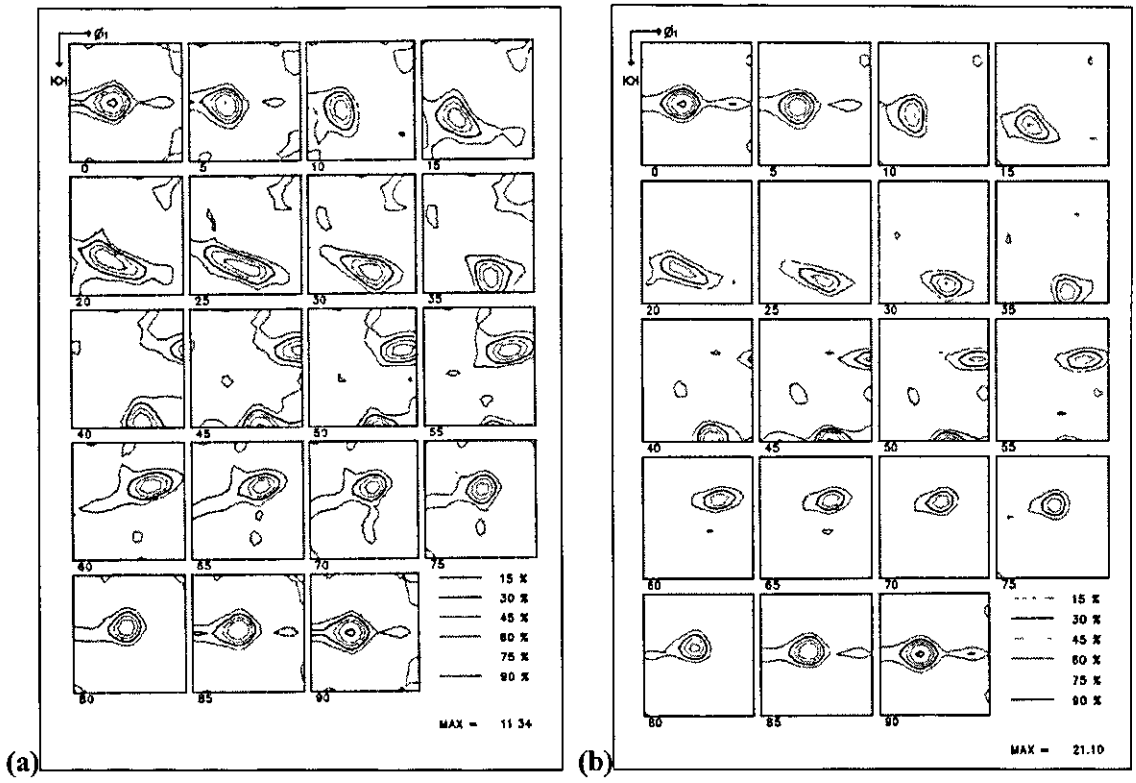

Figure 5.13 ODF plots representing as deformed textures after PSC tests at deformation temperatures of (a) room temperature and (b) 400°C, (for a constant strain of ε = 2.7 and at a constant strain rate of 1 s^{-1}).

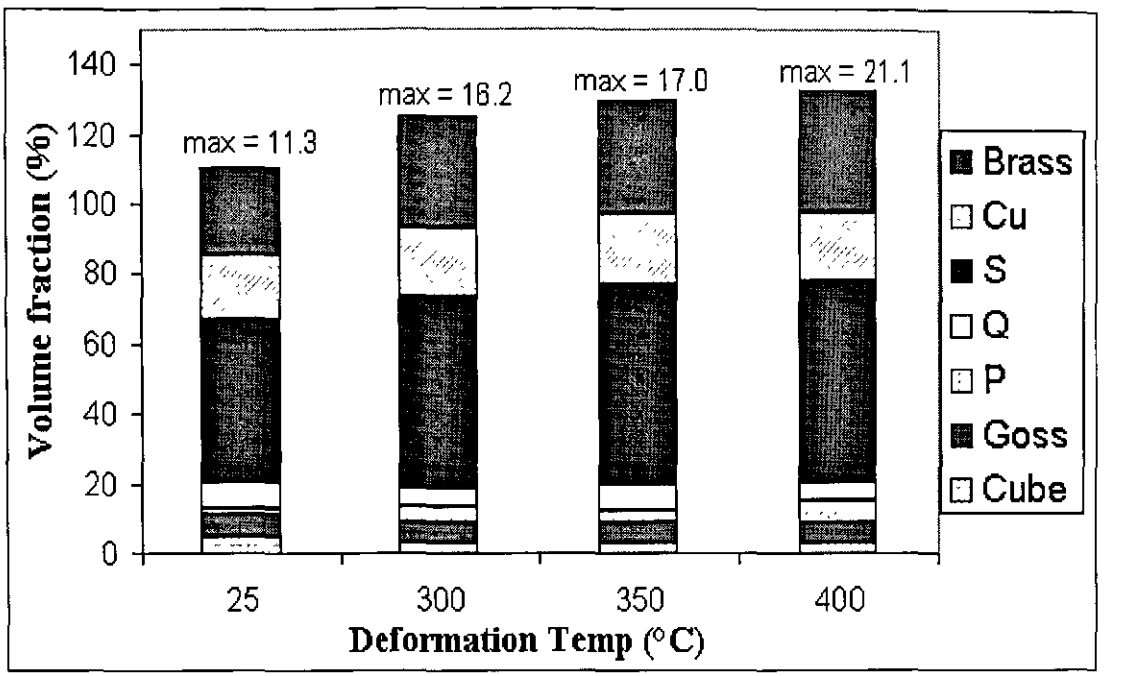

Figure 5.14 The effect of deformation temperature on the volumes of the different deformation texture components (for a constant strain of $\varepsilon = 2.7$ and a constant strain rate = 1 s^{-1}). Max values refer to maximum intensity levels of corresponding ODF plots.

5.3 Recrystallisation Behaviour

5.3.1 Grain Nucleation at Shear Bands

5.3.1.1 Recrystallisation Kinetics

In order to investigate grain nucleation at shear bands following deformation it was necessary to investigate specimens in a partially recrystallised state. To achieve such a state, specimens were subjected to a very short controlled "flash anneal" in a salt bath. The time of the anneal was determined by the recrystallisation kinetics of the particular specimen. Some idea of the recrystallisation kinetics for an annealing temperature of 420°C is given in Figure 5.15. It must be stressed that the inclusion of Figure 5.15 is not an attempt to represent an accurate account of the kinetics of the indicated deformation conditions, due to a low number of data points and an estimation of recrystallised volume fraction. Rather, it serves to indicate the narrow time window available, in terms of annealing time, to achieve a suitable partially recrystallised state. For example, for

deformation conditions of strain $\varepsilon = 2.7$, strain rate = 1 s^{-1} and deformation temperature = room temperature, the time window is approximately 5 seconds. If an ideal partially recrystallised state is defined as between 25 and 65 % recrystallised (when a sufficient quantity of new grains have nucleated and their relationship to the old deformed grains can still be observed), then this time window is further reduced. For the above example, the time window would thus be reduced to approximately 2 seconds. For higher annealing temperatures the effective time window would be even less.

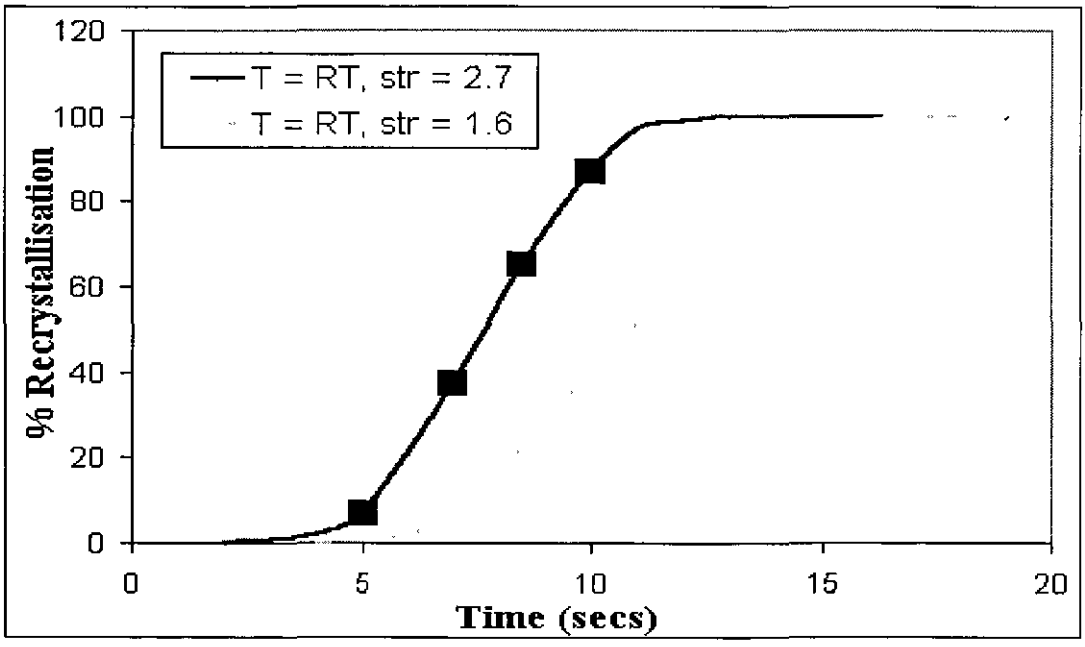

Figure 5.15 An indication of the recrystallisation kinetics for the deformation conditions indicated (annealing temperature = 420°C).

5.3.1.2 Optical Observations

Good evidence of grain nucleation at shear bands was obtained from optical microscopy performed on specimens in partially recrystallised states following deformation at conditions that favoured strong shear band development. Several examples of grain nucleation at shear bands are presented in Figure 5.16. Figure 5.16a represents a typical partially recrystallised microstructure where new small equiaxed grains can be seen to have nucleated at various positions in relation to the old deformed highly elongated grain structure. Grains that appeared to have nucleated at shear bands are shown in Figure 5.16(b-d), while grains at the very beginning stages of nucleation at shear bands are shown in Figure 5.16e and Figure 5.16f.

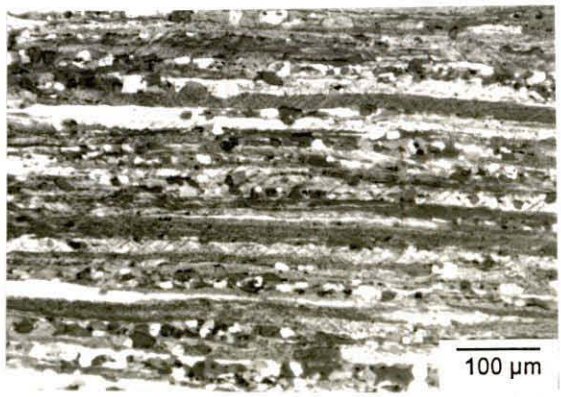

(a)

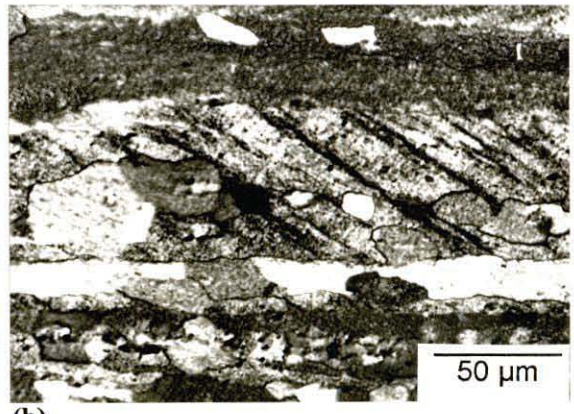

(b)

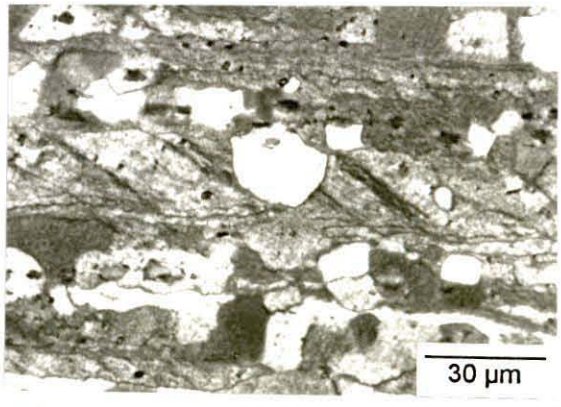

(c)

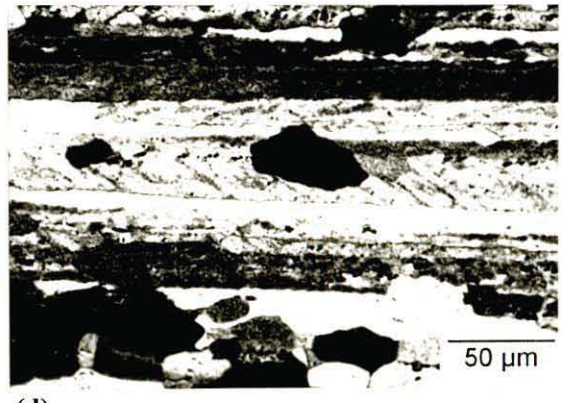

(d)

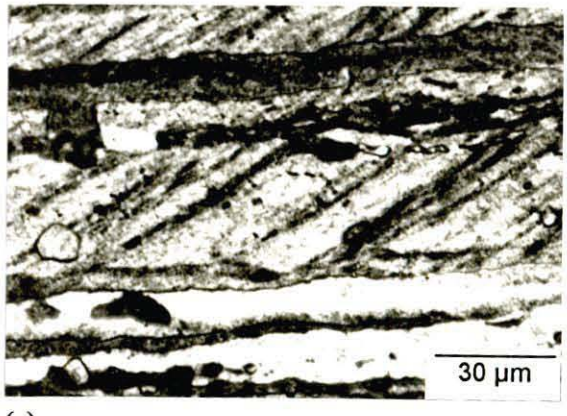

(e)

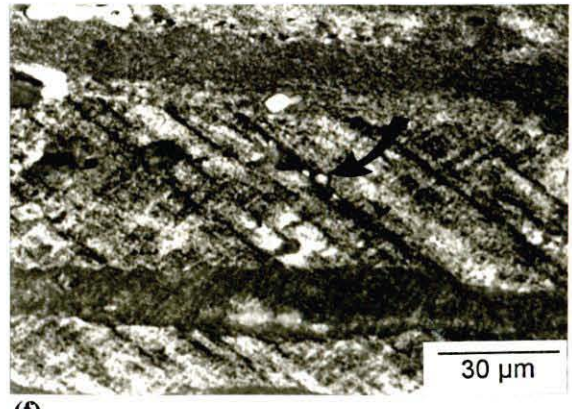

(f)

Figure 5.16 Optical micrographs showing evidence of grain nucleation at shear bands. (a) is a typical example of a partially recrystallised microstructure, (b)-(d) show grains that appear to have nucleated at shear bands and (e) and (f) show grains at the beginning stages of nucleation at shear bands (eg grain indicated by arrow in (f)).

5.3.1.3 Local Orientation Measurements

An attempt was made at measuring the orientations of individual grains thought to have nucleated at shear bands using the SEM based EBSD technique. For a particular field of view, orientation images were built up from electron channelling contrast (ECC) images and in most cases a corresponding optical image. Examples of these images are presented in Figure 5.17 - Figure 5.22. The orientations of particular grains that were measured were related to ideal orientations if the misorientation between the orientation of the measured grain and the orientation of the ideal orientation was less than 15°. The following indexing system was employed: R: Retained rolling, Q: Q, P: P, G: Goss, C: Cube including scatterings around both ND and RD (i.e. $Cube_{ND}$ and $Cube_{RD}$), X: Random. Figure 5.17 - Figure 5.22 reveal no or little evidence of any preferred orientation of grains nucleating at shear bands. In fact, most of the grains that can clearly be seen to have nucleated at shear bands have a random orientation. There is perhaps some evidence of a very weak preference of near Goss and Q orientated grains nucleating at shear bands (see especially Figure 5.17 - Figure 5.20)

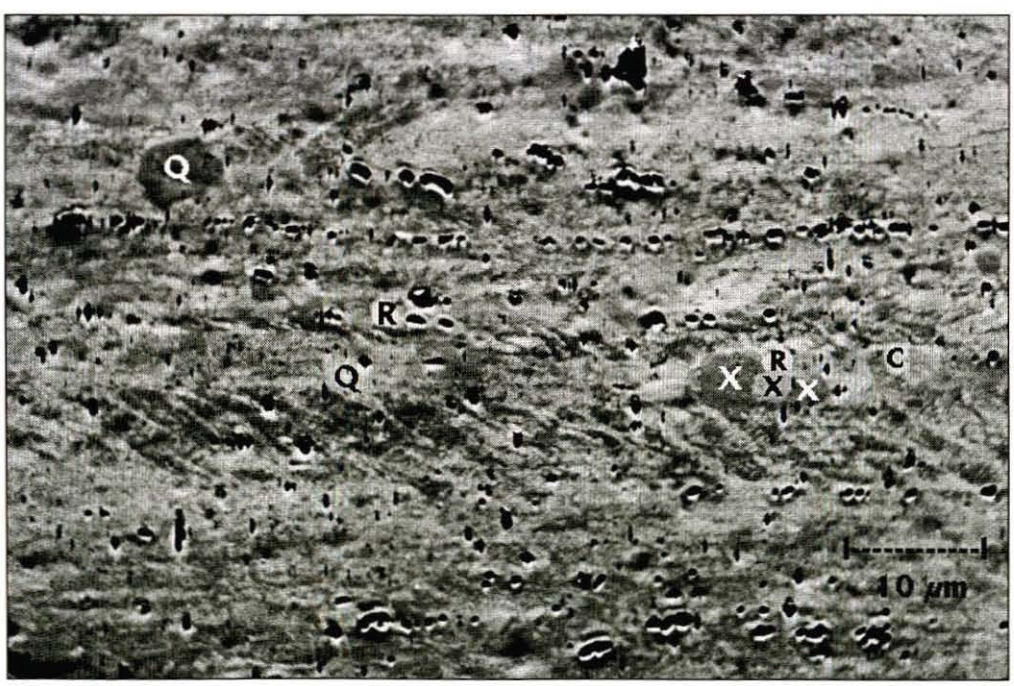

Figure 5.17 ECC orientation image of partially recrystallised PSC specimen. (PSC at room temperature, at a strain rate of 1 s^{-1} and to a strain of $\varepsilon = 1.6$. Annealing at 420°C for 10 secs).

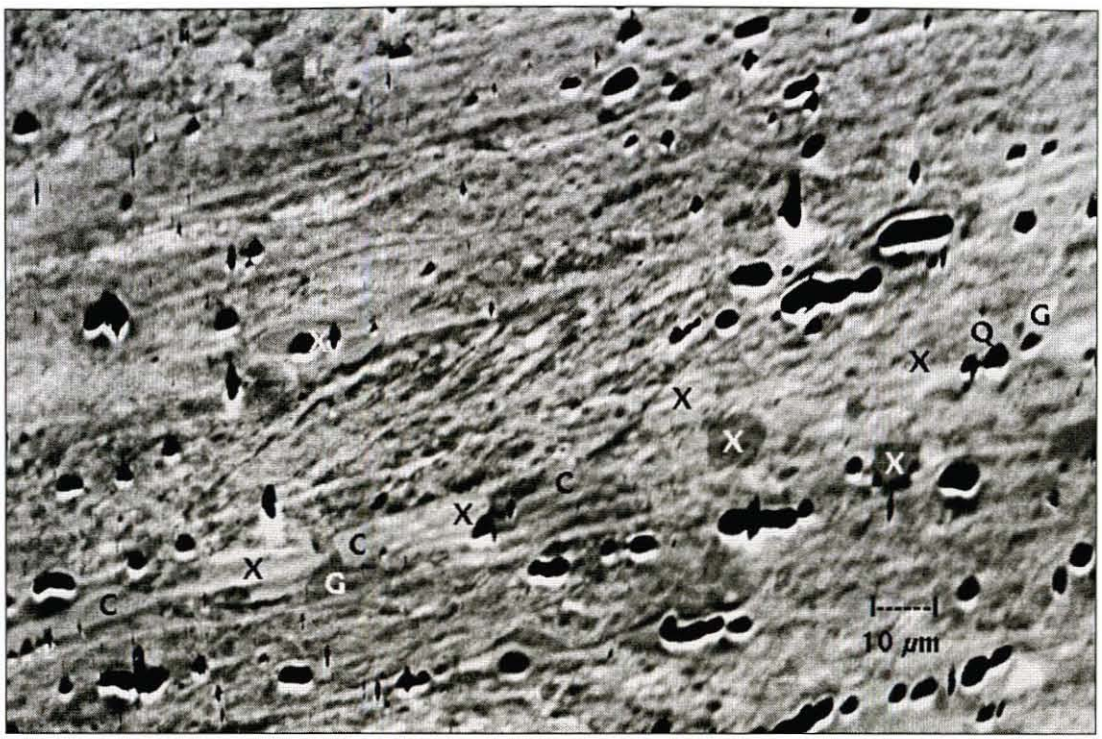

(a)

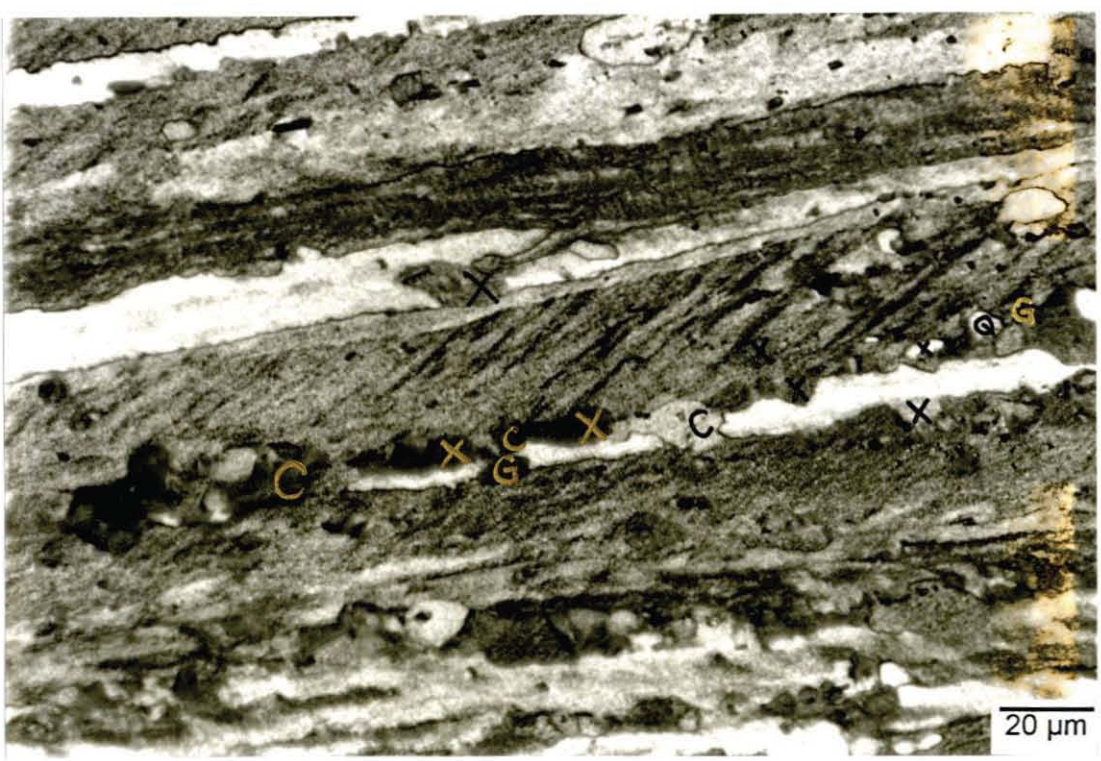

(b)

Figure 5.18 (a) ECC and (b) optical orientation images of the same field of view of partially recrystallised PSC specimen (PSC at room temperature, at a strain rate of 1 s^{-1} and to a strain of $\varepsilon = 1.6$. Annealing at 420°C for 10 secs).

(a)

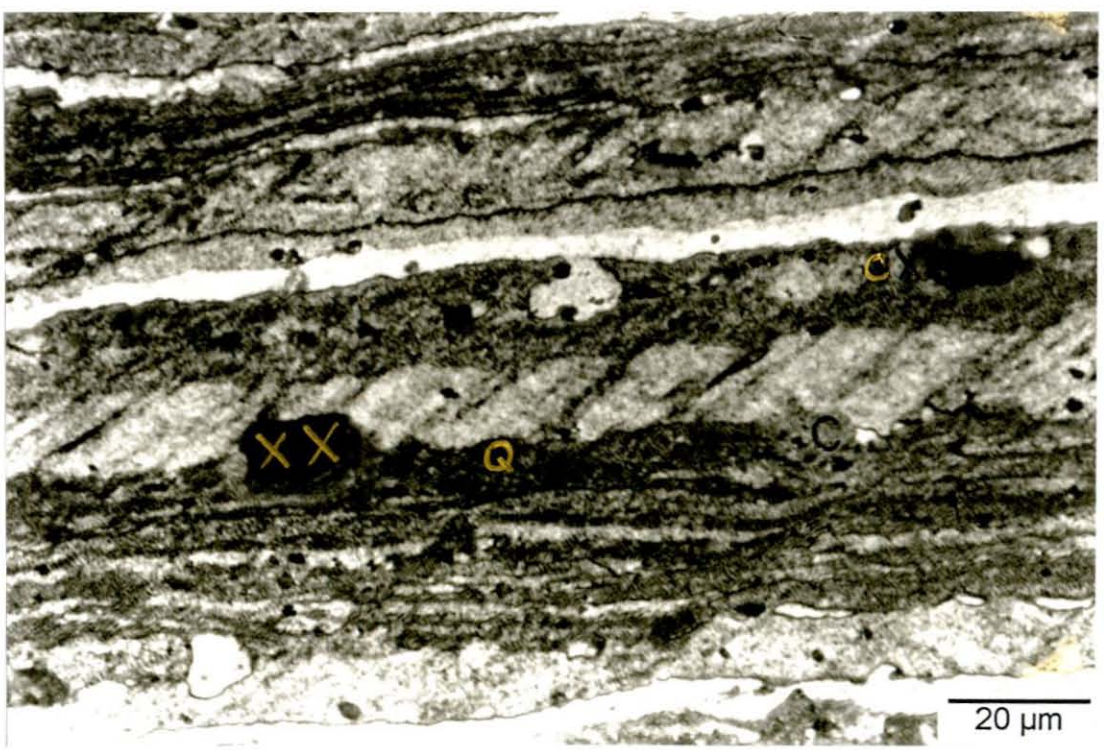

(b)

Figure 5.19 (a) ECC and (b) optical orientation images of the same field of view of partially recrystallised PSC specimen (PSC at room temperature, at a strain rate of 1 s^{-1} and to a strain of $\varepsilon = 2.7$. Annealing at 420°C for 7 secs).

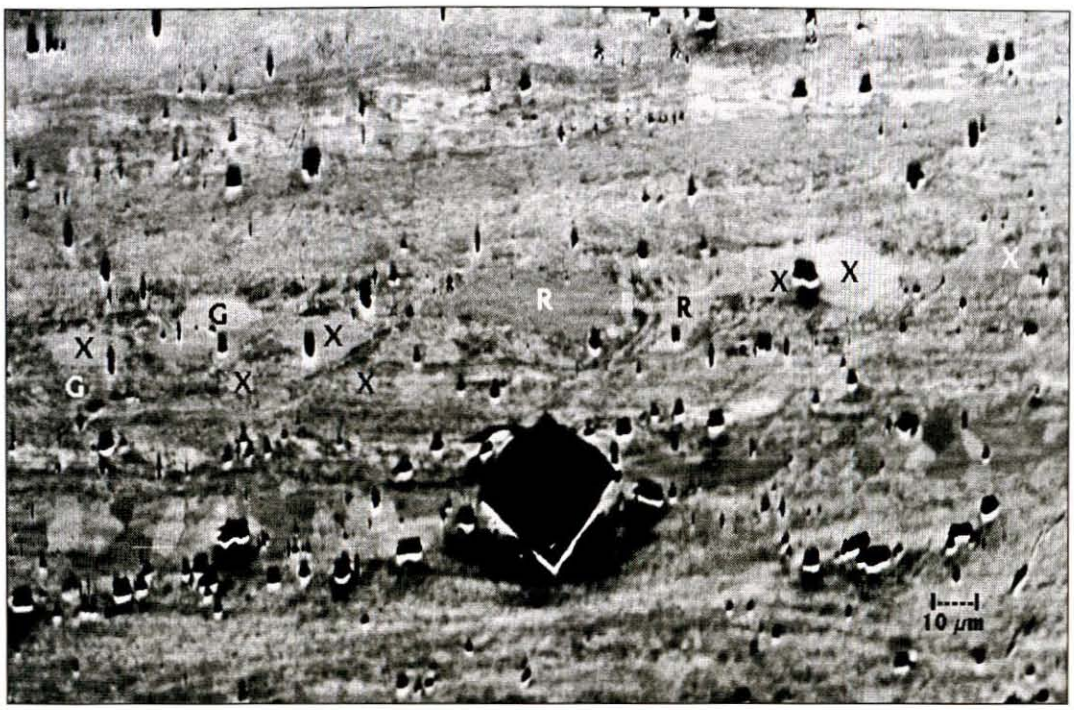

(a)

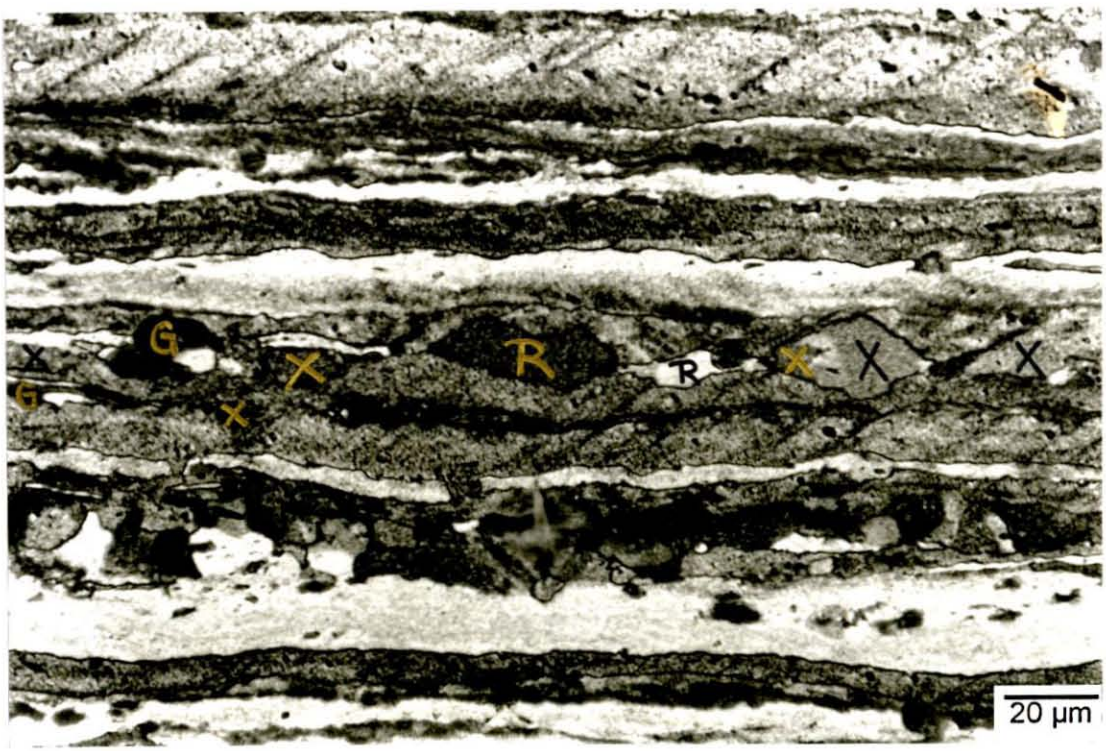

(b)

Figure 5.20 (a) ECC and (b) optical orientation images of the same field of view of partially recrystallised PSC specimen (PSC at room temperature, at a strain rate of 1 s^{-1} and to a strain of $\varepsilon = 2.7$. Annealing at 420°C for 7 secs). Note the micro-hardness indentation mark visible in the lower half of both (a) and (b) that acted as a navigation guide for finding the same field of view.

(a)

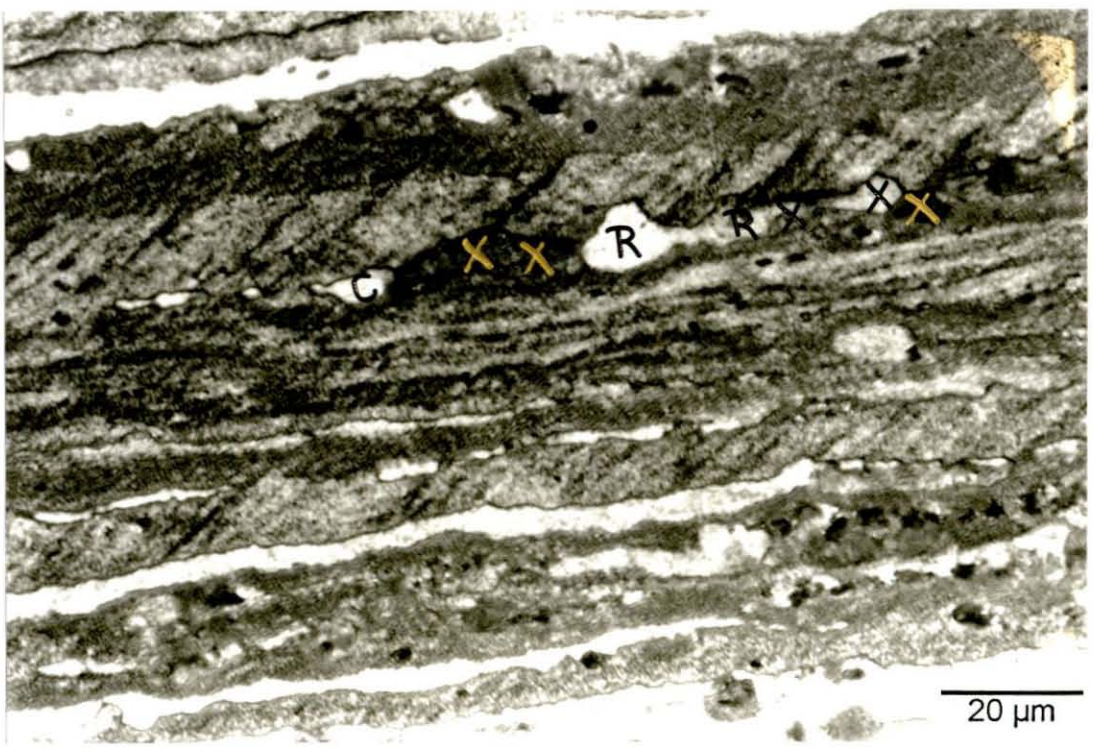

(b)

Figure 5.21 (a) ECC and (b) optical orientation images of the same field of view of partially recrystallised PSC specimen (PSC at room temperature, at a strain rate of 1 s^{-1} and to a strain of $\varepsilon = 2.7$. Annealing at 420°C for 7 secs).

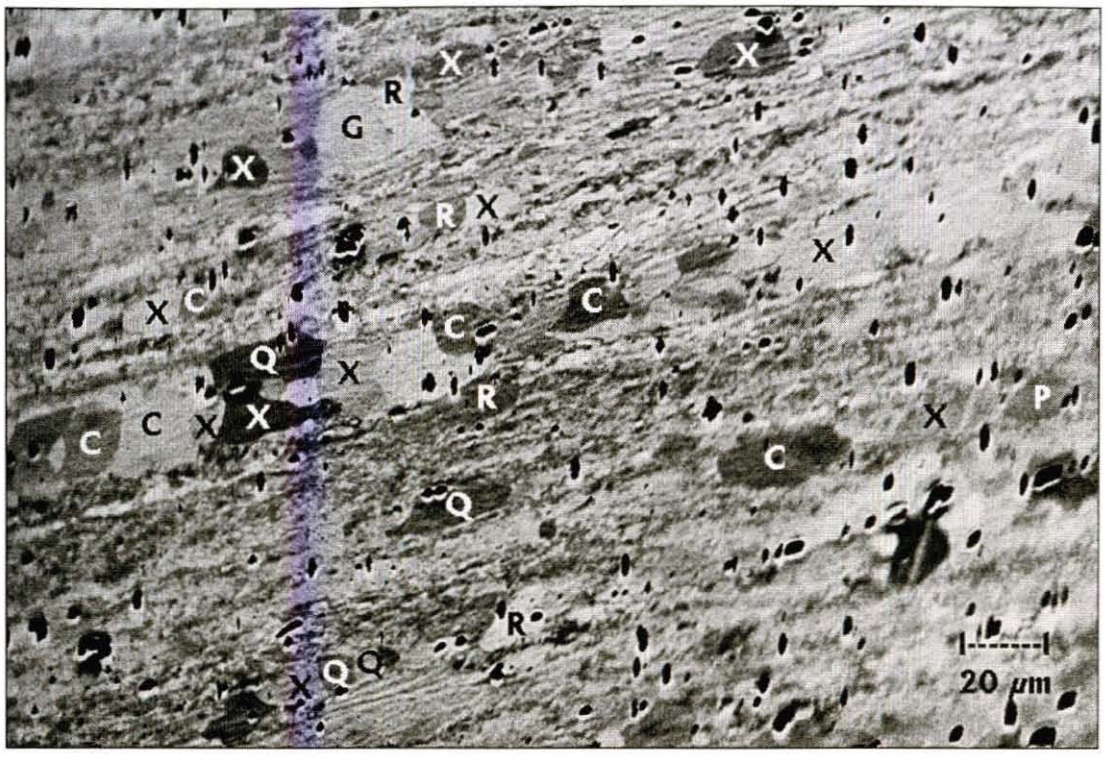

(a)

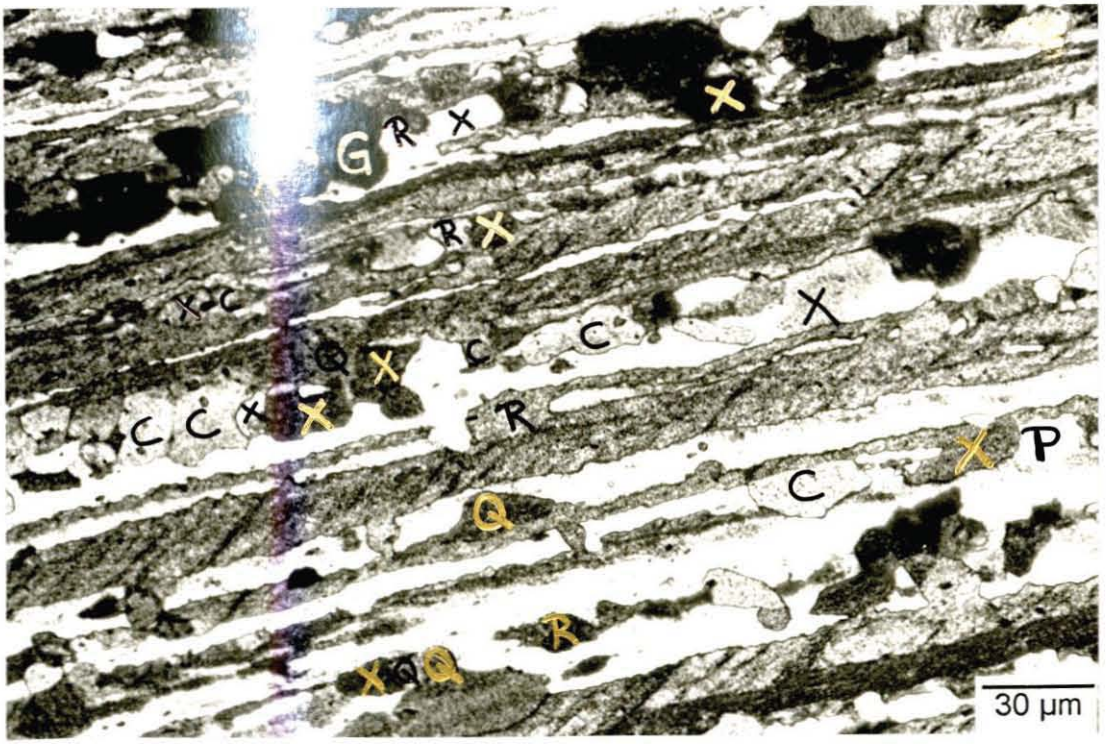

(b)

Figure 5.22 (a) ECC and (b) optical orientation images of the same field of view of partially recrystallised PSC specimen (PSC at room temperature, at a strain rate of 1 s^{-1} and to a strain of $\varepsilon = 2.7$. Annealing at 420°C for 8.5 secs).

might be as a result of these orientated grains nucleating in localised regions containing shear bands.

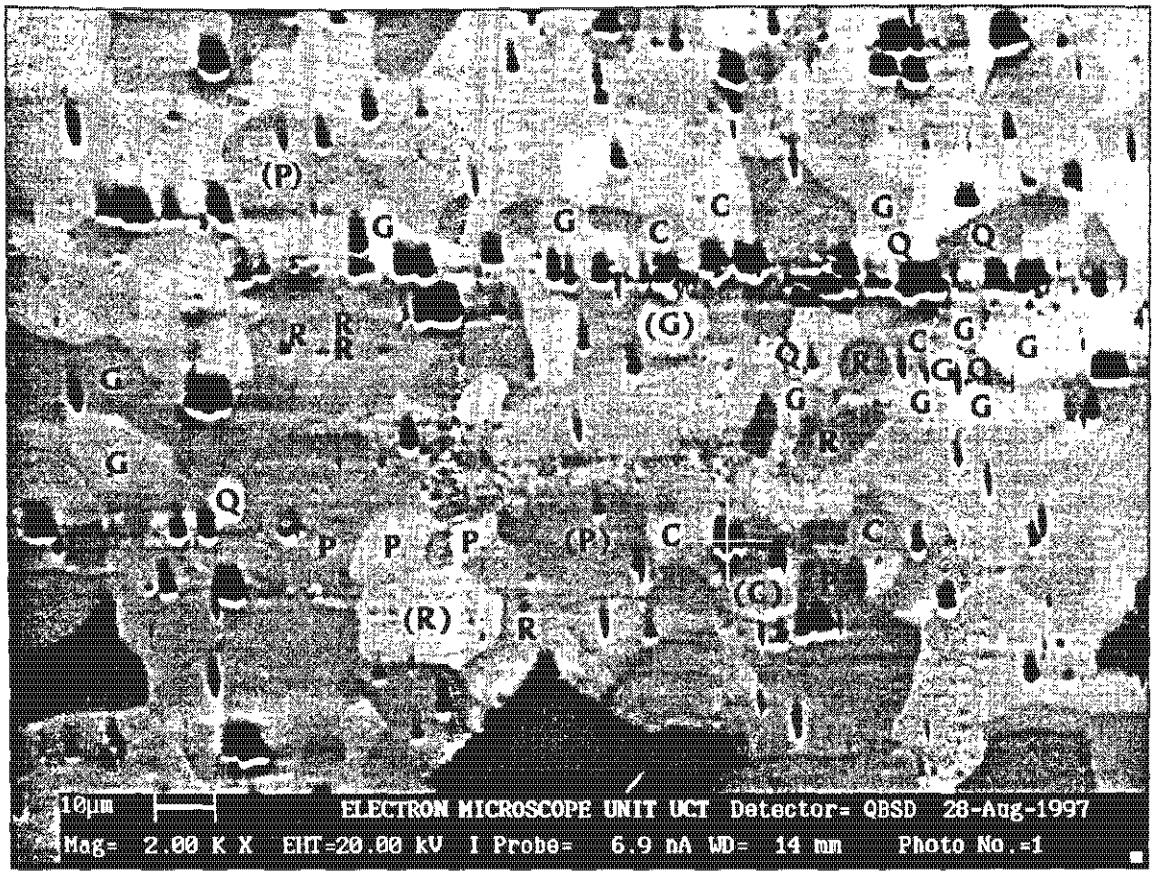

Figure 5.24 ECC orientation image of an almost fully recrystallised PSC specimen (PSC at room temperature, at a strain rate of 1 s^{-1} and to a strain of $\varepsilon = 2.7$. Annealing at 420°C for 10 secs). Letters in brackets reflect a misorientation of between 15° and 20° with the particular ideal orientation.

5.3.2 Bulk Recrystallisation Textures

5.3.2.1 Annealing Conditions

The bulk texture of fully recrystallised conditions was determined from X-ray diffraction measurements performed at the mid-thickness plane of deformed and annealed PSC specimens. The standard annealing condition for most samples consisted of a 3 minute anneal at 420°C in a salt bath unless otherwise indicated.

5.3.2.2 The Effect of Strain

The effect of the amount of strain on recrystallisation textures was investigated by measuring the textures of annealed PSC specimens deformed to strains of ε = 1.6, 2.7 and 3.1 (PSC tests conducted at room temperature and at a strain rate of 1 s^{-1}). ODF plots corresponding to strains of ε = 1.6 and 3.1 are presented in Figure 5.25a and Figure 5.25b respectively. These two plots both represent weak recrystallisation textures with peaks around the Cube, R and, to a lesser extent, Goss, P and Q ideal orientations noticeable. There are no significant differences observable between them. A plot of the relative volume fractions of the different recrystallisation texture components as a function of strain is given in Figure 5.26. There is not much variation of the different components as a function of strain, other than a small increase in the P and Goss components with strain.

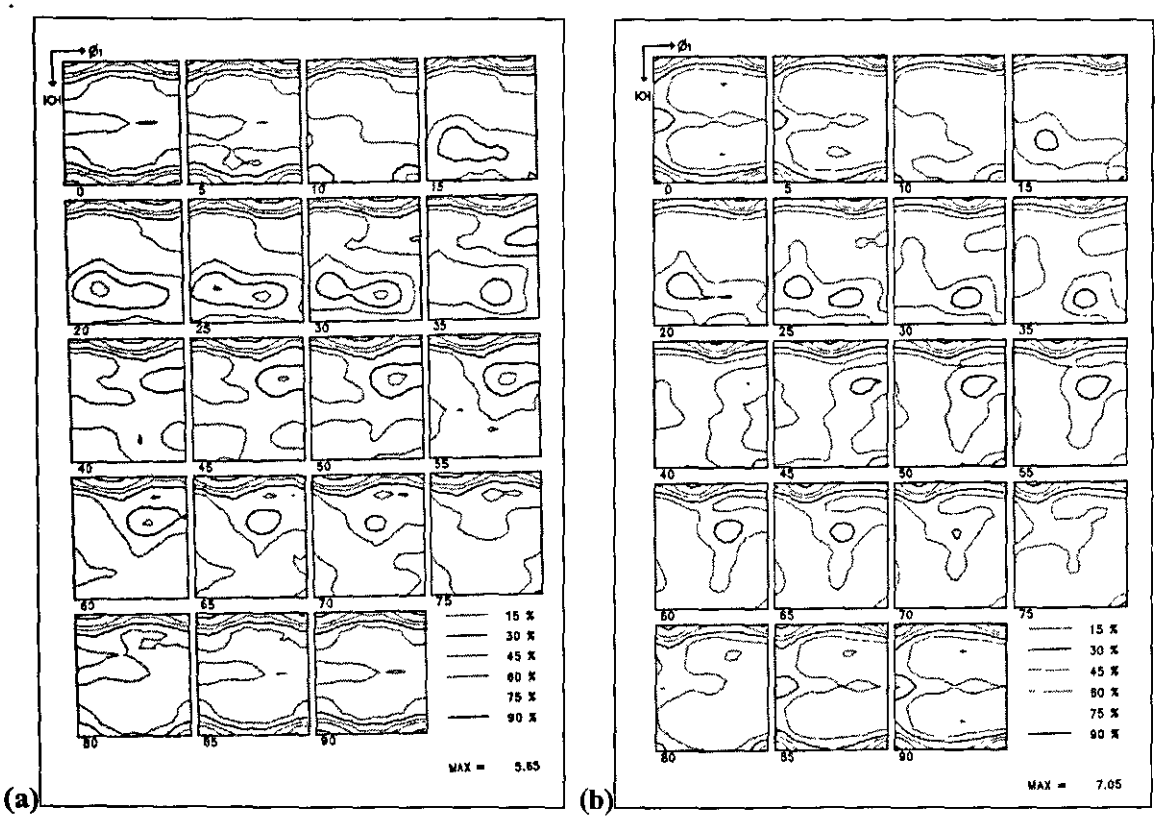

Figure 5.25 ODF plots representing recrystallised textures after annealing subsequent to PSC at (a) a strain of ε = 1.6 and (b) a strain of ε = 3.1, (for a constant deformation temperature = room temperature and at a constant strain rate of 1 s^{-1}).

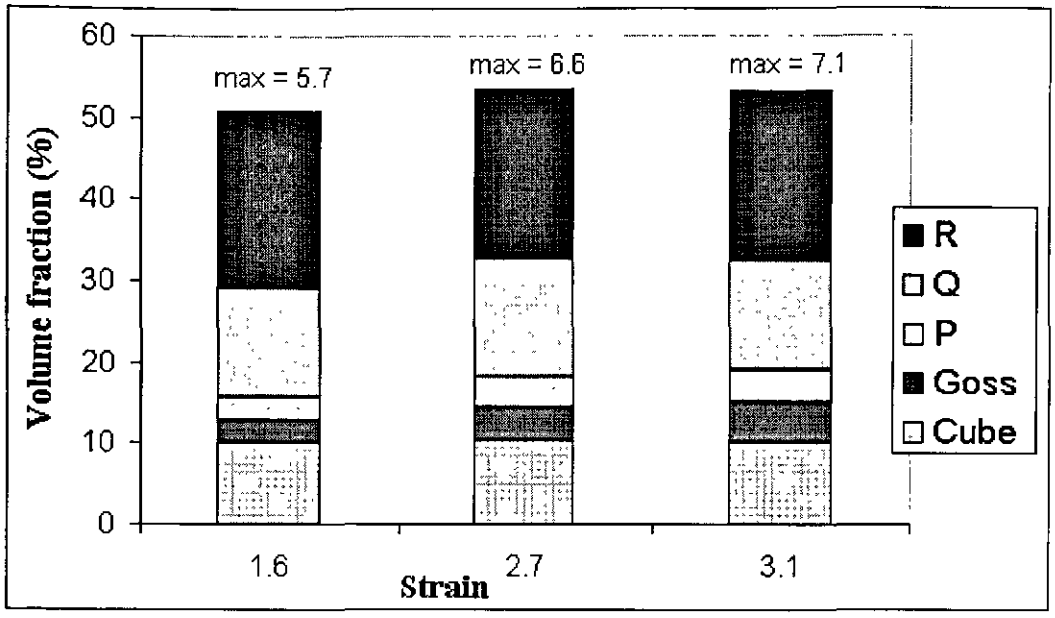

Figure 5.26 The effect of strain on the relative volumes of the different recrystallisation texture components (for a constant deformation temperature = room temperature and for a constant strain rate = 1 s^{-1}). Max values refer to maximum intensity levels of corresponding ODF plots.

5.3.2.3 The Effect of Deformation Temperature

The effect of deformation temperature on recrystallisation texture was investigated by measuring the bulk textures of annealed PSC specimens deformed at temperatures in the range between room temperature and 400°C for strain amounts of both $\varepsilon = 2.7$ and $\varepsilon = 1.6$ (at a constant strain rate of 1 s^{-1}). It was found that deformation temperature had a significant effect on recrystallisation texture and this effect was more marked at the higher strain of $\varepsilon = 2.7$.

ODF plots representing the recrystallised textures of specimens deformed at room temperature, 300°C, 350°C and 400°C (to a strain of $\varepsilon = 2.7$) are included in Figure 5.28. A distinct difference between the plots corresponding to deformation temperatures of room temperature and 400°C (Figure 5.28a and Figure 5.28d respectively) can be noticed. Figure 5.28a represents a weak recrystallisation texture (maximum intensity level = 6.6) with peaks observable around the Cube, R, Goss, P and Q orientations. Figure 5.28d, in comparison, represents a strong recrystallisation texture (maximum intensity level = 45.6) that is dominated by a strong Cube component with very weak peaks around the R and Goss orientations. The ODF plot corresponding to a deformation temperature of 300°C,

with a maximum intensity level = 14.9, (Figure 5.28b) more closely resembles Figure 5.28a than Figure 5.28d. However, the plot corresponding to a deformation temperature of 350°C, with a maximum intensity level = 49.2, more closely resembles Figure 5.28d than Figure 5.28a. These observations are further supported by a plot (Figure 5.27) of the relative volumes of the different recrystallisation texture components as a function of deformation temperature at a constant strain of $\varepsilon = 2.7$. From this plot it can be seen that there is a dramatic increase in the Cube volume fraction as the deformation temperature increases from 300°C to 350°C. At deformation temperatures of 300°C and below the Cube volume fraction remains relatively low (less than 18 %), while at higher deformation temperatures (350°C and 400°C) the Cube volume fraction is significantly higher (about 45%). A similar dependence of the Goss volume fraction with deformation temperature, compared to the Cube volume fraction, can be observed although it is not nearly as marked as that of the Cube. A very small decrease in the Q and P volume fractions as a function of increasing deformation temperature could possibly be inferred from Figure 5.27, while it would seem that the R volume fraction is stable as a function of deformation temperature.

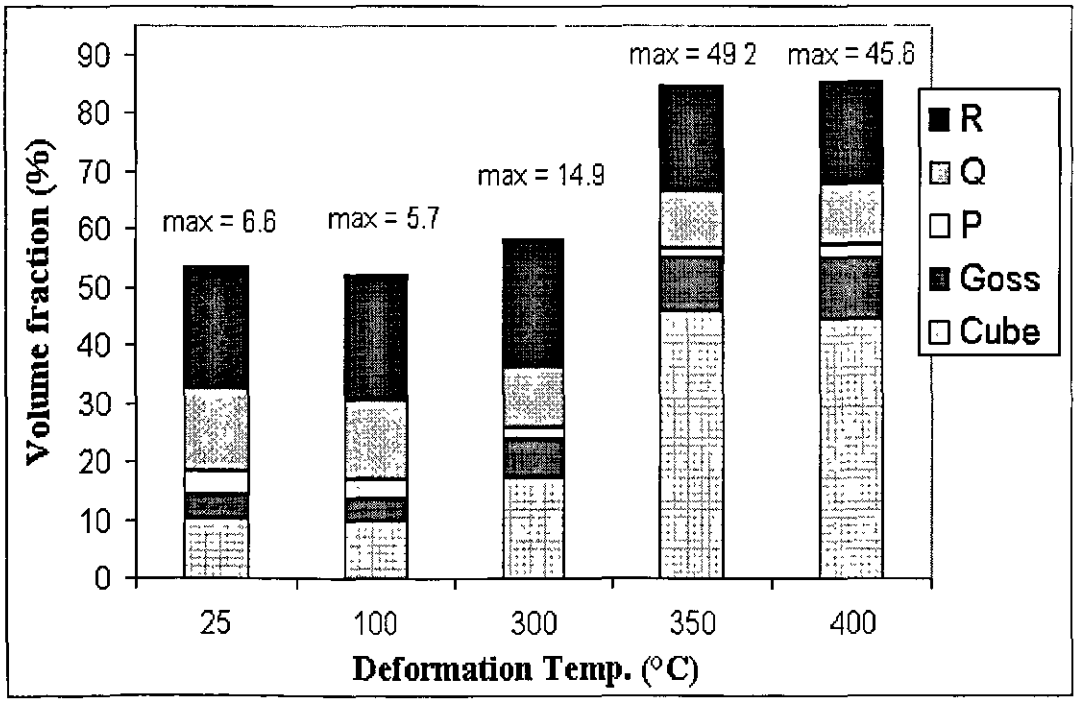

Figure 5.27 The effect of deformation temperature on the relative volumes of the different recrystallisation texture components (to a constant strain $\varepsilon = 2.7$ and for a constant strain rate = 1 s^{-1}). Max values refer to maximum intensity levels of corresponding ODF plots.

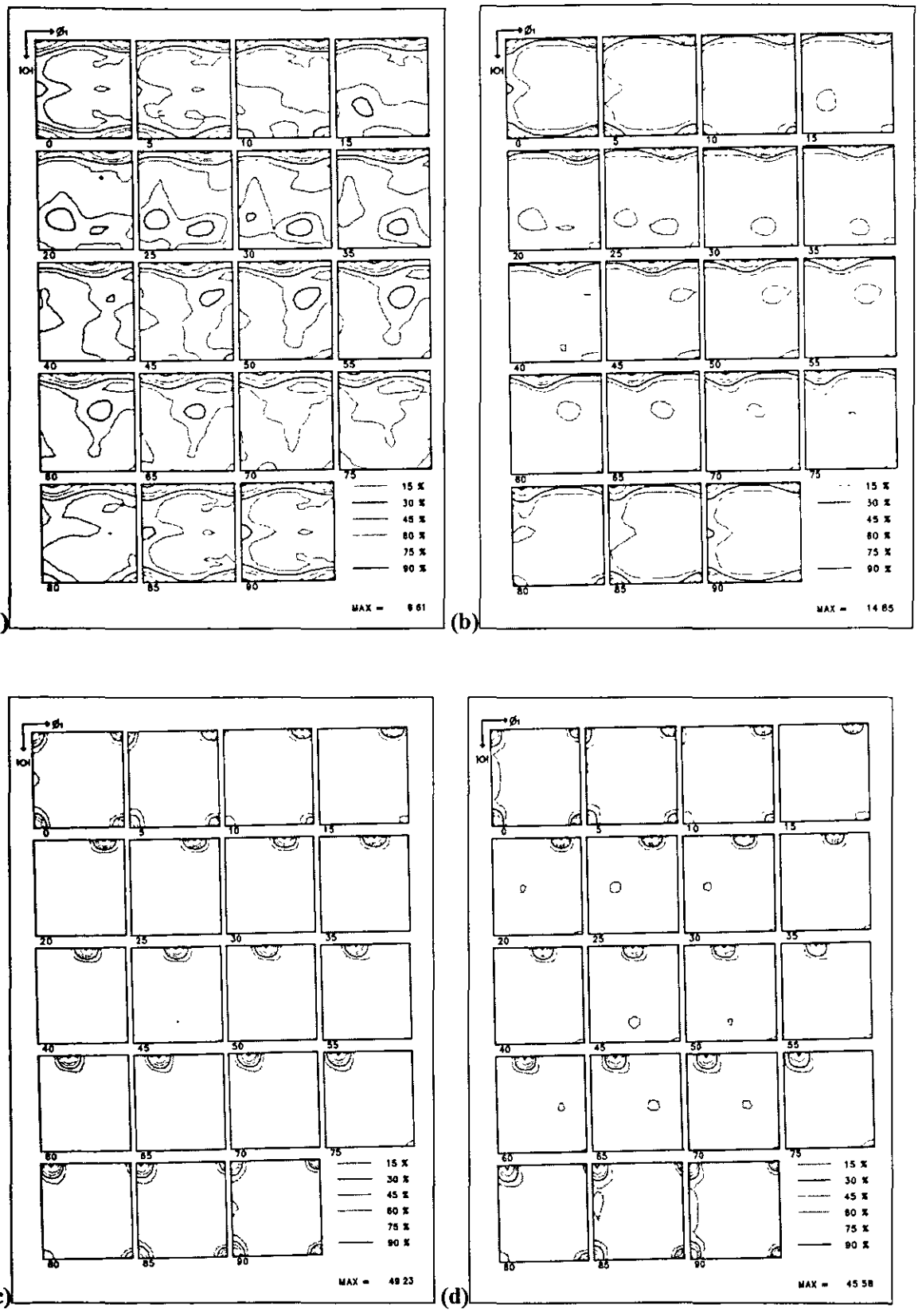

Figure 5.28 ODF plots representing recrystallised textures after annealing subsequent to PSC at deformation temperatures of (a) room temperature, (b) 300°C, (c) 350°C and (d) 400°C (to a constant strain $\varepsilon = 2.7$ and at a constant strain rate of 1 s^{-1}).

The recrystallised textures of specimens deformed at 300°C and 350°C, to a strain of ε = 1.6, are represented by ODF plots in Figure 5.29a and Figure 5.29b respectively. These two plots show a substantial difference in recrystallisation texture caused by an increase in deformation temperature of only 50°C in line with the plots for the higher strain of ε = 2.7. The maximum intensity level of Figure 5.29b is equal to 23 times random, which is more than double the value corresponding to Figure 5.29a (11.1 times random). Figure 5.30 summarises the differences in the relative amounts of the different recrystallisation components for PSC tests conducted at room temperature, 300°C, 350°C and 400°C (to a strain of ε = 1.6). Compared to the plot for ε = 2.7 (Figure 5.27), Figure 5.30 shows a similar increase of the Cube texture component with increasing deformation temperature. Again a significant increase in Cube volume fraction as deformation temperature increases from 300°C to 350°C can be observed, although this increase is not as dramatic as that observed in Figure 5.27. A similar increase of the Goss component with increasing deformation temperature can also observed from Figure 5.30. A decrease in the Q component with increasing deformation temperature might be noticed as well.

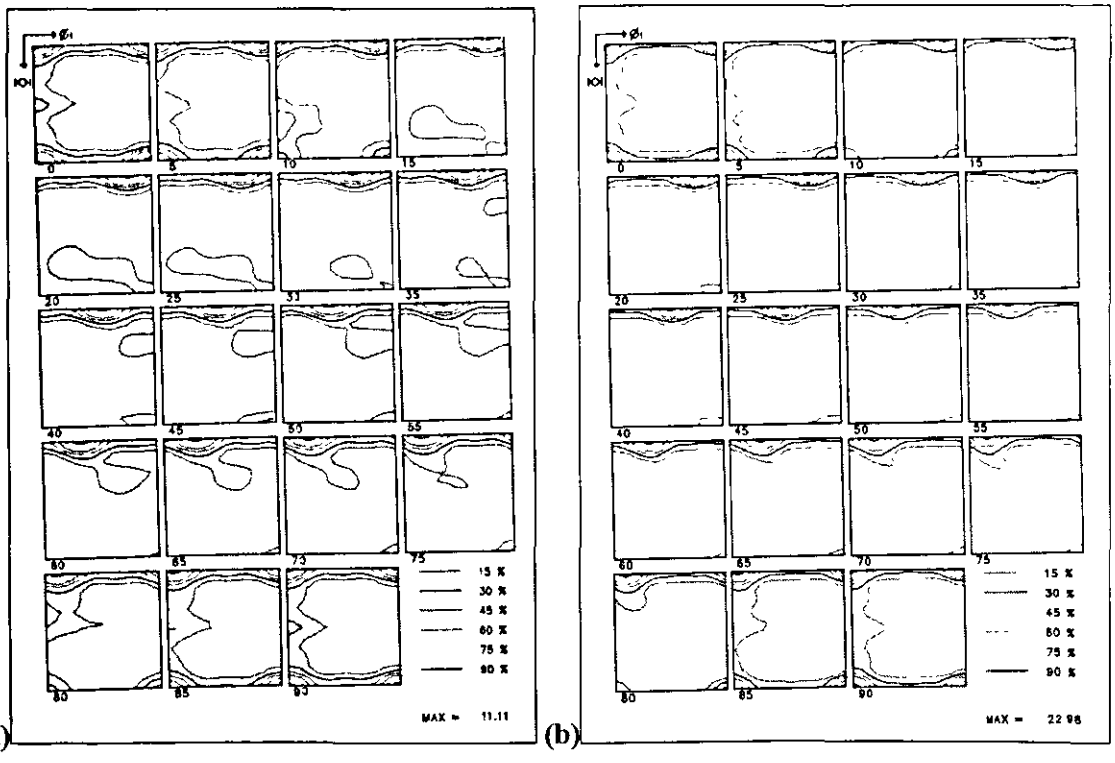

Figure 5.29 ODF plots representing recrystallised textures after annealing subsequent to PSC at deformation temperatures of (a) 300°C and (b) 350°C (to a constant strain ε = 1.6 and at a constant strain rate of 1 s^{-1}).

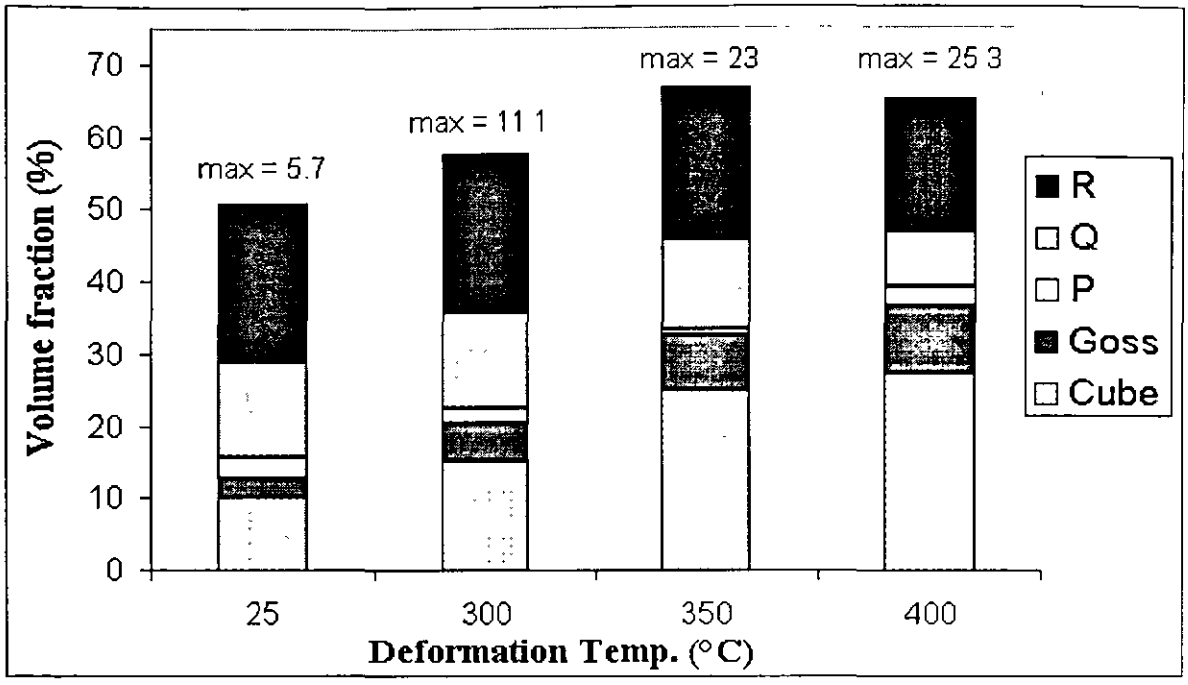

Figure 5.30 The effect of deformation temperature on the relative volumes of the different recrystallisation texture components (to a constant strain $\varepsilon = 1.6$ and for a constant strain rate = 1 s^{-1}). Max values refer to maximum intensity levels of corresponding ODF plots.

5.3.2.4 The Combined Effect of Strain Rate and Deformation Temperature

From the previous section (**5.3.3.2**), it is evident that there is a significant change in recrystallisation texture as the deformation temperature increases from 300°C to 350°C for a constant strain rate of 1 s^{-1}. The combined effect of deformation temperature and strain rate, represented by a single parameter – Z (the Zener-Holloman parameter), was investigated by measuring the recrystallisation textures of two additional annealed specimens. One deformed at an effective temperature of 267°C and at a strain rate of 0.1 s^{-1} and the other deformed at a temperature of 350°C and at a strain rate of 7.5 s^{-1} (both deformed to a strain of $\varepsilon = 2.7$). These deformation conditions correspond to values of Z of 1.3×10^{14} s^{-1} and 9.2×10^{13} s^{-1} respectively. These values lie between those Z values corresponding to deformation at 300°C and 350°C (at a strain rate of 1 s^{-1}). The combined influence of strain rate and deformation temperature can thus be inferred from a plot (Figure 5.31) of the relative volumes of the different recrystallisation components as a function of Z for the four deformation conditions mentioned above. Figure 5.31 shows that the Cube volume fraction increases by a significant amount in a fairly continuous manner as Z decreases over a relatively small range.

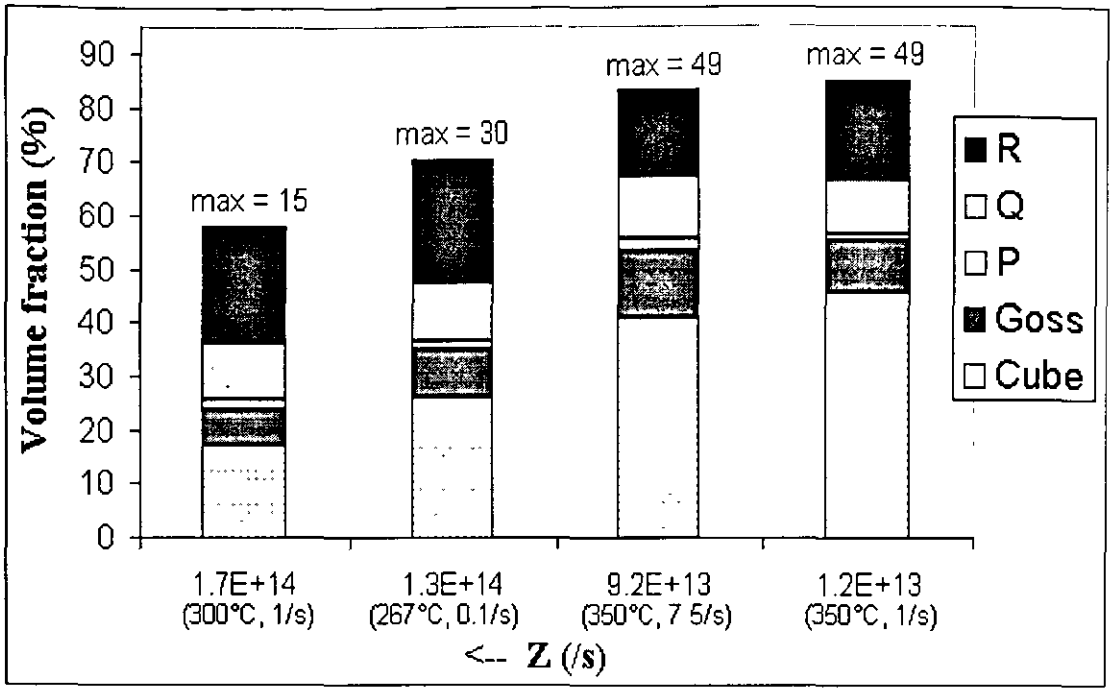

Figure 5.31 The combined effect of strain rate and deformation temperature (represented by Z) on the relative volumes of the different recrystallisation texture components (for a constant strain of ε = 2.7). Max values refer to maximum intensity levels of corresponding ODF plots.

5.3.2.5 The Effect of Annealing Temperature

The effect of annealing at higher temperatures, compared to the standard temperature of 420°C, on recrystallisation texture was also investigated. The recrystallisation textures of specimens deformed at room temperature, at a strain rate of 1 s^{-1} and to a strain of ε = 2.7 and annealed at temperatures of 500°C and 550°C were measured. The recrystallisation texture of a specimen deformed at room temperature, at a strain rate of 1 s^{-1} and to a strain of ε = 3.1 and annealed at a temperature of 550°C was also measured. These two sets of deformation conditions both favour strong shear banding (stronger for a strain of ε =3.1). The recrystallisation textures after annealing at 500°C and 550°C (for a strain of ε = 2.7) are illustrated in ODF plots in Figure 5.32a and Figure 5.32b respectively. Annealing at 500°C compared to annealing at 420°C (compare Figure 5.32a to Figure 5.28a) was seen to cause little observable difference in the recrystallisation texture produced. Annealing at 550°C compared to annealing at 420°C (compare Figure 5.32b to Figure 5.28a), however, caused an observable difference in recrystallisation texture. The texture produced after annealing at 550°C was stronger, with the Cube component increasing in strength at the expense of the P and Q components. This observation is also reflected in a plot of

recrystallisation texture components as a function of annealing temperature for a strain of ε = 2.7 (see Figure 5.33). From this plot it can be seen that the Cube volume fraction increases slightly as annealing temperature increases and that the Q volume fraction decreases correspondingly as a function of increasing annealing temperature. An increase in Cube volume fraction with annealing temperature is also apparent from a similar plot of recrystallisation texture component volume fractions versus annealing temperature for a strain of ε = 3.1 (see Figure 5.34).

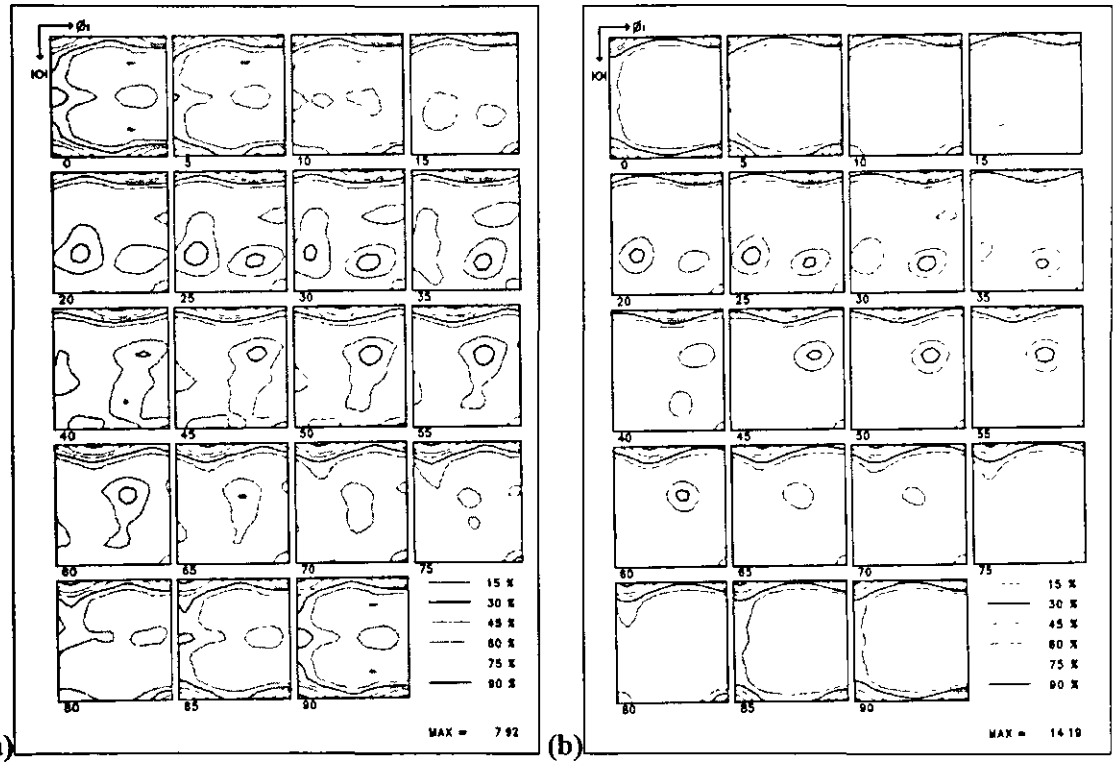

Figure 5.32 ODF plots representing recrystallised textures after annealing at (a) 500°C and (b) 550°C subsequent to PSC to a strain of ε = 2.7, at a deformation temperature = room temperature and at a strain rate of 1 s^{-1}.

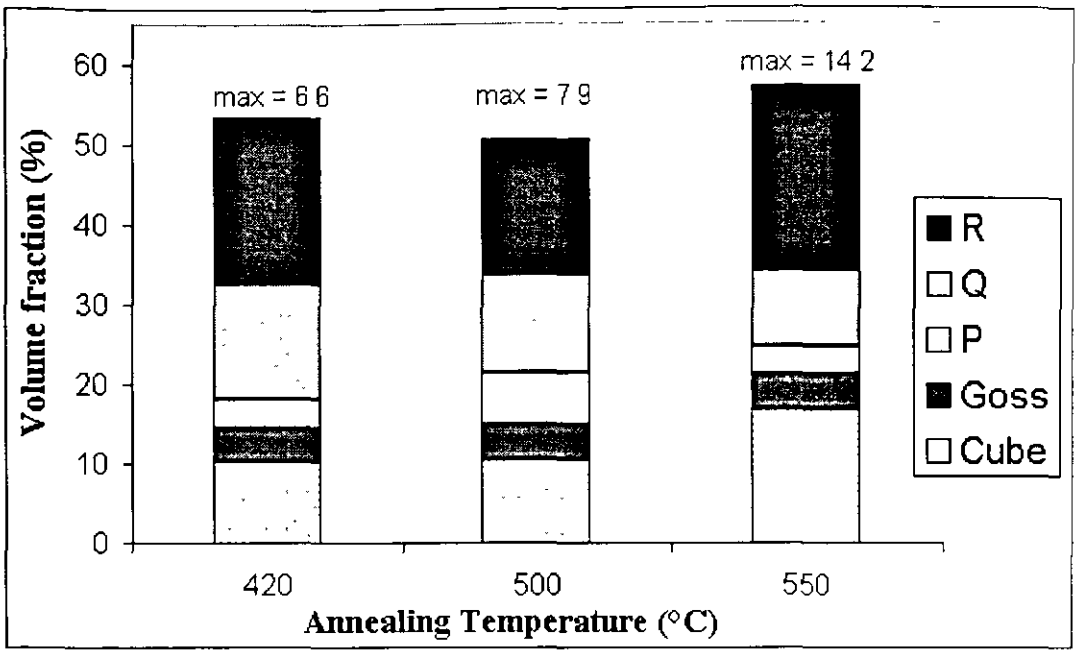

Figure 5.33 The effect of annealing temperature on the relative volumes of the different recrystallisation texture components (deformation at room temperature, strain rate = 1 s^{-1} and to a strain of $\varepsilon = 2.7$). Max values refer to maximum intensity levels of corresponding ODF plots.

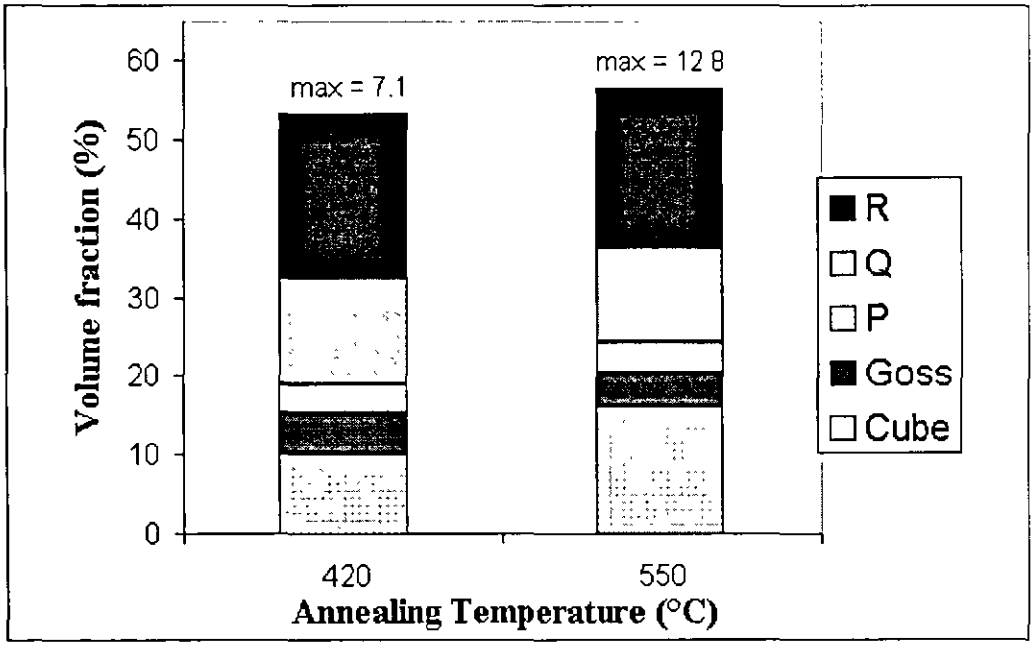

Figure 5.34 The effect of annealing temperature on the relative volumes of the different recrystallisation texture components (deformation at room temperature, strain rate = 1 s^{-1} and to a strain of $\varepsilon = 3.1$). Max values refer to maximum intensity levels of corresponding ODF plots.

5.3.3 Grain Size Measurements

Grain size measurements were performed on fully recrystallised annealed PSC samples corresponding to the same conditions for which bulk texture measurements were conducted (section **5.3.2**).

5.3.3.1 The Effect of Strain

The amount of strain during deformation had only a small influence on the average recrystallised grain size measured (Figure 5.35). For an increase in strain of $\varepsilon = 1.6$ to $\varepsilon = 3.1$ (deformation at room temperature and at a strain rate of 1 s^{-1}), the average grain size was found to decrease dependently from a value of 17.7 μm to a value of 15.4 μm.

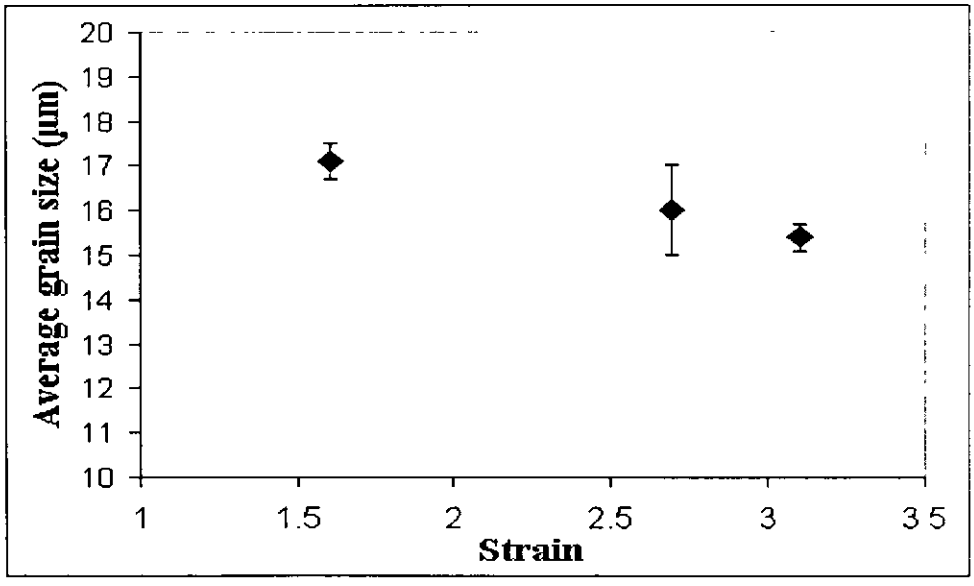

Figure 5.35 The effect of strain on average recrystallised grain size. Deformation performed at room temperature and at a strain rate of 1 s^{-1}. Annealing performed at 420°C for 3 minutes.

5.3.3.2 The Effect of Deformation Temperature

From Figure 5.36 it can be seen that deformation temperature had a significant effect on recrystallised grain size for strains of $\varepsilon = 1.6$ and $\varepsilon = 2.7$ (for a constant strain rate of 1 s^{-1}). Grain size can clearly be seen to increase as deformation temperature increases, with the most rapid rate of change between deformation temperatures of 300°C and 350°C. For a strain of $\varepsilon = 2.7$, grain size was found to increase from a value of 19 μm after deformation at 300°C to a value of 33 μm after deformation at 350°C.

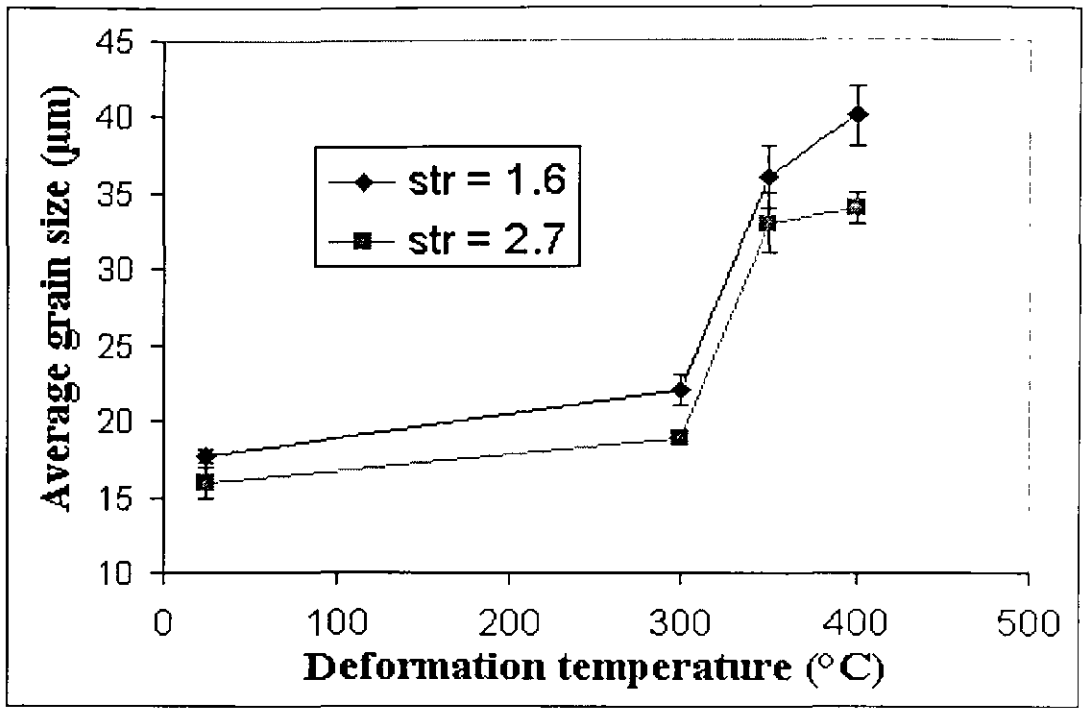

Figure 5.36 The effect of deformation temperature on average recrystallised grain size. Deformation performed to strains of ε = 1.6 and ε = 2.7 (at a strain rate of 1 s^{-1}). Annealing performed at 420°C for 3 minutes. (Lines in graph serve merely to connect points corresponding to the same amount of strain).

5.3.3.3 The Combined Effect of Strain Rate and Deformation Temperature

The dependency of recrystallised grain size on the Zener-Holloman parameter, Z, which represents both strain rate and deformation temperature, is shown in Figure 5.37. An inverse dependency, albeit not a definite one, of grain size on Z may be made out from Figure 5.37. Recrystallised grain size thus appears to increase as Z decreases over the range corresponding to a deformation temperature between 300°C and 350°C (for a strain rate of 1 s^{-1}).

5.3.3.4 The Effect of Annealing Temperature

The value of annealing temperature was found to have a significant influence on recrystallised grain size following deformation at strains of both ε = 2.7 and ε = 3.1 (at room temperature and at a strain rate of 1 s^{-1}) as can be seen in Figure 5.38. For a strain of ε = 2.7, grain size was found to increase in size from a value of 16 μm after annealing at 420°C to a value of 45 μm after annealing at 550°C (an increase by a factor of nearly three).

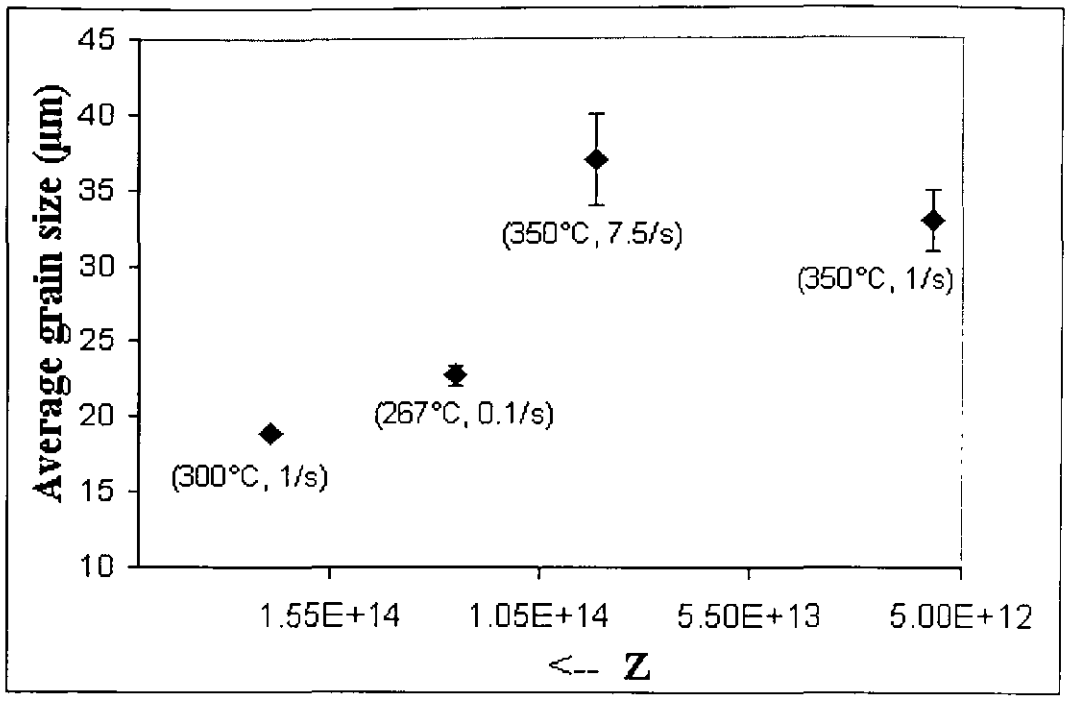

Figure 5.37 The combined effect of strain rate and deformation temperature (represented by Z) on average recrystallised grain size. Deformation performed to a strain of ε = 2.7. Annealing performed at 420°C for 3 minutes.

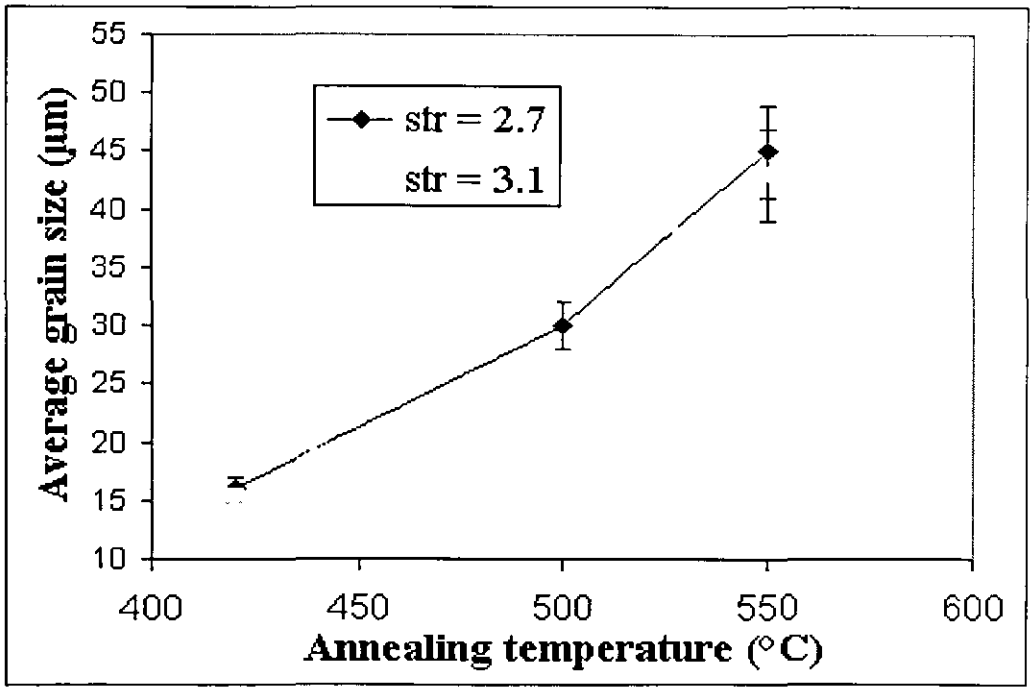

Figure 5.38 The effect of annealing temperature on average recrystallised grain size. Deformation performed at room temperature, to strains of ε = 2.7 and ε = 3.1, and at a strain rate of 1 s^{-1}. (Lines in graph serve merely to connect points corresponding to the same amount of strain).

6. Discussion

6.1 Shear Band Formation

6.1.1 Dependence on Deformation Variables

6.1.1.1 Strain

Shear banding was observed to increase in strength as strain increases (Figure 5.1 and Figure 5.2). This is in agreement with what has been reported by a number of researchers[85,87,92,96] and reflects the continued accommodation of strain by shear bands. At low amounts of strain shear bands were observed to be generally restricted to single grains while at high amounts of strain shear bands were commonly observed to cross grain boundaries. This would tend to confirm the transition of the nature of shear bands from crystallographic to non-crystallographic as strain increases as suggested by Korbel and Martin[86].

6.1.1.2 Deformation Temperature

Deformation temperature was observed to have very little influence on shear band formation up to a temperature of 250°C. At a deformation temperature of 300°C some weakening of shear banding was observed, while at a temperature of 350°C and above a significant weakening in shear band formation was observed (Figure 5.2 and Figure 5.3). It is contended that the significant weakening observed is a true observation of deformation events and is not masked or caused by possible static recovery or recrystallisation that might have occurred in the time period (1 - 2 s) between the end of deformation at high temperature and subsequent quenching. Evidence for this contention is gained from a comparison of the as deformed microstructure after deformation at 350°C and 400°C (Figure 5.3d and Figure 5.7b) with that of partially recrystallised microstructures after deformation at room temperature and annealing (Figure 5.16 and Figure 5.18 - Figure 5.22). The partially recrystallised microstructures still reveal clearly defined shear bands in the unrecrystallised deformed part of the microstructure despite being annealed at a temperature

of 420°C for several seconds. The annealing temperature of 420°C was higher than the deformation temperatures of 350°C and 400°C for which a significant weakening of shear band formation was observed and the annealing time (7 – 10 s) was longer than the delay before quenching. Furthermore, a dependence of shear band formation on deformation temperature has also been observed by Ridha and Hutchinson[10] for copper and by Nakayama and Morii[85] for single crystals of Al-3Mg. Nakayama and Morii[85] found that no shear bands formed after rolling at 200°C compared to rolling at room temperature which did produce shear bands.

6.1.1.3 Zener-Holloman parameter (Z)

Shear band formation was also found to depend on the Zener-Holloman parameter (Z), which takes into account the combined effects of deformation temperature and strain rate (Figure 5.7). The dependency of shear band formation on Z was investigated between those Z values corresponding to deformation at 300°C (strain rate of 1 s^{-1}) and 350°C (strain rate of 1 s^{-1}). These two deformation conditions (Z values of $1.7x10^{14}$ s^{-1} and $1.2x10^{13}$ s^{-1} respectively) corresponded to conditions of still strong shear banding and very weak or no shear banding respectively. The value of Z below which a significant weakening of shear banding occurred was thus further narrowed down to approximately $1.0x10^{14}$ s^{-1} (between $1.3x10^{14}$ s^{-1} and $9.2x10^{13}$ s^{-1}). The rolling experiments performed by Nakayama and Morii[85] mentioned in the previous section (6.1.1.2) were performed at a strain rate of the order of 10^{-2} s^{-1}. The deformation conditions for which they observed no shear banding (deformation temperature of 200°C and strain rate of 10^{-2} s^{-1}) corresponds to a Z value of approximately $1x10^{15}$ s^{-1}. Although slightly above the critical value of $1.0x10^{14}$ s^{-1} obtained for this study, it still compares favourably if it is considered that different modes of deformation and different alloys were employed and that the study by Nakayama and Morii[85] was conducted on single crystals as opposed to polycrystalline material.

6.1.2 Dynamic Recovery

6.1.2.1 General change in dynamic recovery

An increase in deformation temperature clearly causes an increase in the rate of dynamic recovery as can be observed from the systematic drop in measured flow stress with increasing deformation temperature during PSC (Figure 5.5). The observed drop in as

deformed hardness with deformation temperature (Figure 5.6) is also indicative of an increased rate of dynamic recovery during deformation. Dynamic recovery involves dislocation annihilation (of dislocations of opposite sign) and dislocation rearrangement into more stable (lower energy) configurations such as low angle boundaries. These processes are facilitated by dislocation movement in the form of glide, climb and cross-slip. Climb and cross-slip depend in turn on the SFE of the material. The higher the SFE, the more likely climb and cross-slip will occur. The addition of Mg to aluminium is thought to reduce the SFE of the alloy[2,52]. The addition of 1 % Mg is believed to cause the SFE of pure aluminium to drop from about 170-200 $mJ.m^{-2}$ to about 50-60 $mJ.m^{-2}$. A higher deformation temperature allows for faster dynamic recovery due to the increased thermal energy available for this dislocation movement. During deformation dynamic recovery offsets the effects of work hardening, which is due to an increase in dislocation density and the continued trapping of newly created mobile dislocations by existing dislocations. This is reflected as a decrease in flow stress, which is what has been observed. The drop in hardness observed reflects a decrease in the stored energy after deformation, due to a lower dislocation density caused by increased dynamic recovery.

A decrease in strain rate similarly leads to an increase in dynamic recovery as can be seen by the drop in flow stress with strain rate in Figure 5.8. A lower value of strain rate implies that there is more time available for the basic recovery processes of dislocation glide, climb and cross-slip to take place to offset the effects of work hardening. A decrease in Z was also observed to lead to an increase in dynamic recovery as can be seen from the drop in as deformed stored energy (reflected in hardness values) with a decrease in Z (Figure 5.9).

6.1.2.2 Sudden increase in dynamic recovery

The plot of as deformed hardness as a function of deformation temperature (Figure 5.6) not only shows a general drop in hardness with deformation temperature, but also reveals a sharp drop in hardness between a deformation temperature of 300°C and 350°C. This suggests a sharp increase in dynamic recovery during deformation at deformation temperatures between 300°C and 350°C, which exactly coincides with the observed significant weakening of shear band formation during deformation between 300°C and 350°C. If Figure 5.6 and Figure 5.9 are effectively combined, a plot of as deformed hardness as a function of Z for a large range of Z values is obtained (Figure 6.1). This plot

also reveals a sharp drop in hardness, and therefore a sharp increase in dynamic recovery, over a narrow range of Z values centred at approximately $1.0x10^{14}$ s^{-1}. This value of Z is the same as that which is thought to mark the transition from strong shear banding to very weak or no shear banding. It may be speculated that the observed drop in hardness in Figure 6.1 is due, or at least due in part, to static recovery that occurs in the time period between the end of deformation and quenching. Furthermore, the amount of static recovery that occurs should be proportional to the deformation temperature. It is unlikely however that this static recovery is responsible for the sudden step-like drop in hardness seen in Figure 6.1 as a function of Z. The data points plotted as descending values of Z do not all represent ascending values of deformation temperature.

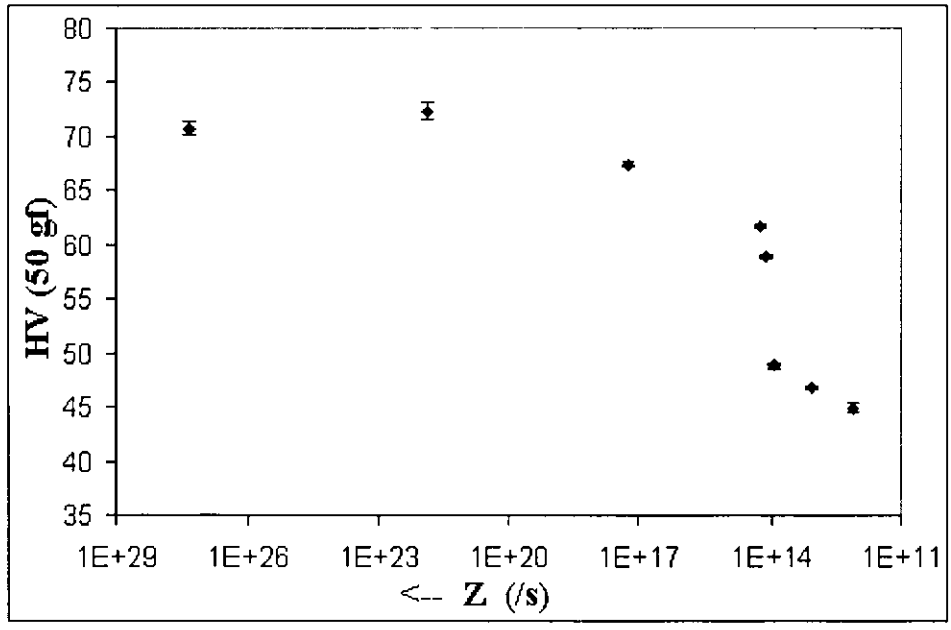

Figure 6.1 As deformed hardness as a function of Z for all deformation conditions measured (for a constant strain of $\varepsilon = 2.7$).

The coincidence of the deduced sharp increase in dynamic recovery and the observed significant weakening of shear band formation over the same narrow range of deformation variables, suggests a sudden change in dynamic recovery events which leads to the sudden change in shear band strength. Before considering the cause of the sharp increase in dynamic recovery, it is instructive to first examine the microstructures corresponding to instances of strong and weak shear banding respectively (Figure 5.4). The structure corresponding to a strong shear banding case (Figure 5.4a) possesses a high dislocation density and is characterised by parallel dislocation walls or microband lamellae. The

structure corresponding to a weak shear banding case (Figure 5.4b), in contrast, exhibits a lower relative dislocation density and is characterised by equiaxed subgrains similar to what is normally observed in a dynamically recovered structure corresponding to pure aluminium. These observations are well supported by the very similar observations made by Nakayama and Morii[85]. It is assumed that the observed rapid change in dynamic recovery over a narrow range of deformation conditions (Z) is linked to the transition of microstructure from one characterised by microbands (strong shear banding case) to one characterised by equiaxed subgrains (weak or no shear banding case). The suddenness of the transition suggests that an activation potential or energy needs to be overcome. Based on this premise two plausible processes (possibly simultaneous) present themselves:

1) The unpinning of dislocations from Mg atom atmospheres: The addition of Mg to aluminium results in the pinning of otherwise mobile dislocations. This pinning of dislocations is thought to be responsible for the Portevin – Le Chatelier dynamic strain ageing behaviour typical of Al-Mg alloys[59]. Korbel et al[87] have suggested that it is also responsible for the prevention of subgrain formation during the deformation of Al-Mg alloys at low temperatures. Microbands are thought to form instead by the co-operative movement of these pinned dislocations. The unpinning of dislocations from Mg atom atmospheres obviously requires a critical amount of energy and time, or temperature and strain rate in terms of deformation variables. Once the dislocations are unpinned then normal subgrain formation can take place. At the same time shear band formation would decrease or disappear if it assumed that microband formation is pre-essential for shear band formation.
2) The onset of non-octahedral slip: Maurice and Driver[12] have provided evidence for the onset of non-octahedral slip (slip on planes other than {111} planes) during deformation at temperatures above 300°C on single crystals of Al and Al-1Mn. They have also provided some indirect evidence of non-octahedral slip during high temperature deformation of polycrystalline Al-1Mg-1Mn[21]. If non-octahedral slip does take place during the high temperature deformation of polycrystalline aluminium alloys then it is likely that its onset is sudden in terms of exceeding an activation potential. It is possible that the onset of non-octahedral slip would greatly enhance the dynamic recovery processes due to an increased number of active slip systems, and would therefore enable a subgrain structure rather than microbands to develop.

The changes in dynamic recovery behaviour as a function of deformation variables (represented by Z) that have been discussed are summarised in Figure 6.2. Figure 6.2 attempts to show how specific dynamic recovery events lead to specific dislocation structures, which in turn determine whether or not shear bands are likely to form.

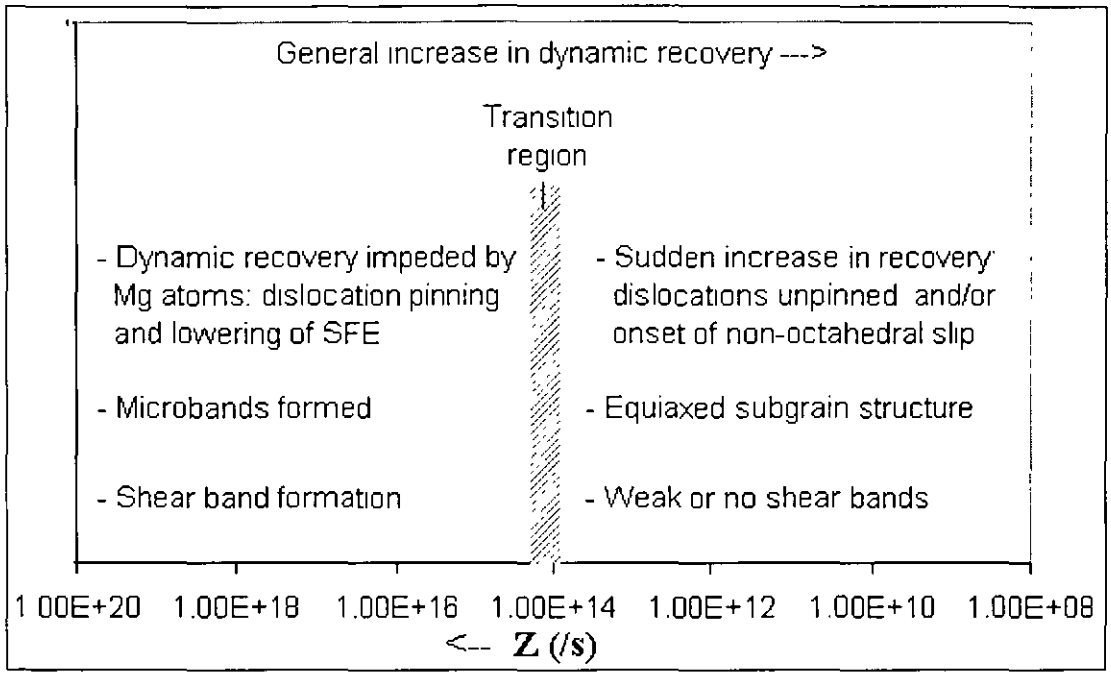

Figure 6.2 The influence of deformation variables (Z) on dynamic recovery which influences the formation of shear bands.

6.2 Deformation Textures

6.2.1 The Effect of Strain

The influence of the amount of strain during deformation on the deformation textures measured was negligible (Figure 5.11 and Figure 5.12). This seems somewhat surprising as a stronger deformation texture with increased strain might be expected. An increase in the main deformation texture components - Brass, Copper and S – in particular might be expected as a function of increasing strain. Figure 5.12 shows that this in not the case and that in fact these components remain relatively stable for the values of strain indicated. A possible reason for this could be due to the inhomogeneous deformation that is associated

with shear banding. It has been shown (see Figure 5.1) that shear bands tend to accommodate increasing amounts of strain as the nominal strain of deformation increases and that at very high strains shear bands cause substantial distortion of the deformed microstructure. This might very well counter the normal strengthening of the deformation texture as a function of strain. A further possible explanation for the observed non-strengthening of deformation texture with strain is related to the nature of the starting microstructure. The starting microstructure (see Figure 3.2b) was partially recrystallised containing elongated deformed grains and therefore the associated starting texture (see) contained a fairly well developed deformation texture. Therefore during subsequent deformation the material may have reached a saturation limit for texture strengthening at a relatively low strain. The starting microstructure is also thought to influence the strength of shear banding as a function of strain. The onset of strong shear banding might occur at higher strains for a fully recrystallised starting microstructure

It has been suggested by Wagner et al[89,92] that the Goss and Q orientations are associated with TD rotations during shear band formation. If this were so then it might be expected that the Goss and Q orientation components would increase as the strength and frequency of shear banding increases, or in this case, as strain increases. This, in fact, has not been what has been observed. There would seem to be no dependence of the Goss and Q deformation texture components on the amount of strain for the strains considered (Figure 5.12). It might be worth noting that the strains considered were $\varepsilon = 1.6$ to $\varepsilon = 3.1$. At a strain of $\varepsilon = 1.6$ shear banding was already noticed to be quite strong. Had a deformation texture corresponding to a lower amount of strain (when shear banding was still weak) been measured, then some dependence of the Goss and Q components on strain might have been noticed. Another point worth considering is that the likely volume fractions of Goss and Q orientations associated with shear banding are probably not very high and consequently any variation would be difficult to detect.

6.2.2 The Effect of Deformation Temperature

The deformation textures measured appeared to increase in strength as deformation temperature increased (Figure 5.13 and Figure 5.14). Two of the main rolling texture components (Brass and S) in particular displayed a small but clear increase in volume

fraction with deformation temperature. This effect is believed to be due to the general enhanced dynamic recovery that occurs at higher deformation temperatures, that results in a deformed microstructure with a lower dislocation density. A more recovered microstructure would therefore be expected to cause stronger diffraction of the X-rays used in texture measurements. Similar observations and views have been presented by Engler et al[78] for the deformation textures corresponding to Al-1Mn-1Mg PSC samples.

No dependence of the Goss, Q and P components was observed as a function of deformation temperature. A decrease in the Goss and Q components with increasing deformation temperature might have been expected due to the suspected association of these components with shear banding. In particular, a decrease in these components corresponding to a significant weakening in shear band formation (i.e. between a deformation temperature of 300°C and 350°C) was not observed. However, it must again be pointed out that the volume fractions of the Goss and Q components that might be produced by shear banding are likely to be very small and therefore any dependent variation of these components associated with shear banding would be very difficult to pick up.

It has been reported and suggested that Cube orientated grains present in the microstructure are more stable at higher deformation temperatures[12,16-22] and that this explains the increase in the Cube component of the recrystallisation texture with increasing deformation temperature. The recrystallised Cube component was indeed observed to increase as a function of increasing deformation temperature in this study, but no increase in the deformed Cube component was observed as a function of increasing deformation temperature. There is thus no support for the above mentioned theory of Cube metastability at high deformation temperatures. The observed dependence of the recrystallised Cube texture component on deformation temperature will be explained in section 6.3.2.

6.3 Recrystallisation Behaviour

6.3.1 Grain Nucleation at Shear Bands

6.3.1.1 Potential Nucleation Sites

Very good evidence that shear bands act as good potential nucleation sites during recrystallisation has been provided. Figure 5.16 and Figure 5.17 - Figure 5.22 all show examples of grains that appear to have nucleated at shear bands. For example, Figure 5.16f shows a grain (indicated by an arrow) that looks very much as if it has just nucleated from within the shear band it is situated. There is also ample support from published research[6 10,90,92 96 112 110] of nucleation at shear bands in copper and aluminium alloys. The nucleation of grains at shear bands in not exactly surprising if one considers that shear bands in theory are very good potential sites for heterogeneous nucleation. They are areas of highly localised strain and are thus areas of high dislocation density which provides the driving force necessary for the recovery events associated with nucleation. They are also areas with high misorientations with respect to the surrounding matrix, which facilitates the boundary movement associated with nucleation and growth.

6.3.1.2 Preferred Orientation of Grains Nucleating at Shear Bands

The orientation of grains suspected of having nucleated at shear bands have been measured in an attempt to establish if there is any preferred orientation, or texture, of nucleation at shear bands. It must be emphasised from the outset that any sort of truly quantitative analysis in this regard is, and has proven to be, very difficult. Part of the problem lies in obtaining an ideal partially recrystallised microstructure for analysis; that is a microstructure containing a sufficient number of grains that can be seen to have clearly nucleated at shear bands. For example, a microstructure that was say 70 % recrystallised would contain an abundance of recrystallised grains but their relationship to the deformed microstructure (and hence also to the shear bands) would be lost. A further problem is that inherent in the relatively poor channelling contrast image quality obtainable for aluminium, in relation to other metals, that is used in the local orientation measurements. The image quality and resolution of the deformed regions of the microstructure in particular is not very

good. Nevertheless, it is possible to make some reasonably sound qualitative deductions based on the measurements made.

Figure 5.17 -Figure 5.22 all show good evidence of grains with random orientation (i.e. not within 15° in orientation space of the Cube, $Cube_{ND}$, $Cube_{RD}$, R, Goss, Q or P orientations) nucleating at shear bands. There is some evidence, although more limited, of grains with Q and Goss orientations also nucleating at shear bands that is in line with the observations and suggestions made by Lücke, Engler, Wagner, Heckelmann, Hirsch and colleagues[6,90,92,93,109,112]. This group of researchers contend that the Goss and Q orientations nucleate from regions of positive and negative TD rotation in and adjacent to shear bands. They also suggest that the P orientation could nucleate from regions at shear bands where Q orientated regions are thought to diverge to the P orientation after further strain. Little evidence of P orientated nucleation at shear bands was found to support this though.

Some attempt to quantify the local orientation measurements was made by means of generating ODFs (Figure 5.23) from all the measurements corresponding to a particular condition. It was hoped that the bias in selecting certain grains for analysis would generate an approximate texture corresponding to grain nucleation at shear bands. When these ODFs are compared to those of bulk texture measurements (see Figure 5.25a and Figure 5.28a) which represent the average orientations of recrystallised grains that have nucleated at all potential sites, some differences may be observed. The peaks around the Goss component appear to be a lot more pronounced at the expense of those around the Cube component for the ODFs representing the local orientation measurements compared to those representing the bulk texture measurements. There also appears to be stronger, although sometimes misplaced, peak around the Q component for the local orientation ODFs. These observations lend some weight to a possible weak preference for the nucleation of Goss and Q orientated grains at shear bands.

The orientation image of an almost fully recrystallised sample that had demonstrated strong shear banding during formation (Figure 5.24) reveals a certain amount of grouping of Goss and Q orientated grains. This observation lends further support to the suspected nucleation of these orientated grains at regions in and adjacent to shear bands. Figure 6.3 shows

schematically how nucleation of Goss and Q orientated grains at shear bands could lead to the observed groupings. Goss orientated grains are believed to nucleate from regions within shear bands that have experienced a negative TD rotation during deformation while Q orientated grains are believed to nucleate from regions within and adjacent to shear bands that have experienced a positive TD rotation during deformation[89,92]. According to this theory it would thus be quite likely for a Goss orientated grain to nucleate from a region within a shear band and have as a neighbouring grain a Q orientated grain that has nucleated in an adjacent region.

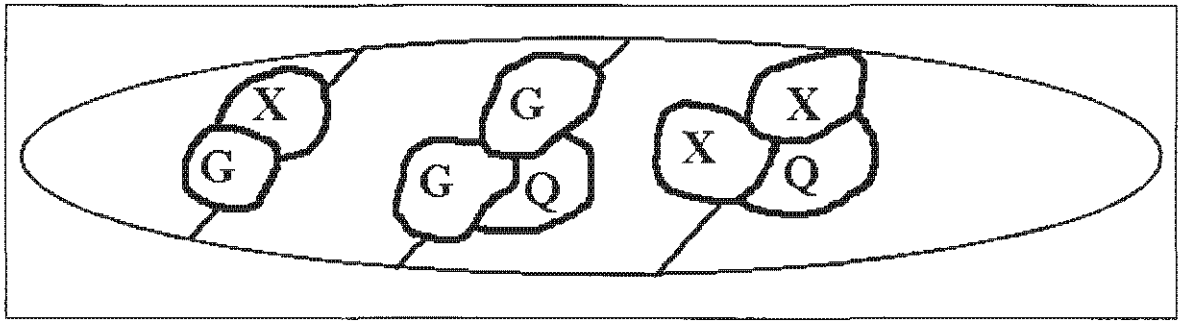

Figure 6.3 Schematic representation of Goss (G), Q and randomly (X) orientated grains nucleating in regions in and adjacent to shear bands in a deformed structure. An example of a resultant grouping of Goss and Q orientated grains is shown in the central region of the diagram.

It is worth examining the bulk recrystallisation texture measurements for evidence of any preference for Goss and Q (and even P) orientated grains nucleating at shear bands. Any increase of the Goss, Q and P volume fractions with a change in deformation conditions that favour stronger shear banding would represent such evidence. Figure 5.26 reveals a small but steady increase in the Goss recrystallised volume fraction as a function of strain and therefore also as a function of stronger shear band formation. No trend is apparent for the Q recrystallised volume fraction. Figure 5.27 (representing deformation to a strain of $\varepsilon = 2.7$) and Figure 5.30 (representing deformation to a strain of $\varepsilon = 1.6$) both reveal a general increase in the Q recrystallised volume fraction as a function of decreasing deformation temperature, i.e. as a function of stronger shear band formation. However, the exact opposite trend for the Goss volume fraction is apparent from Figure 5.27 and Figure 5.30. That is, an increase in the Goss volume fraction with increasing deformation temperature is shown. This is most likely linked with the similar, but far more noticeable, increase in Cube volume fraction with deformation temperature (which will be discussed in detail in

section **6.3.2**). The increase in Goss with deformation temperature is thus thought to be a result of the increase in the TD scatter of the Cube component as it increases, which would mask any downward trend caused by reduced nucleation at shear bands. No trend for the P recrystallised volume fraction as a function of strain (Figure 5.26) or as a function of deformation temperature (Figure 5.27 and Figure 5.30) could be detected.

6.3.2 Cube Texture

One of the most striking features of the results of this study is the very sharp increase in the recrystallised Cube volume fraction that was noticed over a very narrow range of the deformation parameters of deformation temperature and strain rate (Figure 5.27, Figure 5.30 and Figure 5.31). These observations are summarised in Figure 6.4 where Cube volume fraction is plotted as a function of Z for the two separate strains of $\varepsilon = 2.7$ and $\varepsilon = 1.6$. The average recrystallised grain size as a function of Z is plotted on the same graphs for direct comparison. The sharp increase of Cube volume fraction that can be observed for a value of $Z \approx 1.0 \times 10^{14}\ s^{-1}$ after strains of both $\varepsilon = 2.7$ (Figure 6.4a) and $\varepsilon = 1.6$ (Figure 6.4b) is seen to coincide almost exactly with a similar sharp increase in the average recrystallised grain size.

Besides the dramatic increase in the Cube texture strength at $Z \approx 1.0 \times 10^{14}\ s^{-1}$, a more general increase in Cube texture strength with decreasing Z can also be observed from Figure 6.4. It is believed that the increased stability of the Cube texture at lower values of Z, as has been observed and discussed by other researchers[12,16-22], accounts for this general increase but does not account for the sudden increase in Cube texture strength. As discussed previously (see section 6.2.2), no increase in the Cube deformation texture strength with increasing deformation temperature was observed (Figure 5.14). Certainly no variation of the cube deformation texture strength was observed between a deformation temperature of 300°C (for which a weak recrystallised Cube texture was observed) and 350°C (for which a strong recrystallised Cube texture was observed).

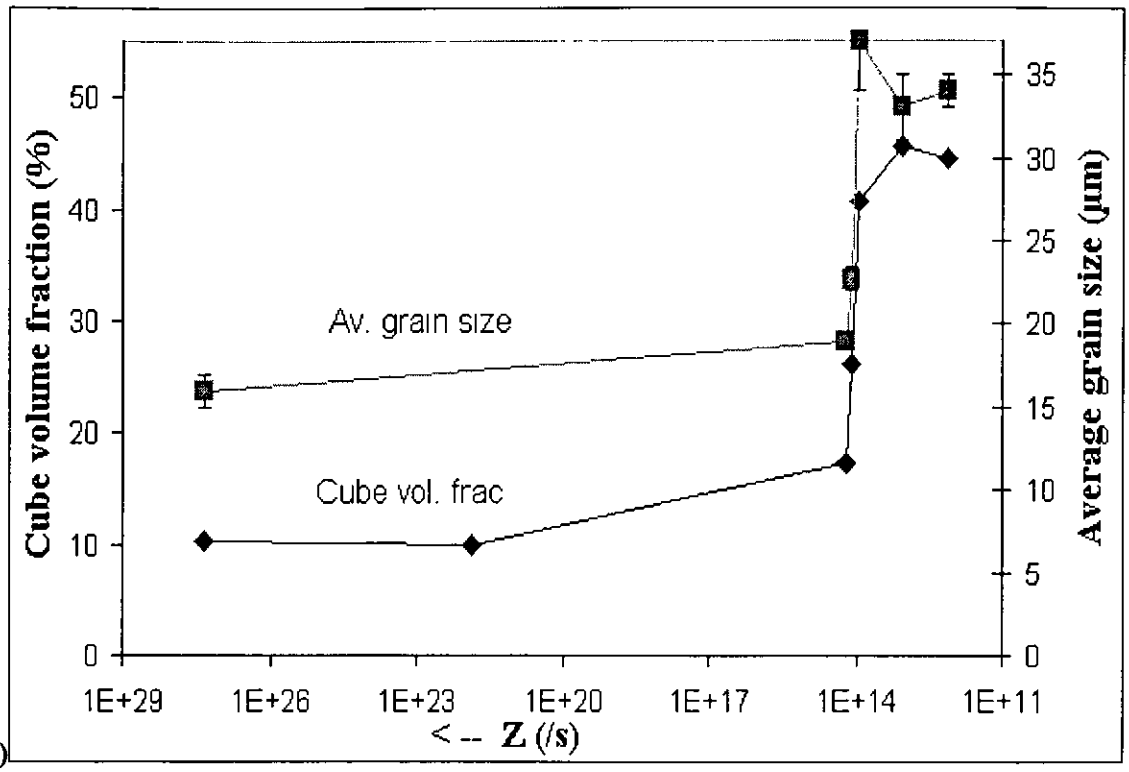

(a)

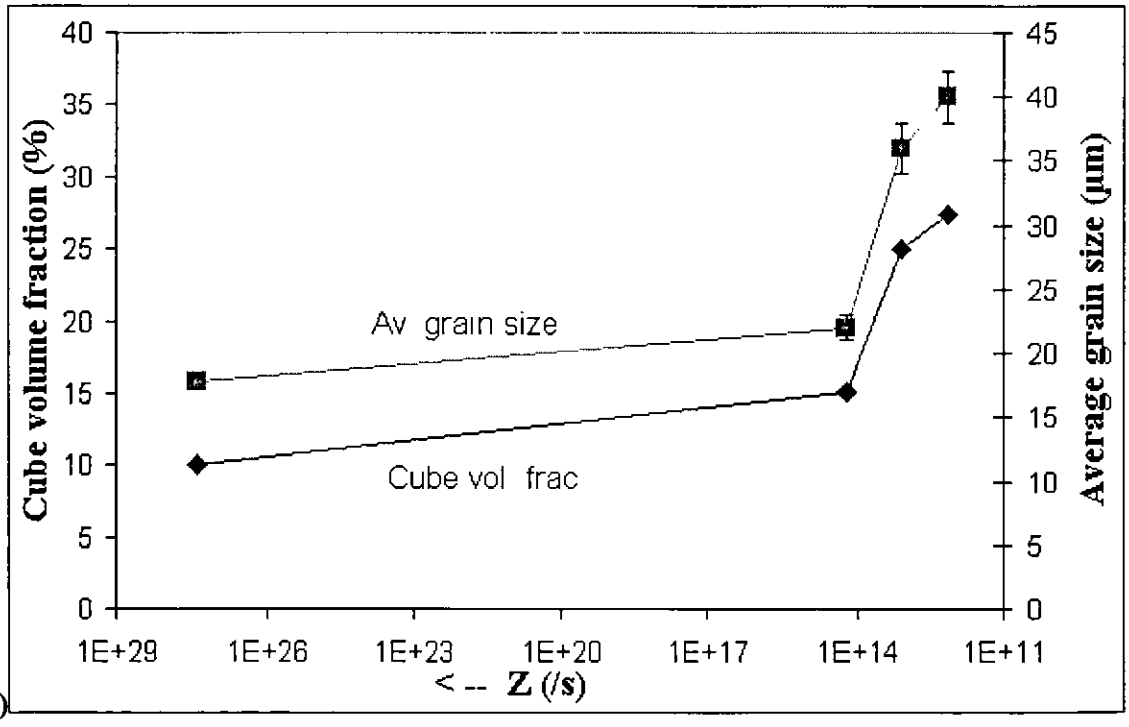

(b)

Figure 6.4 The coincidence of the dependency of the recrystallised Cube volume fraction and the average recrystallised grain size as a function of the deformation parameters of temperature and strain rate, expressed as a value of Z, for strains of (a) $\varepsilon = 2.7$ and (b) $\varepsilon = 1.6$.

6.3.2.1 Influence of Shear Bands

The sharp increase in recrystallised Cube volume fraction that is seen (Figure 6.4) to occur after deformation conditions within the narrow range of Z values at about $1.0x10^{14}$ s^{-1} corresponds very closely to the observed significant weakening of shear band formation over the same narrow range of Z (Figure 6.2). Due to this very close correspondence, it is suggested that shear band formation during deformation impedes the development of a strong Cube texture after subsequent annealing. Possible mechanisms that would explain how this could result include:

1. Competition of nucleation sites: It has been shown and discussed that shear bands offer good potential nucleation sites and consequently also offer alternative nucleation sites to other sites. These other sites include particles, grain boundaries, transition bands and retained Cube orientated grains present before deformation. Nucleation at transition bands and retained Cube orientated grains is known to lead to a Cube texture due to the favoured nucleation and growth preferences of Cube orientated grains. In the absence of competition from non-Cube orientated grains nucleating at other sites, the Cube texture is known to become very dominant in the overall recrystallisation texture. It is believed that nucleation at shear bands leads to the development of fairly randomly orientated grains with a small preference of Goss and Q orientated grains. Competitive nucleation at shear bands is thus thought to cause a weakening of the Cube texture. In the absence or significant weakening of shear band formation this competitive nucleation no longer exists and hence the Cube texture becomes dominant.
2. Destruction of Cube nucleation sites: It is obvious (see Figure 5.1) that shear bands cause a severe distortion of the deformation microstructure due to the very localised shear inherent in a shear band. This distortion could possibly destroy potential Cube nucleation sites in transition bands and retained Cube orientated grains. The reduction in the number of Cube nucleation sites would then lead to an associated weakening of the Cube texture. As soon as shear banding disappeared or its formation significantly weakened, potential nucleation sites would be 'restored' and a strong Cube texture would develop once again.

It is of course possible, and quite likely, that both of the above two mechanisms are active in reducing the strength of the Cube texture. However, by examining the recrystallised

grain size in comparison to the Cube texture as a function of Z (Figure 6.4), it is possible to infer which of the two mechanisms appears to be dominant. The coincidence of the sharp increase in the recrystallised grain size with the sharp increase in the Cube volume fraction at $Z \approx 1.0x10^{14}$ s^{-1}, suggests that the sudden increase in Cube texture strength is linked with a sudden decrease in the number of nucleation sites. The nucleation sites that disappear or become inactive below this value of Z are most likely those associated with shear bands, because of the precise coincidence of the weakening of shear banding that is observed below this same value of Z. Therefore it would seem that the first of the above two mentioned mechanisms is dominant in reducing the strength of the Cube texture.

6.3.2.2 Influence of PSN

The sharp increase in the Cube recrystallisation texture observed at a value of $Z \approx 1.0x10^{14}$ s^{-1} could perhaps equally well be explained by the influence of particle stimulated nucleation (PSN). Second phase particles offer, just as shear bands do, alternative nucleation sites to cube nucleation sites during recrystallisation. PSN is thought to cause a randomising effect on the total recrystallisation texture[42,44-46], and thereby weaken the Cube texture, as well as possibly be responsible for weak peaks around the P and ND rotated Cube components[49-51]. An increase in deformation temperature and / or a decrease in strain rate, that is a decrease in Z, which has been shown to cause an increase in dynamic recovery, will result in PSN being less effective. A decrease in PSN will cause a corresponding strengthening of the Cube texture

An increase in dynamic recovery is thought to cause a reduction in PSN by influencing the two criteria necessary for PSN to occur:

1. the formation of the deformation zones necessary for nucleation
2. the growth of the nuclei beyond the deformation zones into the deformed matrix

Humphreys and Kalu[118] have demonstrated that for low values compared to higher values of Z, the formation of the deformation zones around second phase particles is influenced by the nature of the dislocation-particle interactions. For lower values of Z dislocations are able to bypass particles by a process of climb and so the formation of deformation zones is prevented. The critical strain rate for the formation of a deformation zone around a particle of diameter, d, is given by Humphreys and Kalu[118] as:

Eqn 6.1

$$\dot{\varepsilon} = \frac{K_1 \exp\left(\frac{-Q_v}{RT}\right)}{Td^2} + \frac{K_2 \exp\left(\frac{-Q_b}{RT}\right)}{Td^3}$$

where Q_v and Q_b are the activation energies for volume and boundary diffusion, T is the deformation temperature, and K_1 (= 1712 $m^2s^{-1}K$) and K_2 are constants. If particles of size, $d > 1$ μm, are considered as potential nucleation sites, then the second term in Eqn 6.1 can be neglected. The critical size, d_f, of a second phase particle necessary for the formation of a deformation zone can thus be expressed in terms of Z (from Eqn 2.4 and Eqn 6.1) as:

Eqn 6.2

$$d_f = \left(\frac{K_1}{ZT}\right)^{\frac{1}{2}}$$

The critical size (expressed as a radius) of a particle that is necessary for the growth of a nucleus that has formed in the deformation zone adjacent to the particle has been given in Eqn 2.2. This critical size expressed as a diameter, d_g, is:

Eqn 6.3

$$d_g = \frac{4\gamma_b}{P_d}$$

From Eqn 6.3 it can be seen that d_g is inversely proportional to the driving force provided by the stored dislocation energy in the surrounding matrix, P_d. An increase in dynamic recovery during deformation will reduce the stored energy of the matrix and consequently reduce this driving force, which implies a larger value of d_g necessary for PSN to continue. The driving force, P_d, in Eqn 6.3 can be expressed in terms of the average subgrain size (expressed as, s, instead of, d, to avoid confusion with the critical particle diameter) if it assumed that at low values of Z dynamic recovery has led to a subgrain microstructure similar to that in Figure 5.4b:

Eqn 6.4

$$P_d \approx \frac{3\gamma_s}{s}, \qquad \gamma_s \text{ - } \textit{specific energy of low angle boundaries}$$

By combining Eqn 2.5 and Eqn 2.6 (from the work of Castro-Fernandez et al[75]), the subgrain size may be expressed in terms of Z as:

Eqn 6.5

$$\frac{1}{s} = C + D \cdot \ln Z, \qquad \textit{C and D are constants}$$

Eqn 6.3, Eqn 6.4 and Eqn 6.5 can then be combined to give an expression for the critical particle size for the growth criterion of PSN in terms of Z as:

Eqn 6.6
$$d_g = \frac{4\gamma_b}{3\gamma_s(C + D\ln Z)}$$

The ratio of specific grain boundary energy to specific low angle boundary energy (γ_b/γ_s), may expressed in terms the misorientations across high angle boundaries (θ_b) and low angle boundaries (θ_s) from the Read Shockley[119] equation as:

Eqn 6.7
$$\frac{\gamma_b}{\gamma_s} = \frac{\theta_b}{\theta_s\left(1 - \ln\frac{\theta_s}{\theta_b}\right)}$$

If θ_b is estimated to be 15° and θ_s is estimated to be 5° for low values of Z then Eqn 6.6 reduces to:

Eqn 6.8
$$d_g = \frac{1.9}{(C + D\ln Z)}$$

An expression for the critical particle size for the growth criterion for PSN, d_g, is also given by Sellars[120]. This expression has been empirically derived to fit observations for Al-1Mg:

Eqn 6.9
$$d_g = \frac{0.37}{(TZ)^{1/3}}$$

Eqn 6.2, Eqn 6.8 and Eqn 6.9 can be solved for $Z \approx 1.0\text{x}10^{14}$ s^{-1}, the value of Z at which a sharp increase in the Cube texture was observed. Solving Eqn 6.2 yields a value of $d_f \approx 0.2$ μm if a deformation temperature of 325°C is used. If it is assumed that particles of size, d > 1 μm, are responsible for PSN then it is clear that the formation criterion for PSN is not responsible for the observed strengthening of the Cube texture. All potential particles contributing towards PSN will satisfy the formation criterion (all larger than 0.2 μm) at 325°C and for $Z \approx 1.0\text{x}10^{14}$ s^{-1} and so a possible reduction in PSN (and consequent increase in Cube texture strength) cannot be explained in this way. Solving Eqn 6.8, for C = -3.87x10^6 m^{-1} and D = 0.165x106 m^{-1} (these are the values given by Castro-Fernandez et al[75] for the not too dissimilar alloy, Al-1Mg-1Mn), yields a value of $d_g \approx 1.3$ μm. Solving Eqn 6.9 (for a deformation temperature of 325°C) yields a comparatively similar value of $d_g \approx$

0.95 μm. So it would appear that the growth criterion for PSN could be responsible for the observed strengthening of the Cube texture. A more critical examination of this possibility requires a careful comparison of the range of Z values over which the Cube strengthening has been observed with the particle size distribution. The particle size distribution (Figure 3.3) reveals that the majority of particles (within one standard deviation of the mean) have a diameter that lies in the range between 1.1 μm and 4.2 μm. Figure 6.4 reveals that the sharp increase in Cube texture strength occurs between a very narrow range of Z values (at least for a strain of $\varepsilon = 2.7$), between $Z \approx 1.0 \times 10^{14} s^{-1}$ and $Z \approx 1.0 \times 10^{13} s^{-1}$. This range of Z values results in a critical particle size range for the growth criterion for PSN, d_g, of between 1.3 μm and 1.8 μm after solving for Eqn 6.8, and a similar range of between 0.95 μm and 2.0 μm after solving for Eqn 6.9. If it were so that a reduction in PSN, caused by the growth criterion, resulted in the observed sharp increase in the Cube texture, then the calculated size range (approximately between 1.0 μm and 2.0 μm) should correspond to the measured size range of particles (between 1.1 μm and 4.2 μm). These ranges do not completely correspond. In fact, there is at best a 50 % correspondence, which means that at least half the particles in the material satisfy the growth criterion (larger than 2.0 μm). It is therefore concluded that a reduction in PSN (from the dependence of the growth criterion on Z) can not entirely be responsible for the observed sharp increase in Cube recrystallisation texture as a function of Z.

6.3.2.3 Combined Influence of Shear Bands and PSN

The most plausible explanation for the observed sharp increase in the Cube recrystallisation texture over a narrow range of Z is the combined influence of nucleation at shear bands and PSN. The Z range over which the Cube increase is noticed has been shown to coincide with the same Z range over which a sharp increase in dynamic recovery is noticed. This sharp increase in dynamic recovery simultaneously leads to a severe reduction in shear band formation and a decrease in the effectiveness of PSN. Both nucleation at shear bands and PSN have been shown or are known to cause an effective randomisation of the total recrystallisation texture, or at least cause a weakening of the Cube texture. In the absence - or severe reduction of - nucleation at shear bands and of PSN, the Cube texture becomes dominant. Which of nucleation at shear bands or PSN is more effective in competing with the Cube texture is quite difficult to say. The evidence for nucleation at shear bands competing with Cube orientated nucleation is quite compelling from this study. The

precise coincidence or the significant weakening of shear band formation that has been observed with the observed sharp increase in Cube texture strength over the identical narrow range of Z provides strong evidence. The evidence for the effect of PSN competing with Cube orientated nucleation is more indirect and has been inferred from a theoretical analysis. (Certainly much has been published in support of the competition between PSN and Cube orientated nucleation[42,44-46].) In addition, the analysis is not altogether convincing since the calculated critical particle size range for the growth criterion for PSN does not coincide with the measured particle size distribution.

6.3.3 Effect of Annealing Temperature

The effect of annealing temperature on recrystallisation texture, following deformation that leads to strong shear band formation, was characterised by an increase in both the overall texture intensity and in the Cube texture (see Figure 5.32 - Figure 5.34). This corresponded with quite a substantial increase in average recrystallised grain size as a function of increasing annealing temperature (see Figure 5.38). These observations would at first hand seem to contradict those made by Wagner et al[92] and Heckelmann et al[111], who noticed an increase in the random and Q recrystallisation components and a corresponding weakening of the Cube texture as annealing temperature was increased for Al-3Mg. This was attributed to the decrease in the growth preference of Cube orientated nuclei at higher recrystallisation temperatures. The present study would therefore appear to offer no support for this theory. However, it must be considered that the annealing times employed by Wagner et al[92] and Heckelmann et al[111] differed for each annealing temperature such that recrystallisation was just complete and no grain growth occurred. In the present study a fixed annealing time was employed for all annealing temperatures so that grain growth did occur as can be gathered from Figure 5.38. It is proposed therefore, that faster grain growth has occurred for Cube orientated grains during recrystallisation (as distinct from the growth characteristics of Cube orientated nuclei) such that after higher annealing temperatures the Cube texture is stronger due to the increased normal grain growth at higher annealing temperatures. This ideal will be discussed in further detail in the next section (**6.3.4**). The present observations do not therefore directly contradict those of Wagner et al[92] and Heckelmann et al[111].

6.3.4 Orientated Growth versus Orientated Nucleation

A dominant Cube texture after recrystallisation has for many years been a subject of intense investigation and research[9-30]. Over the past 50 years two major alternative models have evolved to explain the formation of a strong recrystallisation texture – usually described as 'Orientated (or Oriented) Nucleation (ON)' and 'Orientated (or Oriented) Growth (OG)'. Orientated Nucleation is the model that grains, with an orientation that will eventually dominate the fully recrystallised texture, nucleate more frequently than do grains of other orientations. Orientated Growth is the model that grains, with an orientation that will eventually dominate the fully recrystallised texture, grow more rapidly out of a random orientated spread of nuclei.

Before considering these two models in accounting for the observations of this study, or alternatively, in considering the observations of this study in support of either of these models, it is instructive to consider the process of recrystallisation in some detail. Recrystallisation involves the formation and migration of high angle boundaries driven by the stored energy of deformation. Heterogeneous recrystallisation involves two apparently distinct steps: (i) the initial formation of a new grain (nucleation) and (ii) the growth of the new grain. Nucleation is thought to occur in pre-existing structures of the deformed microstructure that (i) possess high angle misoriented boundaries associated with high mobilities and (ii) are of sufficient size for growth into the deformed regions. These pre-existing structures include pre-existing grain boundaries, transition bands, deformation zones surrounding large particles and regions within and adjacent to shear bands. The nucleation process might thus involve subgrain coalescence near a high angle boundary in one of these structures to form an embryo or nucleus of sufficient size and the further movement or growth of this embryo into the deformed region. Once a nucleus is of sufficient size it is referred to as a new grain and will continue to grow until it impinges on other growing grains. Some orientated grains with special high angle boundaries are known to grow faster than other orientated grains. An example of a special high angle boundary is $\Sigma 7$, the 38° misoriented tilt boundary with a common <111> rotation axis.

The term 'growth' is therefore somewhat ambiguous in describing the various recrystallisation events. In view of this it is perhaps better to rename the models of

Orientated Nucleation and Orientated Growth as: (i) the grain frequency effect and (ii) the grain size effect as was recently suggested by Doherty et al[121] in their comprehensive review on current issues in recrystallisation.

The behaviour of the Cube recrystallisation texture as a function of Z that has been observed in this study can be explained by, or alternatively, confirms the grain frequency effect. The relative frequency of cube orientated nuclei increases dramatically when a significant number of non-cube orientated nuclei disappear. This happens below a certain value of Z when nuclei at shear bands and large particles are no longer available or are no longer viable. The weak preferred recrystallisation texture associated with nucleation at shear bands (slight preference of Goss and Q orientated grains) is also thought to be a grain frequency effect. Goss and Q orientated nuclei are thought to possess high angle boundaries of comparatively high mobility and thus more likely to form viable nuclei. This effect has been termed a 'micro-growth' effect[49]. Perhaps it should more accurately be termed a 'micro-frequency' effect.

The grain size effect is thought to account, at least indirectly, for the observed increase in the Cube recrystallisation texture as a function of increasing annealing temperature. Normal grain growth may occur subsequent to the end of primary recrystallisation; that is once significant grain impingement occurs. The driving force for normal grain growth is some two orders of magnitude lower than that for primary recrystallisation and therefore grain growth is very dependent on annealing temperature with significant growth only occurring at very high annealing temperatures. During primary recrystallisation Cube orientated grains are thought to possess a growth rate advantage over other orientated grains due to their near $\Sigma 7$ misorientation to S (a major component of the deformation texture) orientated grains[23]. At the end of primary recrystallisation (and therefore at the start of normal grain growth) Cube orientated grains thus have a size advantage over other orientated grains. During normal grain growth this size advantage allows Cube orientated grains to grow at the expense of smaller non-Cube orientated grains. The volume fraction of the Cube orientation is in this way effectively increased. Increased normal grain growth at higher annealing temperatures results in a higher volume fraction of the Cube orientation.

7. Conclusions

1. A plane strain compression (PSC) apparatus was developed to facilitate the reliable compression of laboratory scale aluminium specimens. The apparatus provided very good control of the deformation variables of deformation temperature, strain and strain rate. The platen / specimen geometry of the apparatus was optimised to ensure that the strain distribution through the specimen was as uniform as possible, while still ensuring that deformation remained acceptably close to plane strain.

2. Asymmetric flow was observed to occur during PSC after high amounts of strain. It is thought to occur as the result of a small lateral movement of the moving platen and is possibly exacerbated by uneven friction conditions along the platen / specimen interface. The relative lateral movement of the platens is believed to cause a rotation of the plastic-rigid exit boundaries of the deforming material and thus result in an asymmetrical slip-line field. Although asymmetric flow compared to symmetric flow is believed to cause an increase in the strength and frequency of shear band formation in the material investigated (Al-1Mg), it was found to have a negligible effect on both the deformation and recrystallisation textures of the samples investigated. This was attributed in part to the selective sampling that was adopted within a deformed specimen.

3. Copper type shear bands were observed to occur in Al-1Mg. Their formation was characterised as a function of the deformation variables of strain, deformation temperature and strain rate by a systematic matrix of PSC testing. Shear band formation was stronger and more frequent with increasing strain. Shear band formation depended quite critically on deformation temperature and strain rate (Z), in that a significant weakening of formation was observed over a very narrow range of Z values at $Z \approx 1.0 \times 10^{14} s^{-1}$. This significant weakening was attributed to a sharp increase in dynamic recovery over the same narrow range of Z values, which led to the formation of a subgrain microstructure instead of a microband microstructure that is considered a prerequisite for shear band formation.

4. Grain nucleation at shear bands was observed to occur during recrystallisation. The orientations of grains believed to have nucleated at shear bands were measured in an attempt to describe their texture. From the single grain orientation measurements made and from the generated ODFs of these measurements, a random texture with weak peaks around the Goss and Q ideal orientations was described.

5. Grain nucleation at shear bands had a profound influence on the bulk recrystallisation textures measured as a function of deformation variables. In particular, nucleation at shear bands was observed to influence the strength of the potentially dominant Cube recrystallisation texture. At high values of Z (low deformation temperatures and / or high strain rates leading to strong shear band formation) weak recrystallisation textures were observed which coincided with nucleation at shear bands. At low values of Z (high deformation temperatures and / or low strain rates leading to weak or no shear band formation) strong recrystallisation textures dominated by the Cube orientation were observed. Shear bands are believed to offer alternative nucleation sites to Cube orientated nucleation sites and additionally are also believed to destroy Cube orientated nucleation sites. When shear bands form during deformation, they effectively weaken the Cube recrystallisation texture formed after annealing. If they do not form during deformation, then the Cube recrystallisation texture dominates the total recrystallisation texture after annealing.

6. Nucleation at particles (PSN) is also believed to moderate the strength of the Cube recrystallisation texture in much the same way as nucleation at shear bands does. Particles offer alternative nucleation sites to Cube orientated nucleation sites. When PSN is effective (i.e. at high values of Z), it weakens the Cube texture. When PSN is less effective (i.e. at low values of Z), due to dynamic recovery effects, its moderation of the Cube texture is also reduced.

7. Some insight into the rival theories of Orientated Nucleation (ON) and Orientated Growth (OG) of recrystallisation has been provided. ON (referred to as the grain frequency effect) is thought to account for the strengthening of the Cube

recrystallisation texture as a function of Z. When nucleation at shear bands (and also at particles) is no longer viable the relative frequency of Cube orientated nuclei increases.

8. Recommended Further Work

8.1 Shear Band Formation

This study has revealed a very clear dependence of shear band formation in Al-1Mg on deformation temperature. A dependence on Z (the Zener-Holloman parameter), which combines the influence of deformation temperature and strain rate, has also been shown. Although the dependence on Z is also very clear it is based on a more limited number of observations. It is therefore recommended that the dependence of shear band formation on deformation temperature and strain rate be more extensively investigated by performing a matrix of PSC tests over a wide range of strain rates and deformation temperatures. It might thus be possible to obtain at least an empirical relationship that describes the dependence of shear band formation on one or more of the parameters of Z, deformation temperature and strain rate. Of interest would be to observe if such a relationship reflects a critical dependency on the deformation parameters of a sudden transition from strong shear band formation to weak shear band formation. The systematic characterisation of the deformed microstructure by the use of transmission electron microscopy would assist in the understanding of any such transition.

8.2 Grain Nucleation at Shear Bands

Further work is recommended for a detailed study of grain nucleation at shear bands. In particular it is recommended that the orientations of a statistically relevant number of grains positively identified as having nucleated at shear bands be measured. This would be more feasible with a sophisticated automatic EBSD system of the type currently available on the market. It is also recommended that the local orientations of deformed regions adjacent to the nucleated grains be measured in order to establish misorientation relationships. In this way a more definite deduction could be made concerning the texture produced from nucleation at shear bands. As has been mentioned, this type of study is non-trivial due to the

experimental difficulties involved. However, it is felt that it is worth pursuing due to the fundamentally important information that would be gained.

8.3 The Influence of Shear Bands on Recrystallisation Texture

It is felt that further bulk texture (both deformation and recrystallisation) studies be pursued to ascertain more comprehensively the influence of shear bands on recrystallisation and in particular on the Cube recrystallisation texture. It is felt that the range of deformation variables should include very high amounts of strain: $\varepsilon \geq 3.45$ (≥ 95 % reduction) which would lead to extremely strong and extensive shear band formation. Any texture associated with nucleation at shear banding would thus be more obvious to describe. The range of deformation variables should also be expanded to include more fully the effects of strain rate on recrystallisation texture. Observations thus made would have to be related closely to observed shear band formation over the same deformation conditions (see section 8.1).

Appendix A:

Source Code Listing for Control of PSC

```
//rollsim7.cpp
//This programme controls the PSC apparatus built at the Department of
//Materials Engineering, University of Cape Town.
//
//Written by:       Alan Duckham
//Last Updated:     March 1997
//Compiler used:    TURBO C++, ver 3.0


#include <stdio.h>
#include <stdlib.h>
#include <constrea.h>
#include <time.h>
#include "pc30esh2.h"
#include "pc30.h"

int main(void)
{
       int stroke_zero1 = 0;
       int stroke_zero2 = 0;
       int stroke_zero3 = 0;
       int *stroke_zero, load_zero;
       float area, gauge_length;
       float stroke_distance = 0, szero = 0, h0, strainrate;
       int num_passes, pass;
       struct variables vpass1, vpass2, vpass3, *pass_variables;
       struct comp_data dpass1, dpass2, dpass3, *stroke_load;
       char response;
       clock_t ti;
       float t;


       clrscr();
       ini_board();

       printf("Enter contact area (in square metres): \n");
       scanf("%f", &area );
       printf("Enter gauge length of specimen (in millimetres ):\n");
       scanf("%f", &gauge_length );
       printf("Enter number of rolling pass simulations (maximum of 3):\n");
       scanf("%d", &num_passes);
       printf("\n");
       load_zero = set_zero(2);

       for( pass = 1; pass <= num_passes; ++pass )
       {
              switch(pass)
              {
                     case 1:
                            pass_variables = &vpass1;
                            break;
                     case 2:
                            pass_variables = &vpass2;
                            break;
                     case 3:
                            pass_variables = &vpass3;
```

```
            }
            get_variables( pass, pass_variables );
      }
      do
      {
            printf("\n Accept and continue? [y/n] \n");
            scanf("%c", &response);
            if( response == 'n' | response == 'N')
                  exit(0);
      }
      while( response != 'y' && response != 'Y' );


      for( pass = 1; pass <= num_passes; ++pass )
      {
            switch(pass)
            {
                  case 1:
                        stroke_load = &dpass1;
                        pass_variables = &vpass1;
                        stroke_zero = &stroke_zero1;
                        h0 = gauge_length;
                        set_temperature( pass_variables );
                        break;
                  case 2:
                        stroke_load = &dpass2;
                        pass_variables = &vpass2;
                        stroke_zero = &stroke_zero2;
                        h0 -= vpass1.comp_distance;
                        cooldown( vpass1.temperature, vpass2.temperature,
vpass2.interpasstime );
                        break;
                  case 3:
                        stroke_load = &dpass3;
                        pass_variables = &vpass3;
                        stroke_zero = &stroke_zero3;
                        h0 -= vpass2.comp_distance;
                        cooldown( vpass2.temperature, vpass3.temperature,
vpass3.interpasstime );
            }
            *stroke_zero = set_zero( 1 );
            szero = stroke_distance;
            stroke_distance += pass_variables->comp_distance;
            strainrate = pass_variables->strain_rate;
            compres4( szero, stroke_distance, h0, strainrate, load_zero,
stroke_load);
      }

      clean();
      da_out( 0, fmap_mti( 20 ) );
      clrscr();
      for( pass = 1; pass <= num_passes; ++pass )
      {
            switch(pass)
            {
                  case 1:
                        stroke_load = &dpass1;
                        stroke_zero = &stroke_zero1;
                        h0 = gauge_length;
                        break;
                  case 2:
                        stroke_load = &dpass2;
                        stroke_zero = &stroke_zero2;
                        h0 -= vpass1.comp_distance;
```

```
                        break;
                case 3:
                        stroke_load = &dpass3;
                        stroke_zero = &stroke_zero3;
                        h0 -= vpass2.comp_distance;
                }
                write_disk( area, pass, h0, *stroke_zero, load_zero, stroke_load );
        }

        for( t = 0, ti = clock(); t <= 5.0;
        t = (clock()-ti)/CLK_TCK, da_out( 0, fmap_mti(-(4.0*t - 20.0)) ) );
        da_out( 0, fmap_vti(0) );

        return( 0 );
}


/*Function that initializes the pc30 board*/
#define BADD        0x700
#define data_30
void ini_board(void)
{
        int i;
        set_base(BADD);
        i = diag();
        printf("\nPC-30 diagnostics report the following :\n");
        if (i != 0)
        {
                printf("\nPC-30 not found, or failed.");
                exit(0);
        }
        else
        {
                switch (get_type()) {
                case found_30 : printf("PC-26/PC-30 found, operating correctly.");
                    break;
                case found_39 : printf("PC-39 found, operating correctly.");
                    break;
                case found_30bc : printf("PC-30B/PC-30C found, operating
correctly.");
                    break;
                case found_30d : printf("PC-30D found, operating correctly.");
                    break;
                case found_30pg : printf("PC-30PG found, operating correctly.");
                    break;
                case found_126 : printf("PC-126 found, operating correctly.");
                    break;
                }
                printf("\n\n");
                init();
        }
}


int set_zero( int chan )    //function that determines the zero values for
{                           // displacement or load.
        char response;
        int volt_zero, temp, i;
        long sum = 0;

        for( i = 1; i <= 100; ++i)
                {
                init();
                clean();
```

```
                ad_in( chan, &temp );
                sum += temp;
                }
        volt_zero = sum / 100;

        return( volt_zero );
}


// function to get deformation variables from user
void get_variables( int pass, struct variables *pass_variables)
{
        printf("Enter the starting temperature (in %cC) for pass %d\n:", 248, pass
);
        scanf("%f", &pass_variables->temperature );
        printf("Enter the compression distance (in millimetres) for pass %d:\n",
pass );
        scanf("%f", &pass_variables->comp_distance );
        printf("Enter the strain rate (per second) for pass %d\n:", pass );
        scanf("%f", &pass_variables->strain_rate );

        if( pass > 1 )
                {
                printf("Enter cooling time (in seconds) between pass %d and %d\n",
pass-1, pass );
                scanf("%f", &pass_variables->interpasstime );
                }

         printf("\n");
}


// function to set temperature before compression
# void set_temperature( struct variables *pass_variable )
{
        int temp_i, temp;
        float temp_f = 0;
        long i, sum;
        clock_t ti;

        clrscr();
        printf("Adjusting temperature to %f\n", pass_variable->temperature );
        while( temp_f < pass_variable->temperature )
                {
                init();
                clean();
                for( i = 1, sum = 0; i <= 100; i++)
                        {
                        ad_in( 3, &temp );
                        sum += temp;
                        }
                temp_i = sum / 100;
                temp_f = fmap_itt( temp_i );
                printf("temperature read in is: %.0f%cC\r", temp_f, 248);
                if( temp_f < pass_variable->temperature )
                        {
                        clean();
                        da_out( 1, fmap_vti( ON )  );
                        }
                else
                        {
                        clean();
                        da_out( 1, fmap_vti( OFF )  );
                        }
```

```
        }

    init();
    clean();
    for( i = 1, sum = 0; i <= 100; i++)
        {
        ad_in( 3, &temp );
        sum += temp;
        }
    temp_i = sum / 100;
    temp_f = fmap_itt( temp_i );

    printf("\n\nStablising temperature at %f\n", pass_variable->temperature);
    for( ti=clock(); (clock()-ti)/CLK_TCK < 30; )
        {
        if( temp_f < pass_variable->temperature )
            {
            clean();
            da_out( 1, fmap_vti( ON )  );
            }
        else
            {
            clean();
            da_out( 1, fmap_vti( OFF )  );
            }
        init();
        clean();
        for( i = 1, sum = 0; i <= 100; i++)
            {
            ad_in( 3, &temp );
            sum += temp;
            }
        temp_i = sum / 100;
        temp_f = fmap_itt( temp_i );
        printf("temperature read in is: %.0f%cC,   holding time is: %.0f
secs\r", temp_f, 248, (clock()-ti)/CLK_TCK);
        }

    while( pow((temp_f-pass_variable->temperature),2) > 6)
        {
        if( temp_f < pass_variable->temperature )
            {
            clean();
            da_out( 1, fmap_vti( ON )  );
            }
        else
            {
            clean();
            da_out( 1, fmap_vti( OFF )  );
            }
        init();
        clean();
        for( i = 1, sum = 0; i <= 100; i++)
            {
            ad_in( 3, &temp );
            sum += temp;
            }
        temp_i = sum / 100;
        temp_f = fmap_itt( temp_i );
        printf("temperature read in is: %.0f%cC\r", temp_f, 248);
        }

    printf("\n");
```

```
        clean();
        da_out( 1, fmap_vti( OFF ) );
}


// function to control rate of cooling between each compressive event
void cooldown( float temphigh, float templow, float intpasstime )
{
        int temp_i, temp;
        float temp_f = 0, coolingrate, time = 0;
        long i, sum;
        clock_t timestart;

        timestart = clock();                        //start timer

        coolingrate = (temphigh - templow) / intpasstime;//calculate
                                                        //cooling rate
        clrscr();
        printf("Adjusting temperature to %f\n", templow );
        time = (clock() - timestart) / CLK_TCK;          //update time

        while( time < (0.95*intpasstime) )
                {
                init();
                clean();
                for( i = 1, sum = 0; i <= 500; i++)
                        {
                        ad_in( 3, &temp );          //sample temperature
                        sum += temp;                //a number of times
                        }                           //to average
                temp_i = sum / 500;
                temp_f = fmap_itt( temp_i );

                time = (clock() - timestart) / CLK_TCK; //update time

                if( temp_f < (temphigh - coolingrate * time) )
                        {
                        clean();                        //transformer switched
                        da_out( 1, fmap_vti( ON )  );   //on
                        }
                else
                        {
                        clean();                         //transformer switched
                        da_out( 1, fmap_vti( OFF )  );   //off
                        }

                printf("temperature read in is: %.0f%cC. interpass time = %.0f
seconds\r", temp_f, 248, time);
                }

        if( (temp_f-templow) != 0 )
                {
                while( pow((temp_f - templow),2) > 25)       //to ensure compression
                        {                                   //at correct temperature
                        clean();
                        for( i = 1, sum = 0; i <= 500; i++)
                                {
                                ad_in( 3, &temp );          //sample temperature
                                sum += temp;                //a number of times
                                }                           //to average
                        temp_i = sum / 500;
                        temp_f = fmap_itt( temp_i );

                        if( (temp_f-templow) == 0 )
```

```
                        break;

                    time = (clock() - timestart) / CLK_TCK; //update time

                    if( temp_f < templow )
                        {
                        clean();                        //transformer switched
                        da_out( 1, fmap_vti( ON )  );   //on
                        }
                    else
                        {
                        clean();                        //transformer switched
                        da_out( 1, fmap_vti( OFF )  );  //off
                        }

                    printf("temperature read in is: %.0f%cC. interpass time =
%.0f seconds\r", temp_f, 248, time);
                    }
                }


        printf("\n");

        clean();                                        //transformer switched
        da_out( 1, fmap_vti( OFF ) );                   //off for beginning of
}                                                        //compression


// compres4.cpp
// function that samples from the stroke and load outputs of the ESH, as well
// as the temperature of deformation. The data is stored in an array and then
// corrected for the zero points.
// Compression is simultaneously controlled at a constant strain rate
// ESH compliance is corrected for during compression
void compres4( float szero, float stroke_distance, float h0, float strain_rate,
int load_zero, struct comp_data *stroke_load )
{
        int i, j;
        int temp1 = 0, temp2 = 0, temp3 = 0;
        long  loadi = 0;
        long sum1 = 0, sum2 = 0, sum3 = 0;
        float t, d, load, rig_comp = 0;
        clock_t ti;

        printf("\nNOW COMPRESSING\n\n");

        for( j = 1; j <= 25; j++ )          //sample load and calculate
                {                           //rig_comp before compression
                clean();
                ad_in( 2, &temp2 );
                sum2 += temp2;
                }
        loadi = sum2 / 25;
        if (loadi < load_zero)
                {
                loadi -= load_zero;
                load = fmap_dtk(-loadi);
                rig_comp = pow(load, 0.65) / 23.0;
                }

        for( i = 0, t = 0, ti = clock(), d = szero;
        d <  (stroke_distance + rig_comp) && i < MAX_POINTS;
        t = (clock()-ti)/CLK_TCK, d = szero + rig_comp + h0*( 1.0 - exp(-
strain_rate*t)), i++)
```

```
            {
            sum1 = 0;
            sum2 = 0;
            sum3 = 0;
            clean();
            da_out( 0, fmap_mti(-d) );
            for( j = 1; j <= 25; j++ )
                  {
                  ad_in( 1, &temp1 );
                  ad_in( 2, &temp2 );
                  ad_in( 3, &temp3 );
                  sum1 += temp1;
                  sum2 += temp2;
                  sum3 += temp3;
                  }
            stroke_load->stroke[i] = sum1 / 25;
            loadi = sum2 / 25;
            stroke_load->load[i] = loadi;
            stroke_load->temperature[i] = sum3 / 25;
            if (loadi < load_zero)
                  {
                  loadi -= load_zero;
                  load = fmap_dtk(-loadi);
                  rig_comp = pow(load, 0.65) / 23.0;
                  }
            }

      da_out( 0, fmap_mti(-(stroke_distance + rig_comp)) );//to ensure correct
                                                            //compression

      for( ;(clock()-ti)/CLK_TCK < 0.4; i++ )        //sample data for at
            {                                        //least 0.4 seconds
            sum1 = 0;
            sum2 = 0;
            sum3 = 0;
            for( j = 1; j <= 25; j++ )
                  {
                  ad_in( 1, &temp1 );
                  ad_in( 2, &temp2 );
                  ad_in( 3, &temp3 );
                  sum1 += temp1;
                  sum2 += temp2;
                  sum3 += temp3;
                  }
            stroke_load->stroke[i] = sum1 / 25;
            loadi = sum2 / 25;
            stroke_load->load[i] = loadi;
            stroke_load->temperature[i] = sum3 / 25;
            if (loadi < load_zero)
                  {
                  loadi -= load_zero;
                  load = fmap_dtk(-loadi);
                  if (load > 20)
                        {
                        rig_comp = pow(load, 0.65) / 23.0;
                        clean();
                        da_out( 0, fmap_mti(-(stroke_distance + rig_comp)) );
                        }
                  }
            }

//    clean();
//    rig_comp = (pow(load, 0.65) / 23.0) * 0.70;    //load relieved
//    clean();
```

```
//      da_out( 0, fmap_mti(-(stroke_distance + rig_comp)) );

        printf("i = %d \n", i);

        if( i >= MAX_POINTS )
                {
                printf("array bounds exceeded");
                exit(0);
                }

        stroke_load->stroke[i] = -5000;
}


/* function that writes an array of data in memory to a file (named by user)
   on disk                                                              */
// Updated March 1994: To calibrate displacement for rig stifness
// Updated October 1995: Stress and strain calculations adjusted by factor of
// 1.155
// Updated February 1997: Deformation temperature data also written to file.
void write_disk( float area, int pass, float h0, int stroke_zero, int load_zero,
struct comp_data *stroke_load )
{
        FILE *stroke_file;
        char file[30], response;
        int i;
        float load, millimetre, stress, strain, calib_fact, temperature;
        float zero_correction = 0;

        do
                {
                printf("Do you want to write sampled data from pass %d to file?
[y/n]\n", pass);
                scanf("%c", &response );
                if( response == 'n' | response == 'N' )
                        return;
                }
        while( response != 'y' && response != 'Y' );

//      printf("h0 = %f\n", h0);
        printf("Enter name of file : \n");
        scanf("%s", file );

        if( stroke_file = fopen( file, "wt") )          // writing data to disk
                for(i = 0 ; stroke_load->stroke[i] != -5000 && i < MAX_POINTS; ++i)
                        {
                        stroke_load->stroke[i] -= stroke_zero;// correcting for zero
                        millimetre = fmap_dtm( -(stroke_load->stroke[i]) );//points
                        if( stroke_load->load[i] < load_zero)
                                {
                                stroke_load->load[i] -= load_zero;
                                load =  fmap_dtk( -(stroke_load->load[i]) );  //in kN

                                if( (i==0) && (load > 5.0) )
                                        zero_correction = pow( load, 0.65) / 23.0;

                                calib_fact = pow( load, 0.65) / 23.0;
                                //calibrating for rig stiffness
                                millimetre = millimetre + zero_correction - calib_fact;
                                }

                        strain = log( h0 / (h0 - millimetre) ) * 1.155;
                        stress = load / (area * 1000 * 1.155);  //in MPa
                        temperature = fmap_itt( stroke_load->temperature[i] );
```

```
                    fprintf( stroke_file, "%f  %f     %f\n", strain, stress,
temperature );
                    printf(" i = %d\r", i);
                    }
        else
                {
                printf("Unable to open file \n");
                exit(0);
                }
        fclose( stroke_file);
}


/* Function that maps an voltage value to a integer value to be outputted */
/* For RANGE 10:                    0 volts   <-------->    +10 volts  */
/*                  is mapped to      0      <-------->      4096     */
/* For RANGE 20:                  -10 volts   <-------->     10 volts  */
/*                  is mapped to     4096    <-------->       0      */
int fmap_vti( float voltage)
{
        float finteger = 0;
        int integer = 0;

        switch (RANGE)
        {
              case 10:
               finteger = voltage * 4096 / 10 ;
               break;
              case 20:
               finteger = (-voltage * 2048 / 10 ) + 2048 ;
        }
        integer = (int) finteger;
        return( integer );
}


/* Function that maps a voltage integer value read in to a voltage value
   in volts */
/* for RANGE    5                              0  <---------->   4096     */
/*                    is mapped to      -5 volts <---------->  +5 volts  */
/* for RANGE   10                              0  <---------->   4096     */
/*                    is mapped to       0 volts <---------->  +10 volts */
/* for RANGE   20                              0  <---------->   4096     */
/*                    is mapped to     -10 volts <---------->  +10 volts */
float fmap_itv( int integer )
{
        float finteger = 0;
        float voltage = 0;

        finteger = (float) integer;
        switch( RANGE )
        {
              case 5:
                 voltage = (finteger - 2048) * 5 / 2048;
                 break;
              case 10:
                 voltage = finteger * 10 / 4096;
                 break;
              case 20:
                 voltage = (finteger - 2048) * 10 / 2048;
        }
        return( voltage );
}
```

```
/* function that maps a stroke value in millimetres to a voltage value in
   integers to be outputted   */
/* for RANGE 10                          0 mm    <---------> 50 mm
                 is mapped to             0     <---------> 4096
   for RANGE 20                        -50 mm    <---------> 50 mm
                 is mapped to         4096      <---------> 0       */
int fmap_mti(  float mm )
{
       float finteger = 0;
       int integer = 0;

       switch( RANGE )
              {
              case 10:
                     finteger = mm * 4096 / 50;
                     break;
              case 20:
                     finteger = ( -mm * 2048 / 50 ) + 2048;
              }
       integer = (int)finteger;
       return (integer) ;
}


/* Function that maps a voltage difference integer value to a stroke value in
   millimetres or a load value in K Newtons  */
/* for RANGE    5                              0  <---------->   4096     */
/*                      is mapped to          0 mm <---------->   50 mm    */
/* for RANGE   10                              0  <---------->   4096     */
/*                      is mapped to          0 mm <---------->   50 mm    */
/* for RANGE   20                              0  <---------->   4096     */
/*                      is mapped to          0 mm <---------->   100 mm   */
float fmap_dtm( int integer )
{
       float finteger = 0;
       float stroke   = 0;

       finteger = (float) integer;
       switch( RANGE )
       {
              case 5:
              case 10:
                     stroke = finteger * 50 / 4096;
                     break;
              case 20:
                     stroke = finteger * 100 / 4096;
       }
       return( stroke );
}


//function that maps a voltage integer read in to a temperature in degrees
//Celsius
//an amplified voltage signal of max range     0 volts <--------> 10 volts
//                        RANGE 5       0      <--------> 4096
//is mapped to a temperature of     -250 deg C <--------> 250 deg C
//                        RANGE 10      0      <--------> 4096
//is mapped to                    0 deg C      <--------> 500 deg C
//                        RANGE 20      0      <--------> 4096
//is mapped to                 -500 deg C      <--------> 500 deg C
float fmap_itt( int integer )
{
       float finteger = 0;
```

```
        float temperature;

        finteger = (float)integer;

        switch( RANGE )
        {
                case 5:
                        temperature = (finteger - 2048 ) * 250 / 2048;
                        break;
                case 10:
                        temperature = finteger * 500 / 4096;
                        break;
                case 20:
                        temperature = (finteger - 2048 ) * 500 / 2048;
        }

        return( temperature );
}


/* Function that maps a voltage difference integer value to a load value in
   K Newtons  */
/* for RANGE    5                              0  <---------->   4096     */
/*                      is mapped to          0 kN <---------->   250 kN   */
/* for RANGE   10                              0  <---------->   4096     */
/*                      is mapped to          0 kN <---------->   250 kN   */
/* for RANGE   20                              0  <---------->   4096     */
/*                      is mapped to          0 kN <---------->   500 kN   */
float fmap_dtk( int integer )
{
        float finteger = 0;
        float load   = 0;

        finteger = (float) integer;
        switch( RANGE )
        {
                case 5:
                case 10:
                        load = finteger * 250 / 4096;
                        break;
                case 20:
                        load = finteger * 500 / 4096;
        }
        return( load );
}
```

Appendix B:

Source Code for Misorientation Calculations

```
//tmatch.cpp
//This programme calculates minimum misorientation angles between several
//ideal orientations and measured orientations.  The ideal orientations
//can be for either FCC or BCC structures.  The measured orientations are
//read in from a file with a format created by EBSD measurements
//conducted at the University of Cape Town and subsequently processed by
//the programme "combine".  Output is to file in the form of the minimum
//misorientation angles calculated for the relevant (BCC or FCC) ideal
//orientations for each measured orientation. From these results the
//closest matching orientation can by chosen by identifying the smallest
//misorientation angle.
//
//Written by:       Alan Duckham
//                  Dept. of Materials Engineering
//                  University of Cape Town
//
//Last Update:      September 1997
//Compiler used:    TURBO C++, ver 3.0


#include <fstream.h>
#include <iostream.h>
#include <iomanip.h>
#include <conio.h>
#include <process.h>
#include <math.h>
#include <string.h>

void bcc( float texture [3] [3], float minangle [11]);
void fcc( float texture [3] [3], float minangle [11]);
void invert_matrix(float matrix [3][3], float matrix_i [3][3]);
void user_matrix(float array1 [3], float array2 [3], float matrix [3] [3]);
void matrix_prod(float matrix1 [3] [3], float matrix2 [3] [3], float prod [3]
[3]);
float minAng(float misO [3] [3]);

float PI = 3.141592654;
int N_CRYST_ELEMS = 24;
float CRYST_ELEMS [24] [3] [3] = {1,0,0,0,1,0,0,0,1, -1,0,0,0,1,0,0,0,-1,
                          -1,0,0,0,-1,0,0,0,1, 1,0,0,0,-1,0,0,0,-1,
                          0,1,0,0,0,1,1,0,0, 0,-1,0,0,0,1,-1,0,0,
                          0,-1,0,0,0,-1,1,0,0, 0,1,0,0,0,-1,-1,0,0,
                          0,0,1,1,0,0,0,1,0, 0,0,-1,1,0,0,0,-1,0,
                          0,0,-1,-1,0,0,0,1,0, 0,0,1,-1,0,0,0,-1,0,
                          0,0,-1,0,-1,0,-1,0,0, 0,0,1,0,-1,0,1,0,0,
                          0,0,1,0,1,0,-1,0,0, 0,0,-1,0,1,0,1,0,0,
                          -1,0,0,0,0,-1,0,-1,0, 1,0,0,0,0,-1,0,1,0,
                          1,0,0,0,0,1,0,-1,0, -1,0,0,0,0,1,0,1,0,
                          0,-1,0,-1,0,0,0,0,-1, 0,1,0,-1,0,0,0,0,1,
                          0,1,0,1,0,0,0,0,-1, 0,-1,0,1,0,0,0,0,1};
float ORTHO0 [3][3] = {1,0,0,0,1,0,0,0,1};
float ORTHO1 [3][3] = {-1,0,0,0,1,0,0,0,-1};
float ORTHO2 [3][3] = {1,0,0,0,-1,0,0,0,-1};
float ORTHO3 [3][3] = {-1,0,0,0,-1,0,0,0,1};
```

```
int main()
{
float plane [3], direction [3], texture [3] [3];
float minangle [11];
float lowest_ang;
char fo[30], fi[30];
char ch;
int i = 0;
int a;
int lines = 0;
int lnumber = 0;
int structure = 0;

clrscr();
cout << "This programme calculates minimum misorientation angles between
several\n";
cout << "ideal orientations and measured orientations. The ideal orientations
can\n";
cout << "be for either FCC or BCC structures.\n";
cout << "The measured orientations are read in from a file with a format
created\n";
cout << "by EBSD measurements conducted at the University of Cape Town and\n";
cout << "subsequently processed by the programme 'combine'.\n";
cout << "Output is to file in the form of the minimum misorientation angles\n";
cout << "calculated for the relevant (BCC or FCC) ideal orientations for each\n";
cout << "measured orientation. From these results the closest matching
orientation\n";
cout << "can by chosen by identifying the smallest misorientation angle.\n";
cout << "\n\n";

while( structure != 1 && structure != 2)
       {
       cout << "Enter 1 for BCC or 2 for FCC. ";
       cin >> structure;
       }

cout << "\nEnter name of input file (EBSD measurements): ";
cin >> fi;
cout << "\nEnter name of output file (results file):     ";
cin >> fo;

ofstream fout (fo);
ifstream fin (fi);
if (!fin)
       {
       cerr << "Cannot open " << fi << "for input\n";
       exit(-1);
       }

for( i=0; i!=5; i++)              //eats up 1st 5 lines of text of input file
       {
       fin.get(ch);
       while( ch!='\n')
              fin.get(ch);
       }

switch (structure)          //Write heading to output file
       {
       case 1: fout << "No.       ideal1 ideal2 ideal3 ideal4 ideal5 ideal6 ideal7
       lowest ang\n";
              break;
       case 2: fout << "No.       copper S      brass  goss   cube   cubeND cubeRD R
       Q      P      BR     lowest ang\n";
       }
```

```
while( fin.get(ch) && fout )      //loop intil end of input file
        {
        fin >> lines;        //read line number
        lnumber ++;

        for( i=0; i!=3; i++)       //read in plane co-ordinates
                {
                fin >> plane[i];
                plane[i] /= 1000.0;
                }
        for( i=0; i!=3; i++)       //read in direction co-ordinates
                {
                fin >> direction[i];
                direction[i] /= 1000.0;
                }

        fin.get(ch);
        while( ch!= '\n')   //eat up the rest of the line
                fin.get(ch);

        user_matrix( plane, direction, texture);   //calculate matrix for
                                                   //measured orientation

        fout <<  lnumber << "      ";           //write line number to ouput
                                                 //file

        fout.precision(1);
        lowest_ang = 180;
        switch (structure)                          //calculate minimum
                {                                  //misorientation angles
                case 1:                            //depending on type of
                        {                          //structure chosen
                        bcc( texture, minangle);   //and write to file
                        for( i=0; i!=7; i++)
                                {
                                fout << minangle [i] << "  ";
                                if(minangle [i] < lowest_ang)
                                        {
                                        lowest_ang = minangle [i];
                                        a = i;
                                        }
                                }
                        fout << lowest_ang;
                        switch (a)
                                {
                                case 0: fout << " (ideal1)\n"; break;
                                case 1: fout << " (ideal2)\n"; break;
                                case 2: fout << " (ideal3)\n"; break;
                                case 3: fout << " (ideal4)\n"; break;
                                case 4: fout << " (ideal5)\n"; break;
                                case 5: fout << " (ideal6)\n"; break;
                                case 6: fout << " (ideal7)\n"; break;
                                }
                        }
                        break;
                case 2:
                        {
                        fcc( texture, minangle);
                        for( i=0; i!=11; i++)
                                {
                                fout <<  minangle [i] << " ";
                                if(minangle [i] < lowest_ang)
                                        {
```

```
                                lowest_ang = minangle [i];
                                a = i;
                                }
                        }
                fout << lowest_ang;
                switch (a)
                        {
                        case 0: fout << " (copper)\n"; break;
                        case 1: fout << " (S)\n"; break;
                        case 2: fout << " (brass)\n"; break;
                        case 3: fout << " (goss)\n"; break;
                        case 4: fout << " (cube)\n"; break;
                        case 5: fout << " (cubeND)\n"; break;
                        case 6: fout << " (cubeRD)\n"; break;
                        case 7: fout << " (R)\n"; break;
                        case 8: fout << " (Q)\n"; break;
                        case 9: fout << " (P)\n"; break;
                        case 10: fout << " (BR)\n"; break;
                        }
                }
        }

    }

fin.close();
fout.close();
return (0);
}


void bcc( float texture [3] [3], float minangle [11])
{
float ideal1 [3] [3] = {0.70710678,0.70710678,0.0,
                    -0.70710678,0.70710678,0.0,
                    0.0,0.0,1.0};
float ideal2 [3] [3] = {0.70710678,0.57735027,0.40824829,
                    -0.70710678,0.57735027,0.40824829,
                     0.0,-0.57735027,0.81649658};
float ideal3 [3] [3] = {0.70710678,-0.57735027,0.40824829,
                    -0.70710678,-0.57735027,0.40824829,
                     0.0,-0.57735027,-0.81649658};
float ideal4 [3] [3] = {0.70710678,0.40824829,0.57735027,
                    -0.70710678,0.40824829,0.57735027,
                    0.0,-0.81649658,0.57735027};
float ideal5 [3] [3] = {0.0,0.81649658,0.57735027,
                    -0.70710678,-0.40824829,0.57735027,
                    0.70710678,-0.40824829,0.57735027};
float ideal6 [3] [3] = {-0.40824829,-0.70710678,0.57735027,
                    0.81649658,0.0,0.57735027,
                    -0.40824829,0.70710678,0.57735027};
float ideal7 [3] [3] = {0.40824829,0.70710678,0.57735027,
                    -0.81649658,0.0,0.57735027,
                    0.40824829,-0.70710678,0.57735027};
float sym_matrix [3][3];
float ideal1_s [3][3], ideal2_s [3][3],  ideal3_s [3][3], ideal4_s [3][3];
float ideal5_s [3][3], ideal6_s [3][3],  ideal7_s [3][3];
float ideal1_i [3][3], ideal2_i [3][3],  ideal3_i [3][3], ideal4_i [3][3];
float ideal5_i [3][3], ideal6_i [3][3],  ideal7_i [3][3];
float misorien [3][3];
int i,j,m,n;
float angle;

for(m=0;m<7;++m)
```

```
{
minangle[m] = 180.0;
for(n=0;n<4;++n)
        {
        switch (n)
                {
                case 0: for(i=0;i<3;++i)
                        for(j=0;j<3;++j)
                                sym_matrix [i][j] = ORTHO0 [i][j]; break;
                case 1: for(i=0;i<3;++i)
                        for(j=0;j<3;++j)
                                sym_matrix [i][j] = ORTHO1 [i][j]; break;
                case 2: for(i=0;i<3;++i)
                        for(j=0;j<3;++j)
                                sym_matrix [i][j] = ORTHO2 [i][j]; break;
                case 3: for(i=0;i<3;++i)
                        for(j=0;j<3;++j)
                                sym_matrix [i][j] = ORTHO3 [i][j]; break;
                }
        switch (m)
                {
                case 0:
                        {
                        matrix_prod(ideal1, sym_matrix, ideal1_s);
                        invert_matrix(ideal1_s, ideal1_i);
                        matrix_prod(texture,ideal1_i,misorien);
                        } break;
                case 1:
                        {
                        matrix_prod(ideal2, sym_matrix, ideal2_s);
                        invert_matrix(ideal2_s, ideal2_i);
                        matrix_prod(texture,ideal2_i,misorien);
                        } break;
                case 2:
                        {
                        matrix_prod(ideal3, sym_matrix, ideal3_s);
                        invert_matrix(ideal3_s, ideal3_i);
                        matrix_prod(texture,ideal3_i,misorien);
                        } break;
                case 3:
                        {
                        matrix_prod(ideal4, sym_matrix, ideal4_s);
                        invert_matrix(ideal4_s, ideal4_i);
                        matrix_prod(texture,ideal4_i,misorien);
                        } break;
                case 4:
                        {
                        matrix_prod(ideal5, sym_matrix, ideal5_s);
                        invert_matrix(ideal5_s, ideal5_i);
                        matrix_prod(texture,ideal5_i,misorien);
                        } break;
                case 5:
                        {
                        matrix_prod(ideal6, sym_matrix, ideal6_s);
                        invert_matrix(ideal6_s, ideal6_i);
                        matrix_prod(texture,ideal6_i,misorien);
                        } break;
                case 6:
                        {
                        matrix_prod(ideal7, sym_matrix, ideal7_s);
                        invert_matrix(ideal7_s, ideal7_i);
                        matrix_prod(texture,ideal7_i,misorien);
                        } break;
                }
```

```
        angle = minAng(misorien);
        if(angle < minangle[m])
                minangle[m] = angle;
        }
}
}


void fcc( float texture [3] [3], float minangle [11])
{
float copper [3] [3] = {-0.5774,0.7071,0.4082,
                        -0.5774,-0.7071,0.4082,
                        0.5774,0.0,0.8165};
float s [3] [3] = {-0.7682,0.5817,0.2673,
                -0.3841,-0.7528,0.5345,
                0.5121,0.3080,0.8018};
float brass [3] [3] = {0.4082,0.5774,0.7071,
                        -0.4082,-0.5774,0.7071,
                        0.8165,-0.5774,0.0};
float goss [3] [3] = {0.0,0.7071,0.7071,
                        0.0,-0.7071,0.7071,
                        1.0,0.0,0.0};
float cube [3] [3] = {0.0,0.0,1.0,
                        0.0,-1.0,0.0,
                        1.0,0.0,0.0};
float cubend [3][3] = {-0.9487,-0.3162,0.0,
                        0.3162,-0.9487,0.0,
                        0.0,0.0,1.0};
float cuberd [3][3] = {0.0,0.9487,0.3162,
                        0.0,-0.3162,0.9487,
                        1.0,0.0,0.0};
float r [3][3] = {-0.8165,0.5345,0.2182,
                -0.4082,-0.8018,0.4364,
                0.4082,0.2673,0.8729};
float q [3][3] = {-0.5345,0.8452,0.0,
                -0.8018,-0.5071,0.3163,
                0.2673,0.1691,0.9487};
float p [3][3] = {-0.3333,0.9428,0.0,
                -0.6667,-0.2357,0.7071,
                0.6667,0.2357,0.7071};
float br [3][3] = {-0.3030,0.9091,0.2857,
                -0.8081,-0.4041,0.4286,
                0.5051,-0.1010,0.8571};
float sym_matrix [3][3];
float copper_s [3][3], s_s [3][3], brass_s [3][3], goss_s [3][3];
float cube_s [3][3], cubend_s [3][3], cuberd_s [3][3], r_s [3][3];
float q_s [3][3], p_s [3][3], br_s [3][3];
float copper_i [3][3], s_i [3][3], brass_i [3][3], goss_i [3][3];
float cube_i [3][3], cubend_i [3][3], cuberd_i [3][3], r_i [3][3];
float q_i [3][3], p_i [3][3], br_i [3][3];
float misorien [3 ] [3];
int i,j,m,n;
float angle;

for(m=0; m<11; m++)
{
minangle[m] = 180.0;
for(n=0;n<4;++n)
        {
        switch (n)
                {
                case 0: for(i=0;i<3;++i)
                        for(j=0;j<3;++j)
                                sym_matrix [i][j] = ORTHO0 [i][j]; break;
```

```
        case 1: for(i=0;i<3;++i)
                for(j=0;j<3;++j)
                        sym_matrix [i][j] = ORTHO1 [i][j]; break;
        case 2: for(i=0;i<3;++i)
                for(j=0;j<3;++j)
                        sym_matrix [i][j] = ORTHO2 [i][j]; break;
        case 3: for(i=0;i<3;++i)
                for(j=0;j<3;++j)
                        sym_matrix [i][j] = ORTHO3 [i][j]; break;
        }
switch (m)
        {
        case 0:
                {
                matrix_prod(copper,sym_matrix,copper_s);
                invert_matrix(copper_s, copper_i);
                matrix_prod(texture,copper_i,misorien);
                }break;
        case 1:
                {
                matrix_prod(s, sym_matrix, s_s);
                invert_matrix(s_s, s_i);
                matrix_prod(texture,s_i,misorien);
                }break;
        case 2:
                {
                matrix_prod(brass, sym_matrix, brass_s);
                invert_matrix(brass_s, brass_i);
                matrix_prod(texture,brass_i,misorien);
                }break;
        case 3:
                {
                matrix_prod(goss, sym_matrix, goss_s);
                invert_matrix(goss_s, goss_i);
                matrix_prod(texture,goss_i,misorien);
                }break;
        case 4:
                {
                matrix_prod(cube, sym_matrix, cube_s);
                invert_matrix(cube_s, cube_i);
                matrix_prod(texture,cube_i,misorien);
                }break;
        case 5:
                {
                matrix_prod(cubend, sym_matrix, cubend_s);
                invert_matrix(cubend_s, cubend_i);
                matrix_prod(texture,cubend_i,misorien);
                }break;
        case 6:
                {
                matrix_prod(cuberd, sym_matrix, cuberd_s);
                invert_matrix(cuberd_s, cuberd_i);
                matrix_prod(texture,cuberd_i,misorien);
                }break;
        case 7:
                {
                matrix_prod(r, sym_matrix, r_s);
                invert_matrix(r_s, r_i);
                matrix_prod(texture,r_i,misorien);
                }break;
        case 8:
                {
                matrix_prod(q, sym_matrix, q_s);
                invert_matrix(q_s, q_i);
```

```
                matrix_prod(texture,q_i,misorien);
                }break;
        case 9:
                {
                matrix_prod(p, sym_matrix, p_s);
                invert_matrix(p_s, p_i);
                matrix_prod(texture,p_i,misorien);
                }break;
        case 10:
                {
                matrix_prod(br, sym_matrix, br_s);
                invert_matrix(br_s, br_i);
                matrix_prod(texture,br_i,misorien);
                }break;
        }
    angle = minAng(misorien);
    if(angle < minangle[m])
        minangle[m] = angle;
    }
}

}


void invert_matrix(float matrix [3][3], float matrix_i [3][3])
{
int i,j;

for (i=0; i<3; ++i)
    for (j=0; j<3; ++j)
        matrix_i [j][i] = matrix [i][j];
}


void user_matrix(float array1 [3], float array2 [3], float matrix [3] [3])
{
float array3 [3];
int i;

array3 [0] = (array1 [1] * array2 [2] - array1 [2] * array2 [1]);
array3 [1] = (array1 [2] * array2 [0] - array1 [0] * array2 [2]);
array3 [2] = (array1 [0] * array2 [1] - array1 [1] * array2 [0]);

for(i=0; i<3; ++i)
    matrix [i] [0] = array2 [i];
for(i=0; i<3; ++i)
    matrix [i] [1] = array3 [i];
for(i=0; i<3; ++i)
    matrix [i] [2] = array1 [i];
}


void matrix_prod(float matrix1 [3] [3], float matrix2 [3] [3], float prod [3]
[3])
{
int i,j;

for (i=0; i<3; ++i)
    for (j=0; j<3; ++j)
        prod [i] [j] = matrix1 [i] [0] * matrix2 [0] [j]
                     + matrix1 [i] [1] * matrix2 [1] [j]
                     + matrix1 [i] [2] * matrix2 [2] [j];
}
```

```
float minAng(float misO [3] [3])
{
float trace, minAng = PI, Ang;
int j,n;

//ofstream fout ("results.tex");
for(n=0; n<N_CRYST_ELEMS; ++n)
      {
      trace = misO [0] [0] * CRYST_ELEMS [n] [0] [0]
            +      misO [0] [1] * CRYST_ELEMS [n] [1] [0]
            +      misO [0] [2] * CRYST_ELEMS [n] [2] [0];
      trace +=misO [1] [0] * CRYST_ELEMS [n] [0] [1]
            +      misO [1] [1] * CRYST_ELEMS [n] [1] [1]
            +      misO [1] [2] * CRYST_ELEMS [n] [2] [1];
      trace +=misO [2] [0] * CRYST_ELEMS [n] [0] [2]
            +      misO [2] [1] * CRYST_ELEMS [n] [1] [2]
            +      misO [2] [2] * CRYST_ELEMS [n] [2] [2];
      if (trace>=2.999999)
            return 0.0;
      else if (trace<=-0.999999)
            Ang = PI;
      else
            Ang = acos ((trace-1.0)/2.0);
      if (Ang<minAng)
            minAng=Ang;
//    cout << n+1 << "  " << (Ang*180.0/PI) << "\n";
//    fout << n+1 << "  " << (Ang*180.0/PI) << "\n";
      }
return (minAng*180.0/PI);
}
```

References

[1] Sanders, R.E. Jr., Baumann S.F. and Stumpf H.C., "Non-Heat Treatable Aluminium Alloys", *Proc.Int. Conf. on Aluminium Alloys Their Physical and Mechanical Properties*, Charlotteville, vol. 3, 1986, p. 1441.

[2] McQueen H.J., "Micromechansims of Dynamic Softening in Aluminium Alloys During Hot Working", *Proc. Hot Deformation of Aluminum Alloys (Edited: Langdon TG, Merchant HD, Morris JG and Zaidi MA)*, The Minerals, Metals and Materials Society, 1991, p.31.

[3] Taylor G.I., "Plastic Strain in Metals", *Journal of the Institute of Metals*, vol. 62, 1938, p. 307.

[4] Engler O., "Investigation of the Recrystallisation Textures in Al-Alloys", *Proc Int. Conference, Minerals and Materials '96*, Somerset West, South Africa, vol. II, 1996, p.449.

[5] Cahn R.W., "Measurement and Control of Texture", *Materials Science and Technology*, vol.15, 1991, p.429

[6] Lücke K. and Engler O., "Effects of Particles on Development of Microstructure and Texture During Rolling and Recrystallisation in FCC Alloys", *Materials Science and Technology*, vol. 6, 1990, p.1113.

[7] Tucker G.E.G., "Texture and Earing in Deep Drawing of Aluminium", *Acta Metallurgica*, vol. 9, 1961, p. 275.

[8] Panchanadeeswaran S., Richmond O., Fricke W.G. Jr., Lalli L.A., "The Effect of Texture on Earing in Cup Drawing of Rolled High Purity Aluminium Sheets", *Eighth International Conference on Textures and Materials (ICOTOM 8), (edited by Kallen J.S. and Gottstein G.)*, The Metallurgical Society, 1988, p.1103.

[9] Dillamore I.L. and Katoh H., "The mechanisms of Recrystallisation in Cubic Metals with Particular Reference to Their Orientation Dependence", *Metal Science*, vol. 8, 1974, p.73.

[10] Ridha A.A. and Hutchinson W.B., "Recrystallisation Mechanisms and the Origin of Cube Texture in Copper", *Acta Metallurgica*, vol. 30, 1982, p.1929.

[11] Dons A.L. and Nes E., "Nucleation of Cube Texture in Aluminium", *Materials Science and Technology*, vol. 2, 1986, p.8.

[12] Maurice C.I. and Driver J.H., "High Temperature Plane Strain Compression of Cube Oriented Aluminium Crystals", *Acta Metall. Mater*, vol. 41, 1993, p.1653.

[13] Butler J.F., Blicharski M. and Hu H., "The Formation of Dislocation Structure and Nucleation of Recrystallised Grains in an Aluminium Single Crystal", *Textures and Microstructures*, vols. 14-18, 1991, p.611.

[14] Maurice C.I., Driver J.H., Raynaud G.M. and Lequeu Ph., "Texture Evolution During Processing of A 3004 Aluminium Alloy", *Textures and Microstructures*, vol. 14-18, 1991, p.871.

[15] Doherty R.D., Fricke W.G. and Rollett A.D., "Investigations Into the Origin of Cube Recrystallisation Texture in Aluminium Alloys", *Proc. Int. Conference: Aluminium Technology '86*, London, 1986, p.289.

[16] Vatne H.E., Shahani R. and Nes E, "Deformation of Cub-Oriented Grains and Formation of Recrystallised Cube Grains in a Hot Deformed Commercial AlMgMn Aluminium alloy", *Acta Mater.*, vol. 44, 1996, p.4447.

[17] Vatne H.E., Furu T, Ørsund R and Nes, E., "Modelling Recrystallization After Hot Deformation of Aluminium", *Acta Metall*, vol. 44, 1996, p.4463.

[18] Weiland H. and Hirsch J.R., "Microstructure and Local Texture in Hot Rolled Aluminium", *Textures and Microstructure*, vol. 14-18, 1991, p.647.

[19] Saimoto S. and Kamat R.G., "Microstructure and Texture Evolution in Hot Rolled AA 3004 Aluminium Alloy", *Materials Science and Technology*, vol. 8, 1992, p.869.

[20] Panchandeeswaran S. and Field D.P., "Texture Evolution During Plane Strain Deformation of Aluminium", *Acta Metal. Mater*, vol. 43, 1995, p.1683.

[21] Maurice C.I. and Driver J.H., "Hot Rolling Textures of F.C.C. Metals – Part I", *Acta Mater.*, vol. 45, 1997, p.4627.

[22] Hirsh J.R., "Texture Evolution During Hot Rolling in Al Alloys", Proc. *Hot Deformation of Aluminium Alloys (Edited. Langdon TG, Merchant HD, Morris JG and Zaidi MA)*, The Minerals, Metals and Materials Society, 1991, p.379.

[23] Beck P.A. and Hu H., "The Origin of Recrystallisation Textures", *Proc. of Recrystallisation, Grain Growth and Textures (edited by Margolin H.)*, Ohio, 1965, p.393.

[24] Hirsch J. and Lücke K., "The Application of Quantitative Texture Analysis for Investigating Continuous and Discontinuous Recrystallisation Processes of Al-0.01Fe", *Acta Metall*, vol.33, 1985, p.1927.

[25] Hjelen J, Ørsund R. and Nes E., "On the Origin of Recrystallisation Textures in Aluminium", *Acta. Metall. Mater.*, vol. 39, 1991, p.1377.

[26] Doherty R.D., Samajadar I. and Kunze K., "Orientation Imaging Microscopy: Application to the Study of Cube Recrystallisation Texture in Aluminium", *Scripta Metallurgica et Materialia*, vol. 27, 1992, p.1459.

[27] Benum S. and Nes E., "The Effect of Precipitation on the Texture Evolution of Cube Recrystallisation Texture", *Acta Mater.*, vol. 45, 1997, p.4593.

[28] Hirsch J., Mao W. and Lücke K., "Modulation of Rolling and Recrystallisation Textures of Aluminium by Variation of Starting Texture", *Proc. of Int. Conf. Aluminium Technology '86*, London, 1986, p.303.

[29] Akef A., Fortunier R., Driver J.H. and Watanabe T., "Recrystallisation of High Symmetry Aluminium Single Crystals After Plane Strain Compression", *Textures and Microstructures*, vol. 14-18, 1991, p.617.

[30] Nes E. and Solberg J.K., "Growth of Cube Grains During Recrystallisation of Aluminium", *Materials Science and Technology*, vol. 2, 1986, p.19.

[31] Hutchinson W.B. and Ekström H.-E., "Control of Annealing Texture and Earing in Non-Hardenable Aluminium Alloys", *Materials Science and Technology*, vol. 6, 1990, p.1103.

[32] Ito K., Abe H. and Lücke K., "Electronmicroscopical Identification of Second Phases Precipitated During Recrystallisation Annealing of Dilute Al-Fe-Si Alloys", *Journal of the Japanese Institute of Light Metals*, vol. 32, 1982, p.235.

[33] Cigdem M. and Bennet G.H.J., "Effect of Composition on Critical (Cold Working) Strain and Recrystallised Grain Size of Dilute Al-Fe Alloys", *Materials Science and Technology*, vol.7, 1991, p.835.

[34] Morris P.L. and Duggan B.J., "Precipitation and Recrystallisation in an Al-1.8%Mn Alloy", *Metal Science*, January 1978, p.1.

[35] Ito K, Musick R. and Lücke K., "The Influence of Iron Content and Annealing Temperature on the Recrystallisation Textures of High-Purity Aluminium-Iron Alloys", *Acta Metall.*, vol. 31, 1983, p.2137.

[36] Dermarkar S., Guyot P. and Pelissier J., "HVEM Study of Recrystallisation in Aluminium Alloys Containing Second Phase Particles", *Acta Metall.*, vol. 31, 1983, p.1315.

[37] Humphreys F.J., "A Unified Theory of Recovery, Recrystallization and Grain Growth, Based on the Stability and Growth of Cellular Microstructures – I. The Basic Model", *Acta Mater*, vol.45 no. 10, 1997, p.4231.

[38] Humphreys F.J., "A Unified Theory of Recovery, Recrystallisation and grain Growth, Based on the Stability and Growth of Cellular Microstructures – II. The Effect of Second-Phase Particles", *Acta Mater*, vol.45 no.12, 1997, p.5051.

[39] Humphreys F.J., "The Nucleation of Recrystallisation at Second Phase Particles in Deformed Aluminium", *Acta. Metall.*, vol. 25, 1977, p.1323.

[40] Oscarsson A., Hutchinson W.B. and Ekström H.-E., "Influence of Initial Microstructure on Texture and Earing in Aluminium Sheet After Cold Rolling and Annealing", *Materials Science and Technology*, vol. 7, 1991, p.554.

[41] Nes E., "Recrystallisation and Texture Control During Processing", *Proc. Int. Conf. Aluminium Technology '86*, London, 1986, p.280.

[42] Vatne H.E., Engler O. and Nes E., "The Effect of Precipitates on Texture Development", *Materials Science Forum*, vol. 157-162, 1994, p.1501.

[43] Engler O., Tap M., Hirsch J and Gottstein G., "Control of the Recrystallisation Textures in Al-Mg-Si Sheet Alloys", *Proc. Int. Conf. Textures of Materials (ICOTOM 11)*, Xi'an China, 1996, p.405.

[44] Hansen N. and Jensen D.J., "Deformation and Recrystallisation Textures in Commercially Pure Aluminium", *Metallurgical Transactions A*, vol. 17a, 1986, p.253.

[45] Lücke K., Hirsch J., Engler O. and Rickert T., "Rolling and Recrystallisation Textures of Al Alloys in Presence of Precipitation", ", *Proc.Int. Conf. on Aluminium Alloys Their Physical and Mechanical Properties*, Charlotteville, vol. III, 1986, p.1741.

[46] Hutchinson W.B., Oscarsson A. and Karlsson Å, "Control of Microstructure and Earing Behaviour in Aluminium Alloy AA 3004 Hot Bands", *Materials Science and Technology*, vol. 5, 1989, p.1118.

[47] Oscarsson A., "The Effect of Nucleation Sites for Recrystallisation on Annealing Texture and Earing in Aluminium", *Textures and Microstructures*, vol. 14-18, 1991, p.477.

[48] Ferry M. and Humphreys F.J., "The Deformation and Recrystallisation of Particle-Containing {011}<100> Aluminium Crystals", *Acta Mater.*, vol. 44, 1996, p.3089.

[49] Engler O., Yang P. and Kong X.W., "On the Formation of Recrystallisation Textures in Binary Al-1.3%Mn Investigated by Means of Local Texture Analysis", *Acta Mater.*, vol. 44, 1996, p.3349.

[50] Rabet L., Ratchev P, Verlinden B and Van Houte P., "Influence of Constituent Particles on the Recrystallisation of a Cold Rolled Aluminium-Magnesium AA 5182 Alloy", *Proc. 11th Int. Conf. Textures of Materials (ICOTOM 11)*, Xi'an, China, 1996, p.537.

[51] Rickert T., Guldberg S., Furu T., Nes E. and Lücke K., "The Effect of Particles on Texture Evolution in Commercial AlMn", *Textures and Microstructures*, vol. 14-18, 1991, p.721.

[52] Gardener K.J. and Grimes R., "Recrystallisation During Hot Deformation of Aluminium Alloys", *Metal Science*, March-April 1979, p.216.

[53] Perryman E.C., "Recrystallisation Characteristics of Superpurity Base Al-Mg Alloys Containing 0 to 5 Pct Mg", *Journal of Metals*, February 1955, p.1.

[54] Blade J.C., "Recrystallisation in Hot Rolling of Dilute Aluminium Alloys", *Metal Science*, March-April 1979, p.206.

[55] Ueki M., Horie S. and Nakamura T., "Hot Deformation and Dynamic Restoration Processes in a Series of Al-Mg Alloys", *Proc. Int. Conf. on Aluminium Alloys Their Physical and Mechanical Properties*, Charlotteville, vol. I, 1986, p.419.

[56] Raghunathan N. and Sheppard T., "Evolution of Structure in Roll Gap When Rolling Aluminium Alloys", *Materials Science and Technology*, vol. 5, 1989, p.194.

[57] Poschmann I. and McQueen H.J., "Flow Softening and Microstructural Evolution of Al-5Mg During Hot Working", *Scripta Materialia.*, vol. 35, 1996, p.1123.

[58] Lin J.P., "Dynamic Recrystallisation During Hot Compression in Al-Mg Alloy", *Scripta Metallurgica et Materialia*, vol. 26, 1992, p.1869.

[59] MacEwen S.R. and Ramaswami B., "Dynamic Strain Ageing and Jerky Flow in Al-Mg Single Crystals", *Phil. Mag.*, vol. 22, 1970, p. 1025.

[60] Orowan E., "The Calculation of Roll Pressure in Hot and Cold Flat Rolling", *Procedures of the Institute of Mechanical Engineers*, vol. 150, 1943, p. 140

[61] Ford H., "Researches into the Deformation of Metals by Cold Rolling", *Procedures of the Institute of Mechanical Engineers*, vol. 159 no. 39, 1948, p.115.

[62] Watts A.B. and Ford H., "An experimental Investigation of the Yielding of Strip Between Smooth Dies", *Procedures on the Institute of Mechanical Engineers*, vol. 1B no. 10, 1952, p. 448.

[63] Hill, R., Lee, E.H. and Tupper, S.J., "A Method of Numerical Analysis of Plastic Flow in Plane Strain and Its Application to the Compression of a Ductile Material Between Rough Plates", *The American Society of Mechanical Engineers Transactions, Journal of Applied Mechanics*, vol 18, 1951, pp 46-52.

[64] Green, A.P., "A Theoretical Investigation of the Compression of a Ductile Material between Smooth Flat Dies", *Philosophical Magazine*, vol. 42, no. 331, August 1951, pp 900-918.

[65] Collins I.F., "Geometric Properties of Some Slip-Line Fields for Compression and Extrusion", *Journal of the Mechanics and Physics of Solids*, vol. 16, 1968, p.137.

[66] Thomason P.F., "On the Plane-Strain Compression of a Rigid-Plastic Material, With an Entrapped Viscous Lubricant on the Platen Face", *Int. Journal of Mechanical Science*, vol.14, 1972, p.279.

[67] Beynon J.H. and Sellars C. M., "Strain Distribution Patterns During Plane Strain Compression", *Journal of Testing and Evaluation*, vol. 13 no. 1, 1985, p. 28.

[68] Colas R. and Sellars C.M., "Strain Distribution and Temperature Increase During Plane Strain Compression Testing", *Journal of Testing and Evaluation*, vol. 15 no. 6, 1987, p342.

[69] Timothy S.P., Yiu H.L., Fine J.M. and Ricks R.A., "Simulation of Single Pass of Hot Rolling Deformation of Aluminium Alloy by Plane Strain Compression", *Materials Science and Technology*, , vol. 7, 1991, p.255.

[70] Lee C.H. and Kobayashi S., "Elastoplastic Analysis of Plane-Strain and Axisymmetric Flat Punch Indentation by the Finite Element Method", *Int Journal of Mechanical Science*, vol.12, 1970, p.349.

[71] Gelin J.C., Ghouti O. and Shahani R., "Modelling the Plane Strain Compression Test to Obtain Constitutive Equations of Aluminium Alloys", *International Journal of Mechanical Science*, vol. 36 no. 9, p.773.

[72] Machio, C.N., "Optimising Specimen Geometry in Plane Strain Compression", *Final year engineering thesis*, University of Cape Town, November 1996.

[73] Shi H., McLaren A.J., Sellars C.M., Shahani R. and Bolingbroke R., "Hot Plane Strain Compression Testing of Aluminium Alloys", *Journal of Testing and Evaluation*, vol. 25 no. 1, 1997.

[74] Zener C. and Holloman J.H., "Effect of Strain Rate Upon Plastic Flow of Steel", *Journal of Applied Physics*, vol. 15, 1944, p.22.

[75] Castro-Fernandez F.R., Sellars C.M. and Whiteman J.A., "Changes of Flow Stress and Microstructure During Hot Deformation of Al-1Mg-1Mn", *Materials Science and Technology*, vol. 6, 1990, p.453.

[76] Wells M.A., Bolingbroke R., Samarasekera I.V., Hawbolt E.B. and Brimacombe J.K., "Microstructural Changes During Hot Deformation of AA5XXX Aluminium Alloys", *Canadian Institute of Metal Conference*, 1993.

[77] Bolingbroke R.K., Marshall G.J. and Ricks R.A., "The Influence of Initial Microstructure on the Recrystallisation Textures of Aluminium Alloys after Hot Deformation by Laboratory Simulation", *Proc. 10^{h} Int. Conf. On Textures of Materials (ICOTOM 10)*, Clausthal, 1993.

[78] Engler O, Mülders B. and Hirsch J., "Deformation Temperature and Strain Rate Influence on the Recrystallisation Nucleation in Al-Mn1-Mg1", *Z. Mettallkd*, vol. 6, 1996, p.454.

[79] Harren S.V., Dève, H.E., Asaro R.J., "Shear Band Formation in Plane Strain Compression", *Acta Metall.*, vol. 36, 1988, p.2435.

[80] Furu T., Ørsund R. and Nes E., "Substructure Evolution During Hot Deformation Processes of Commercial Non-Heat Treatable Aluminium Alloys", *Materials Science and Engineering*, vol. A214, 1996, p.122.

[81] Zhu Z.G. and Batra R.C., "Analysis of Shear Banding in Plane Strain Compression of a Bimetallic Thermally Softening Viscoplastic Body Containing an Elliptical Void", *Transactions of ASME, Journal of Engineering Materials and Technology*, vol. 113, 1991, p.382.

[82] Bird J.E. and Carlson J.M., "Shear Band Formation During Sheet Forming", *Journal of Metals*, vol. 38, 1986, p.47.

[83] Hatherly M. and Malin A.S., "Shear Bands in Deformed Metals", *Scripta Metallurgica*, vol. 18, 1984, p.449.

[84] Morrii K., Mecking H. and Nakayam Y., "Development of Shear Bands in F.C.C. Single Crystals", *Acta Metall.*, vol. 33, 1985, p.379.

[85] Nakayama Y. and Morii K., "Microstructure and Shear Band Formation in Rolled Single Crystals of Al-Mg Alloy", *Acta. Metall.*, vol. 35, 1987, p.1747.

[86] Korbel A. and Martin P., "Microscopic Versus Macroscopic Aspect of Shear Bands Deformation", *Acta Metall.*, vol. 34, 1986, p.1905.

[87] Korbel A., Embury J.D., Hatherly M., Martin P.L. and Erbsloh H.W., "Microstructural Aspects of Strain Localization in Al-Mg Alloys", *Acta. Metall.*, vol. 34, 1986, p.1999.

[88] Lee W.B. and Chan K.C., "A Criterion for the Prediction of Shear Band Angles in FCC Metals", *Acta Metall. Mater*, vol. 39, 1991, p.411.

[89] Wagner P., Engler O. and Lücke K., "Formation of Cu-Type Shear Bands and Their Influence on Deformation and Texture of Rolled F.C.C. {112}<111> Single Crystals", *Acta. Metall. Mater.*, vol.43, 1995, p.3799.

[90] Engler O., "The Influence of the Initial Grain Size on the Rolling and Recrystallisation Textures in the Alloy Al-1.8%Cu", *Textures and Microstructures*, vol.23, 1995, p.61.

[91] Engler O, Hirsch J. and Lücke K., "Texture Development in Al-1.8wt% Cu Depending on the Precipitation State – I. Rolling Textures", *Acta metall.*, vol. 37, 1989, p.2743.

[92] Wagner P., Engler O. and Lücke K, "Texture Development in Al-3%Mg Influenced by Shear Bands", *Textures and Microstructures*, vols 14-18, 1991, p.927.

[93] Engler O., Heckelmann I., Rickert T., Hirsch J. and Lücke K., "Effect of Pretreatment and Texture on Recovery and Recrystallisation in Al-4.5Mg-0.7Mn Alloy", *Materials Science and Engineering*, vol.10, 1994, p.771.

[94] Jasienski Z., Baudin T., Piatkowski A. and Penelle R., "Orientation Changes Inside Shear Bands Occurring in Channel-Die Compressed (112)[111] Copper Single Crystals", *Scripta Materialia*, vol.35, 1996, p.397.

[95] Jasienski Z., Pospiech J. and Piatkowski A., "Influence of the Specific Local Misorientations Within Shear Bands on the Global Rolling Texture Formation in Polycrystalline Copper and Brass", *Proc. 11th Int. Conf. Textures of Materials (ICOTOM 11)*, Xi'an, China, 1996, p.281.

[96] Koken E. and Embury J.D., "Recrystallisation at Shear Bands in Al-Mg", *Scripta Metallurgica*, vol.22, 1988, p.99.

[97] Dillamore I.L., Roberts J.G. and Bush A.C., "Occurrence of Shear Bands in Heavily Rolled Cubic Metals", *Metal Science*, vol. 13, 1979, p.73.

[98] Asaro R.J., "Geometrical Effects in the Inhomogeneous Deformation of Ductile Single Crystals", *Acta Metallurgica*, vol. 27, 1979, p.445.

[99] Asaro R.J. and Needleman A., "Flow Localization in Strain Hardening Crystalline Solids", *Scripta Metallurgica*, vol. 18, 1984, p.429.

[100] Anand L., "Some Experimental Observations on Localized Shear Bands in Plane-Strain", *Scripta Metallurgica*, vol. 18, 1984, p.423.

[101] Juul Jensen D. and Hansen N., "Flow Stress Anisotropy in Aluminium", *Acta Metall. Mater.*, vol. 38, 1990, p.1369.

[102] Shen Y., "On the Shear Band Formation in f.c.c Metals", *Scripta Metall. Mater*, vol. 25, 1991, 1081.

[103] Hughes D.A., "Microstructural Evolution in a Non-Cell Forming Metal: Al-Mg", *Acta Metall. Mater*, vol. 41, 1993, p.1421.

[104] Winther G., Juul Jensen D. and Hansen N., "Dense Dislocation Walls and Microbands Aligned With Slip Planes – Theoretical Considerations", *Acta Mater.*, vol. 45, 1997, p.5059.

[105] Raghavan M. and Shapiro E., "Structure and Strengthening of Al-Mg Alloys During Hot Working", *Metallurgical Transactions A, vol. 11a, 1980, p.117.*

[106] Cizek P., Parker B.A. and McCulloch D.G., "A Crystallographic Study of Dislocation Cell Arrangement in Aluminium Deformed at an Elevated Temperature", *Materials Science and Engineering A*, vol.194, 1995, p.201.

[107] Godfrey A., Juul Jensen D. and Hansen N., "Slip Pattern, Microstructure and Local Crystallography in an Aluminium Single Crystal of Brass Orientation {110}<112>", *Acta Mater.*, vol. 46, 1998, p.823.

[108] Godfrey A., Juul Jensen D. and Hansen N., "Slip Pattern, Microstructure and Local Crystallography in an Aluminium Single Crystal of Copper Orientation {112}<111>", Acta Mater., vol. 46, 1998, p.835.

[109] Choi C-H, Kwon J-W, Oh K.H. and Lee D.N., "Analysis of Deformation Texture Inhomogeneity and Stability Condition of Shear Components in f.c.c. Metals", *Acta mater*, vol.45, 1997, p.5119.

[110] Jasienski Z., Baudin T., Piatkowski A., Pospiech J., Penelle R. and Paul H., "Development of the Recrystallization Texture in Channel-Die Compressed (112)[111] Copper Single Crystals", *Proc. of 11th Int. Conf. On Textures of Materials (ICOTOM 11)*, Xi'an, China, 1996, p.484.

[111] Heckelmann I., Zhao X.B., Lücke K. and Abbruzzesse G., "Texture Development During Grain Growth", *Textures and Microstructures*, vol. 14-18, 1991, p.769.

[112] Engler O., Hirsch J. and Lücke K., "Texture Development in Al-1.8 wt% Cu Depending on the Precipitation State – II. Recrystallisation Textures", *Acta metall. Mater*, vol.43, 1995, p.121.

[113] Ferguson H, "Physical Simulation Makes Inroads in Advanced Materials Testing", *Advanced Materials and Processes*, vol.143 no. 4, 1993, p.33.

[114] Jahajeeah N, "Design Optimisation of Plane-Strain Compression Dies", *Final year engineering thesis*, University of Cape Town, June1996.

[115] Johnson W and Kudo H., "The Compression of Rigid-.Perfectly-Plastic Material Between Rough Parallel Dies of Unequal Width", *International Journal of Mechanical Sciences*, vol.1, 1960, p.336.

[116] Collins I.F., "Slipline Field Solutions for Compression and Rolling With Slipping Friction", *Int. Journal of Mechanical Science*, vol.11, 1969, p.971.

[117] Collins I.F., "Compression of a Rigid-Perfectly Plastic Strip Between Parallel Rotating Smooth Dies", *Quarterly Journal Of Mechanical and Applied Mathematics*, vol. XXIII part 3, 1970, p.329.

[118] Humphreys F.J. and Kalu P.N., "Dislocation-Particle Interactions During High Temperature Deformation of Two-Phase Aluminium Alloys", *Acta Metall*, vol.35 no.12, 1987, p.2815.

[119] Read W.T. and Shockley W., "Dislocation Models of Crystal Grain Boundaries", *Physical Review*, vol.78 no. 3, 1950, p.275.

[120] Sellars C.M., "Modelling Microstructural Development During Hot Rolling", *Materials Science and Technology*, vol.6, 1990, p.1072.

[121] Doherty R.D., Hughes D.A., Humphreys F.J., Jonas J.J., Juul Jensen D., Kassner M.E., King W.E., McNelley T.R., McQueen H.J. and Rollet A.D., "Current Issues in Recrystallisation: A Review", *Materials Science and Engineering A*, vol.238, 1997, p.219.

[121] Doherty R.D., Hughes D.A., Humphreys F.J., Jonas J.J., Juul Jensen D., Kassner M.E., King W.E., McNelley T.R., McQueen H.J. and Rollet A.D., "Current Issues in Recrystallisation: A Review", *Materials Science and Engineering A*, vol.238, 1997, p.219.